Design of Modern Dispersion-Managed Lightwave Systems

by

Ekaterina Poutrina

Submitted in Partial Fulfillment
of the
Requirements for the Degree
Doctor of Philosophy

Supervised by
Professor Govind P.Agrawal

The Institute of Optics
The College
School of Engineering and Applied Sciences

University of Rochester
Rochester, New York

2003

for my parents

Curriculum Vitae

The author graduated with Master degree in Physics from Moscow State University, Russia, in 1991. During 1991 -1998 she was conducting research at Moscow State University and teaching at the Moscow State Technical University. She began her graduate studies at the Institute of Optics, University of Rochester, in 1998, received the MS degree in Optics in 2003, and carried out her doctoral research in nonlinear fiber optics and optical communications under the supervision of Professor Govind P. Agrawal.

Publications

E. Poutrina and Govind P. Agrawal, "Impact of dispersion fluctuations on 40-Gb/s dispersion-managed lightwave systems ", *J. Lightwave Technol.* **21**, 990-996 (2003).

E. Poutrina and Govind P. Agrawal, "Design rules for dispersion-managed soliton systems", *Opt. Commun.* **206**, 193-200 (2002).

E. Poutrina and Govind P. Agrawal, "Timing jitter in dispersion-managed soliton systems with distributed, lumped, and hybrid amplification ", *J. Lightwave Technol.* **20**, 790-797 (2002).

E. Poutrina and Govind P. Agrawal, "Effect of distributed Raman amplification on timing jitter in dispersion-managed lightwave systems", *IEEE Photon. Technol. Lett.* **14**, 39-40 (2002).

Presentations

E. Poutrina and Govind P. Agrawal, "Impact of dispersion fluctuations on 40-Gb/s dispersion-managed lightwave systems", OSA Annual Meeting, Orlando, FL (2002).

E. Poutrina and Govind P. Agrawal, "Design rules for dispersion-managed soliton systems", OSA Annual Meeting, Orlando, FL (2002).

E. Poutrina and Govind P. Agrawal, "Timing jitter in dispersion-managed soliton systems", OSA Annual Meeting, Long Beach, CA (2001).

E. V. Putrina, N. M. Litchinitser, C. J. McKinstrie, and G. P. Agrawal, "Modulation instability in bulk periodic structures: numerical results", QELS 2000, San Francisco, CA

Acknowledgments

I am deeply grateful to my research advisor, Professor Govind P. Agrawal, for his support, insightful guidance, enthusiasm, understanding and encouragement during all these years. I feel fortunate, for all these years, to be under the influence of such a comprehensive essence of broad and truly encyclopedic knowledge that possesses my advisor. I feel exceptionally grateful for the considerable work he has done shaping me as a researcher; for his prompt and thorough responses to all my questions, for teaching me technical writing, for invariably immediate and careful proofing of the manuscripts, for making my Ph.D work such a positive and memorable experience.

I would like to thank the members of my committee, Professors Wayne H. Knox, Thomas G. Brown, and Philippe Fauchet for their time, for the valuable advises they gave me, and for the questions they asked. Your encouragement and guidance were of a great help for me.

I am grateful to our collaborators, Drs. Dipak Chowdhury and Shiva Kumar, for welcoming us at Corning and for the very fruitful discussions we had about our project.

My very special thanks go to Natasha Litchinitser for her kind friendship, for introducing me into this group, for her help with every aspect at every stage.

I sincerely thank all of the current and former members of our lab for their help, daily conversations, and friendship. I would like to thank especially Quiang Lin and Fatih Yaman for sharing their insights and for their scientific enthusiasm. The numerous stimulating discussions with you were of a great help for me. I am grateful to many other graduate or postdoctoral students, as well as staff members, who were here at one or another time: to Taras Lakoba for being a good friend and for his ready assistance with every mathematical question I asked; to Annick Jehanno (and now Annick Canoglu) for sharing with me her vast experience of laboratory work; to Zhi Liao for introducing me into the project; to Drew Maywar for his friendly assistance during my first year in the group, to Chris Ditchman who was a wonderful teaching assistant in Fourier Optics for us and from whom I learned a lot, to Jayanthi Santhanam and Nick Usechak for many conversations we had during our conference trips as well as here in the Institute, to Per Adamson for laboratory training.

Finally, I would like to thank my whole family for constant support and encouragement they gave me. I am deeply grateful to my mother for the feat she made coming here and taking care of our little son for the whole period of time I was writing this thesis, and to my father who missed her so much.

This research was supported by the National Science Foundation.

Abstract

Dispersion management has proven to be an important technique for designing lightwave communication systems as it can be used to lower the average dispersion of a fiber link even though the group-velocity dispersion is kept relatively large locally for suppressing four-wave mixing. The performance of modern dispersion-managed lightwave systems depends on a large number of factors. Gordon-Haus timing jitter, arising from the presence of amplified spontaneous emission noise, happens to be one of the major limiting factors for long-haul systems, especially at high bit rates exceeding 10 Gb/s. In this thesis, we analyze the role of distributed amplification in controlling timing jitter in dispersion-managed systems. We derive analytical expressions for the timing jitter at any position within the fiber link in the cases of ideal distributed and lumped amplifications and show the possibility of reducing timing jitter by up to 40% using Raman or erbium-based distributed amplification.

It has become apparent in recent years that the dispersion of an optical fiber, designed to have a fixed value, can vary over a considerable range because of unavoidable variations in the core diameter along the fiber length. Even though

such axial variations are static, they can impact the system performance because of the nonlinear nature of the pulse propagation problem. Although dispersion fluctuations rarely impact a 10-Gb/s system, their role on the system performance must be considered for 40-Gb/s lightwave systems for which dispersion tolerance is relatively tight. In this thesis, we present the results of extensive numerical simulations performed to identify the impact of dispersion fluctuations on the performance of 40-Gb/s dispersion-managed lightwave systems, designed using either the chirped-return-to-zero or the soliton format and employing distributed Raman amplification.

We consider also the design of dispersion-managed soliton systems. We use the variational approach to derive approximate analytic expressions for the input pulse parameters and show the existence of a limiting bit rate, which depends only on the dispersion-map configuration. Finally, the design rules are proposed that allow the minimization of the intrachannel pulse interactions in a dispersion-managed soliton system.

Table of Contents

List of Figures

Chapter 1

Introduction

The choice of single-mode silica fibers over copper coaxial cable for designing telecommunication systems was assured by the mid-1980s, and it tremendously improved their performance, reliability, transmission capacity, and cost-effectiveness [1]– [4]. Such systems are nowadays referred to as lightwave systems as they employ an optical carrier in place of a microwave one. Any lightwave system is composed of an optical transmitter, a communication channel, and an optical receiver [1]. The optical transmitter converts an electrical signal into optical pulses and launches the resulting optical signal into an optical fiber. The receiver converts the optical signal back into the original electrical signal at the output end. The transmitter consi sts of an optical source, a modulator and a channel coupler. Semiconductor lasers or light-emitting diodes are usually used as optical sources, and optical signal is generated by modulating the optical carrier wave [1]. The communication channel provides signal propagation while ensuring

a high signal-to noise ratio (SNR) at the receiver end. Modern optical lightwave systems employ a low-loss, usually single-mode, fiber for signal transmission [2].

Although the amount of loss that an optical fiber possesses is quite small (usually around 0.2 dB/km near 1.55 μm) [2], losses accumulate over long distances, so that signal has to be periodically amplified during propagation [1]– [4]. Prior to the advent of optical amplifiers, electronic regenerators were employed to cope with the attenuation of signal along the fiber span. Such regenerators usually include a photodetector to detect the weak incoming light, electronic amplifiers, timing circuitry to maintain the timing of the signals, and a laser along with its driver to launch the signal along the next span [4]. The regenerators raised the cost and limited the transmission capacity of lightwave systems since each channel had to be separately, first, detected, which required a high-speed electronic circuitry, and then regenerated. After erbium-doped fiber amplifiers (EDFAs) were developed around 1990 for travelling-wave amplification near 1.5 μm (the wavelength region in which the fiber losses are minimal), optical amplifiers have been widely used for signal amplification in lightwave systems [4]. The employment of optical amplifiers had a tremendous impact on long-haul networks. It allowed to reduce system cost by eliminating the need to convert an optical signal into electrical domain and back at each regeneration stage. Besides that, optical amplifiers increased dramatically system capacity due to the possibility of amplifying

simultaneously several frequency channels, which enabled the development of the wavelength-division multiplexing (WDM) technique.

The advent of WDM technique has transformed the technology behind modern optical networks. A 1999 book says: "in less than 10 years, the capacity of a single optical fiber equipped with commercial transmission equipment has increased from a single signal, transmitting at a rate of 2.488 Gb/s, to 160 signals, totaling 1600 Gb/s, a factor of close to 1000" [4]. In the latest experiments, long-haul transmission at up to 6.3 Tb/s [5]– [14] and short-haul transmission at up to 10.2 Tb/s [15]– [18] have been achieved employing the WDM technology. While a single-channel rate of 10 Gb/s has been used commercially, higher bit rates of 40 Gb/s [6], [8]– [11], [14]– [19], and up to 320 Gb/s [20], [21] have been used in the laboratory experiments. Transmission of high data rate channels over unregenerated links with lengths of 1000 to 5000 km poses major challenges on WDM technology. Foremost among these problems are the distortion due to transmission effects (including chromatic dispersion, polarization-mode dispersion, and optical nonlinearities), as well as the accumulation of spontaneous emission noise and power nonuniformity arising from optical amplification.

Chromatic dispersion in optical fibers is due to the frequency-dependent nature of the propagation characteristics of light in both the material (the refractive index of glass) and the waveguide structure [1]. Different spectral components of the modulated data travel at different speeds along the fiber. Hence, chromatic

dispersion leads to pulse broadening, which in turn limits the maximum data rate at which information can be transmitted through an optical fiber. The effect of chromatic dispersion is cumulative and increases linearly with transmission distance. Although it is possible to manufacture fibers that induce zero chromatic dispersion [22]– [24], such fibers are incompatible with the deployment of WDM systems since harmful nonlinear effects would be easily generated in this case. For example, zero dispersion creates favorable conditions for phase matching of the four-wave mixing (FWM) [25] process, leading to energy transfer among channels [26]– [34]. Also, nonlinear effects such as self-phase modulation (SPM) and cross-phase modulation (XPM) [25] induce a frequency chirp on optical pulses, which enhances pulse broadening. This chirp could be compensated if a system had an overall small, but nonzero, negative dispersion. Moreover, a dispersion value as small as few ps/(nm km) is sufficient to make XPM and FWM negligible [29] since the different wavelength channels are not phase matched and "walk-off" from each other quickly, thus ensuring that they interact with each other only over relatively short distances.

It turns out that, as long as the WDM technique is implemented in practice, optical fiber used in the system must possess a nonzero amount of chromatic dispersion, while overall dispersion must be compensated. If a system were perfectly linear, it would be irrelevant as to whether the accumulated dispersion along a path is small or large, as long as the overall dispersion is compensated at the

end. However, this is not the case in a real system that possesses some amount of nonlinearity. If too much chromatic dispersion is allowed to accumulate, the data bits will evolve into odd shapes, potentially creating narrow spikes of very high peak power. This will enhance the nonlinear effects and prevent the possibility of restoring data bits at the system output, even though total accumulated dispersion is compensated at the end. The sensitivity with respect to nonlinear effects and chromatic dispersion increases even more at high bit rates (10 Gb/s and larger) because pulse separation in time domain becomes relatively small, while signal power levels required for transmission are large. WDM systems with large number of channels, dense channel spacing, as well as EDFAs that produce large output powers, also lead to the enhancement of the nonlinear effects.

A simple and elegant solution is to create a dispersion map, in which fiber sections with positive and negative dispersion are alternated. In this way, at each point along the fiber link local dispersion has some nonzero value, effectively eliminating FWM and XPM, but the total accumulated dispersion at the end of the link is zero or has a fixed small value, so that minimal pulse broadening is induced. This technique is called *dispersion management*.

Many issues are involved in designing dispersion-managed (DM) systems. One is the choice of the dispersion map. Traditionally, dispersion-compensating fiber (DCF) [35]– [37] has been used inside dispersion-compensation modules. Other more recent techniques include chirped fiber-Bragg gratings (FBGs) [38,39],

higher-order-mode DCFs [40,41], and electronic compensation circuity [42,43]. Besides periodic dispersion compensation, additional compensation modules can be added at the beginning and at the end of the fiber link, providing pre- and post-compensation. The performance of the system can be considerably improved by fine-tuning these end-point modules [44]. With proper dispersion management, even ultra-high bit rate signals can be transmitted through the fiber. As an example, a 640-Gb/s optical time division multiplexed signal was successfully transmitted over the 92-km zero-dispersion-flattened transmission line [45]. The transmission line consisted of single-mode fiber, dispersion-shifted fiber, and reverse-dispersion fiber. Fiber-based dispersion compensation was employed in several recent WDM transmission experiments, which provided total transmission capacity of up to 1.5 Tb/s over transoceanic distances with 40-Gb/s per-channel bit rate [8,9]. Using a fiber-Bragg-grating-based compensator, a 16-channel WDM transmission over nonzero dispersion-shifted fiber was demonstrated at a per-channel rate of 20 Gb/s over 400 km [39]. Tunable dispersion-slope compensation using broadband chirped FBGs [46,47], as well as the employment of higher-order-mode fiber [40] have been shown to provide good dispersion compensation in system demonstrations at 40 Gb/s.

The other important question in designing DM lightwave system is the choice of the kind of amplification scheme one can employ. EDFAs are known to have a very good efficiency, meaning several decibels of gain can be achieved per milliwatt of

power [2]. After the development of efficient, high-power pump sources [48]– [55], there have been a rebirth of interest in Raman amplification in optical fibers [5]– [7], [9]– [11], [56]– [69]. Raman amplification employs the process of inelastic scattering of light through which a photon downshifted in frequency is produced (Stokes wave) together with a vibrating molecule when a pump photon is scattered by silica glass. The advent of high pump power sources has diminished the disadvantage of relatively poor efficiency of Raman amplification in comparison with erbium amplification, while Raman amplifiers do offer several attractive advantages over EDFAs. One very important feature of Raman amplifiers, which makes them attractive for lightwave systems, is their capability of providing gain at any wavelength. In addition to that, Raman amplifiers offer improved noise performance because of several reasons. First, the effective inversion parameter [4] for the Raman scattering process is quite small, close to its quantum-limited value of 1 at room temperature [70]– [72]. Second, accumulated noise power is smaller with distributed amplification [73]. Since Raman process is highly suitable to provide distributed amplification, the signal-to-noise ratio in this distributed amplifier is improved over lumped amplification. Besides the capability of providing gain at arbitrary wavelengths and an improved noise performance, the nonlinear effects in the system can be reduced by using Raman amplification, since the improved SNR allows one to use smaller signal powers [2].

The choice of data propagating format is the next important step in dispersion-

managed system design. Several propagation formats can be used for data transmission in a DM system, including non-return-to-zero (NRZ) [1], chirped return-to-zero (CRZ) [74,75], DM-soliton [76]– [81], and differential phase-shift keying (DPSK) formats [6], [82]– [89]. The return-to-zero (RZ) format is more susceptible to chromatic dispersion than NRZ, but is more robust to nonlinear effects [90]. The CRZ format, in which optical pulses are first prechirped by propagating them thorough a piece of fiber with anomalous dispersion, helps to deal with chromatic dispersion, while keeping the robustness to nonlinear effects that RZ transmission possesses [91]– [93]. DM solitons have an advantage over the CRZ format as they can balance the nonlinear and dispersive effects during pulse propagation. The use of DM solitons also provides a number of other advantages over the conventional solitons occurring in constant-group-velocity-dispersion fibers [1]. However, the design of DM soliton systems requires a careful choice of input parameters (such as the pulse energy, width, and chirp) to ensure that each soliton recovers its input state after each amplification period. A variational technique is commonly used to find the periodic solutions of a dispersion map [94]– [99]. However, its use still requires a numerical approach.

Another important aspect of system design is to ensure the system stability and to optimize the system with respect to parameter variations. It has become apparent in recent years that the dispersion of an optical fiber, designed to have a fixed value, can vary over a considerable range because of unavoidable variations

in the core diameter along the fiber length [100]– [104]. Even though such axial variations are static, they can impact the system performance because of the nonlinear nature of the pulse propagation problem. Another source of dispersion fluctuations is related to environmental changes. For example, if the temperature fluctuates at a given location, the local dispersion would also change in a random fashion. Such dynamic fluctuations can also degrade the system performance. Although dispersion fluctuations rarely impact a 10-Gb/s system, their role on the system performance must be considered for 40-Gb/s lightwave systems for which dispersion tolerance is relatively tight.

The performance of modern DM lightwave systems depends on a large number of other factors, the most important being the noise added by optical amplifiers [1]. Amplified spontaneous emission (ASE) in optical amplifiers introduces random fluctuations in pulse position, pulse phase, and pulse amplitude. While random fluctuations of the latter quantity degrade the SNR, fluctuations in pulse position and phase eventually lead to the Gordon-Haus timing jitter [105,106], which happens to be one of the major limiting factors for long-haul optical communication systems, especially at high bit rates exceeding 10 Gb/s [105]– [113]. A general approach for calculating timing jitter in DM systems was developed by Grigoryan et al. in 1999 [108]. In the past, attention was mostly paid to estimating timing jitter in lightwave systems with lumped amplifiers placed periodically along the DM link [109]– [111]. Although the effect of distributed amplification on timing

jitter has been studied for uniform-dispersion fibers [112,113], the combination of distributed amplification and dispersion management was not yet investigated until our research results were published.

This thesis analyzes several aspects of dispersion-managed systems design. The research work is organized as follows. In Chapter 2, the design of DM soliton systems is considered. We derive analytical expressions for the input parameters that ensure a periodic propagation of DM solitons and analyze how those parameters and the dispersion map can be optimized to increase the possible bit rate in a DM soliton system. Based on the results, simple design rules are proposed that can be quite beneficial in practice. In Chapter 3, the impact of dispersion fluctuations on the performance of 40-Gb/s DM lightwave systems having different modulation formats is investigated. Although dispersion fluctuations have been considered in some recent papers [114]– [119], the emphasis was mostly on the broadening of a single pulse transmitted through the fiber link. In contrast, we model a realistic lightwave system in which a data-coded pulse train consisting of 0 and 1 bits is transmitted through a periodically amplified, dispersion-managed fiber link. The system performance is quantified by the well-known Q parameter that is related to the bit-error rate in a simple way. My emphasis is on identifying how the nonlinear effects are affected by dispersion fluctuations and how the local value of average dispersion affects the interplay among the nonlinear effects and dispersion fluctuations. In Chapter 4, we consider the role of distributed amplifi-

cation in controlling timing jitter in DM systems. We use the approach developed in Ref. [108] to derive analytical expressions for timing jitter in DM systems with ideal distributed and lumped amplifications and compare the two cases. This results, as well as numerical simulations, are then employed to analyze how timing jitter can be reduced using erbium-based distributed, Raman, and hybrid Raman amplification. The main results of this thesis are summarized in Chapter 5.

Chapter 2

Design Rules for Soliton Systems

2.1 Introduction

In this section we consider the DM soliton system design. We introduce basic notation used throughout the text and describe the techniques that are usually used to find the input parameters that ensure periodical pulse propagation in the system. One of these techniques, variational analysis, is then employed to find approximate analytical expressions for the input parameters. The expressions show a good agreement with numerical solutions of variational equations and reveal several interesting results used for designing DM soliton systems. Finally, a system design that allows minimization of intrachannel pulse interactions is described.

2.2 Dispersion Management

The principal scheme of a dispersion map used in a DM lightwave system is shown in Fig. 2.1. Each map period L_m is composed of two fiber sections with opposite dispersion signs, and each amplification period L_A can contain one ore more map periods. When the amplification period contains more than one map period, the system is called dense dispersion-managed system. Dispersion maps composed of alternating-group-velocity-dispersion fibers are attractive for WDM data transmission because their use lowers the average dispersion of the whole system while keeping the group velocity dispersion (GVD) of each section large enough that the four-wave mixing effects remain negligible.

One of the parameters used for characterizing a DM system is the map strength, defined for a two-fiber-section dispersion map as

$$S_{map} = \frac{(\beta_{21} - \bar{\beta}_2)l_1 - (\beta_{22} - \bar{\beta}_2)l_2}{T_{min}^2}, \tag{2.1}$$

where β_{2i} and l_i are the dispersion and the length of the i^{th} fiber section (i = 1,2), respectively, T_{min} is the full width at half maximum (FWHM) of the pulse at the

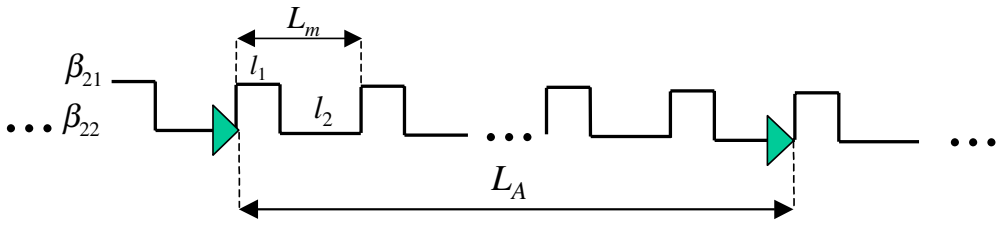

Figure 2.1: Schematic of dispersion map with the notations used

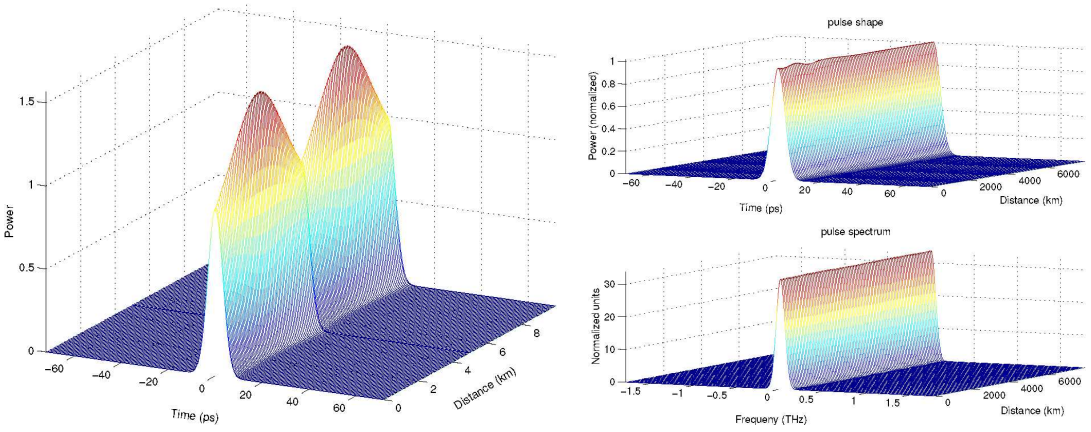

Figure 2.2: Propagation of a DM soliton over one map period (left). Pulse shape and spectrum of a DM soliton while propagating over 100 amplification periods (right).

chirp-free point inside the fiber section, and $\bar{\beta}_2$ is the average dispersion in the system defined as $\bar{\beta}_2 \equiv \sum_{i=1}^{N} \beta_{2i} l_i \Big/ \sum_{i=1}^{N} l_i$, N being the number of fiber sections within the amplification period.

Examples of pulse propagation over one map period of 10 km and over a distance of 8000 km (in the absence of noise) are shown in Fig. 2.2. The graphs on the right represent the pulse shape and spectrum at the output of every amplifier. One can see that, while pulse oscillates noticeably within each fiber section, it almost regains its shape and energy after each amplifier for quite a long propagation distance, so that pulse propagation resembles very much that of a soliton. A DM system having $\beta_{2i} = \pm 4$ ps^2/km, $l_1 \approx l_2 = 5$ km, $\bar{\beta}_2 = -0.01$ ps^2/km, $L_A = 8L_m = 80$ km, and fiber losses of 0.25 dB/km is used for constructing Fig. 2.2. The Gaussian pulse shape was used at the input and the initial pulse

parameters, ensuring periodical pulse propagation, were found numerically using the variational analysis described in section 2.4.

2.3 Nonlinear Schrödinger equation

Pulse propagation in a DM lightwave system is generally described by the nonlinear Schrödinger (NLS) equation. In this section, we outline the derivation of this equation and point out the approximations implied [25].

Similar to all electromagnetic phenomena, the propagation of light in optical fiber is governed by Maxwell's equations, that can be written in SI units as follow:

$$\nabla \times \mathbf{E} = -\partial \mathbf{B}/\partial t, \tag{2.2}$$

$$\nabla \times \mathbf{H} = \mathbf{J}_f + \partial \mathbf{D}/\partial t, \tag{2.3}$$

$$\nabla \cdot \mathbf{D} = \rho_f, \tag{2.4}$$

$$\nabla \cdot \mathbf{B} = 0, \tag{2.5}$$

where $\mathbf{E}$ and $\mathbf{H}$ are, respectively, the electric and magnetic field vectors, $\mathbf{D}$ and $\mathbf{B}$ are the corresponding electric and magnetic flux densities, and $\mathbf{J}_f$ and ρ_f are, respectively, the current density vector and the charge density. Both the last two quantities vanish in the absence of free charges in a medium such as optical fibers.

In a dielectric medium, the flux densities $\mathbf{D}$ and $\mathbf{B}$ are related to the electric and magnetic fields as

$$\mathbf{D} = \varepsilon_0 \mathbf{E} + \mathbf{P}, \tag{2.6}$$

$$\mathbf{B} = \mu_0 \mathbf{H} + \mathbf{M}, \tag{2.7}$$

where ε_0 and μ_0 are, respectively, the vacuum permittivity and permeability, while $\mathbf{P}$ and $\mathbf{M}$ are the induced electric and magnetic polarizations (note that $\mathbf{M}= 0$ for a nonmagnetic media such as an optical fiber).

In a nonlinear medium, electric polarization $\mathbf{P}$ can be represented as a sum of its linear part $\mathbf{P}_L$ and nonlinear part $\mathbf{P}_{NL}$:

$$\mathbf{P}(\mathbf{r},t) = \mathbf{P}_L(\mathbf{r},t) + \mathbf{P}_{NL}(\mathbf{r},t), \tag{2.8}$$

Using the electric-dipole approximation such that the medium response is local, including only the third-order nonlinear effects governed by the third-order susceptibility $\chi^{(3)}$ (noticing that the second order susceptibility $\chi^{(2)}$ vanishes for an isotropic medium like silica glass [25,120]), the linear and nonlinear parts of the induced polarization can be related to the electric field by the general relations [25,121]

$$\mathbf{P}_L(\mathbf{r},t) = \varepsilon_0 \int_{-\infty}^{\infty} \chi^{(1)}(t-t') \cdot \mathbf{E}(\mathbf{r},t')dt', \tag{2.9}$$

$$\mathbf{P}_{NL}(\mathbf{r},t) = \varepsilon_0 \int_{-\infty}^{\infty} \int \chi^{(3)}(t-t_1, t-t_2, t-t_3) \vdots \mathbf{E}(\mathbf{r},t_1)\,\mathbf{E}(\mathbf{r},t_2)\mathbf{E}(\mathbf{r},t_3)\,dt_1 dt_2 dt_3, \tag{2.10}$$

where we assumed also that the optical frequency of the electromagnetic field is far from any resonances of the medium.

Taking curl of Eq. (2.2) and using Eqs. (2.3), (2.4), (2.6), (2.7), and (2.8), we obtain the wave equation

$$\nabla^2\mathbf{E} - \frac{1}{c^2}\frac{\partial^2\mathbf{E}}{\partial t^2} = -\mu_0\frac{\partial^2\mathbf{P}_L}{\partial t^2} - \mu_0\frac{\partial^2\mathbf{P}_{NL}}{\partial t^2}, \tag{2.11}$$

where c is the velocity of light in vacuum and $1/c^2 = \mu_0\varepsilon_0$. In deriving Eq (2.11) we assumed that the nonlinear polarization $\mathbf{P}_{NL}$ is a small perturbation to the total induced polarization and that the dielectric constant ε, defined as

$$\varepsilon(\omega) \equiv 1 + \tilde{\chi}^{(1)}(\omega) + \varepsilon_{NL}, \tag{2.12}$$

is independent of the spatial coordinates for both core and cladding so that the equation $\nabla \cdot \mathbf{D} = \varepsilon\nabla \cdot \mathbf{E} = 0$ can be used, leading to the relation $\nabla \times \nabla \times \mathbf{E} = \nabla(\nabla \cdot \mathbf{E}) - \nabla^2\mathbf{E} = -\nabla^2\mathbf{E}$. In Eq. (2.12), ε_{NL} represents the contribution to the dielectric constant from the nonlinear polarization: $\varepsilon_{NL} \equiv \frac{3}{4}\chi^{(3)}_{xxxx}\left|E(\mathbf{r},t)\right|^2$ [25] and is much less than $1 + \tilde{\chi}^{(1)}$. Also, $\tilde{\chi}^{(1)}(\omega)$ is related to $\chi^{(1)}(t)$ by a Fourier transform.

Several simplifying assumptions are made in order to solve the wave equation (2.11) [25]. First, as it was mentioned, $\mathbf{P}_{NL}$ is a small perturbation to $\mathbf{P}_L$. Second, the optical field is assumed to maintain its polarization along the fiber length so that a scalar approach is valid. Third, the optical field is assumed to be quasi-monochromatic, meaning that its spectrum, centered at ω_0, has a spectral width $\Delta\omega$ such that $\Delta\omega/\omega_0 \ll 1$. For $\omega_0 \sim 10^{15}$ s^{-1} the last assumption is valid for pulses whose width is ≥ 0.1 ps ($\Delta\omega \leq 10^{13}$ s^{-1}). We use now the slowly varying

envelope approximation to separate the rapidly varying part of the electric field by writing it in the form

$$\mathbf{E}(\mathbf{r},t) = 0.5\hat{x}\left[E(\mathbf{r},t)\exp(-i\omega_0 t) + \text{c.c.}\right], \tag{2.13}$$

where c.c. stands for complex conjugate, $\hat{x}$ is the polarization unit vector of the light assumed to be linearly polarized along the x axis, and $E(\mathbf{r},\ t)$ is a slowly varying function of time (relative to the optical period). The polarization components $\mathbf{P}_L$ and $\mathbf{P}_{NL}$ are then expressed in a similar way. Using those expressions in Eqs. (2.9) and (2.10) and making a further simplification assuming that a medium nonlinear response is instantaneous, the Fourier transform $\tilde{E}(\mathbf{r},\ \omega-\omega_0)$ of $E(\mathbf{r},\ t)$ is found to satisfy [25]

$$\nabla^2\tilde{E} + \varepsilon(\omega)\,k_0^2\tilde{E} = 0, \tag{2.14}$$

where $k_0 = \omega/c$, $\varepsilon(\omega)$ is given by Eq. (2.12) and ε_{NL} is assumed to be constant while performing the Fourier transform. We note that by assuming the instantaneous nonlinear response, we neglect the contribution of molecular vibrations to $\chi^{(3)}$, i.e. neglect the Raman effect. The generalized NLS equation that includes this effect can be found in [25].

Equation (2.14) is solved using the method of separation of variables. We assume the solution of the form

$$\tilde{E}(r,\omega-\omega_0) = F(x,y)\,\tilde{A}(z,\omega-\omega_0)\exp(-i\beta_0 z), \tag{2.15}$$

where $\tilde{A}(z,\ \omega)$ is a slowly varying function of z and β_0 is the wavenumber de-

termined later. We use this solution in Eq. (2.14) and obtain the following two equations for $F(x, y)$ and $\tilde{A}(z,\ \omega)$:

$$\frac{\partial^2 F}{\partial x^2} + \frac{\partial^2 F}{\partial y^2} + \left[\varepsilon(\omega) k_0^2 - \beta^2\right] F = 0, \tag{2.16}$$

$$2i\beta_0 \frac{\partial \tilde{A}}{\partial z} + \left(\tilde{\beta}^2 - \beta_0^2\right) \tilde{A} = 0. \tag{2.17}$$

In deriving Eq. (2.17) the second derivative $\partial^2 A/\partial z^2$ is neglected, since $\tilde{A}(z,\ \omega)$ is assumed to be a slowly varying function of z.

As a next step, $\varepsilon(\omega)$ in equation (2.16) is represented as a sum of two parts: $\varepsilon = n^2 + 2n\Delta n$, where n represents the (linear) refractive index and Δn is a small perturbation that includes contributions from the intensity-dependent portion of refractive index and from absorption loss α, $\Delta n = n_2 |E|^2 + \frac{i\alpha}{2k_0}$

We then solve the wave equation (2.16), first, assuming $\Delta n = 0$ to obtain the modal distribution $F(x, y)$ and the wavenumber $\beta(\omega)$. After that, the first-order perturbation theory is used to include the effect of Δn. As a result, the eigenvalue $\tilde{\beta}$ can be represented as

$$\tilde{\beta}(\omega) = \beta(\omega) + \Delta\beta, \tag{2.18}$$

where $\Delta\beta$ represents the part of the eigenvalue affected by Δn and is expressed in terms of Δn and $F(x, y)$ [25].

With the expression (2.18) for the eigenvalue, Eq. (2.17) can be rewritten as

$$\frac{\partial \tilde{A}}{\partial z} = i\left[\beta(\omega) + \Delta\beta - \beta_0\right] \tilde{A}, \tag{2.19}$$

where an approximation $2\beta_0(\tilde{\beta} - \beta_0)$ is used for $\tilde{\beta}^2 - \beta_0^2$.

We now expand $\beta(\omega)$ in a Taylor series, neglecting the terms of the third and higher orders (which is consistent with the requirement $\Delta\omega \ll \omega_0$), and perform an inverse Fourier transform in Eq. (2.14). Using the relation between the $\Delta\beta$ and Δn [25], we finally arrive at the following equation for the propagation of $A(z,t)$:

$$\frac{\partial A}{\partial z} = -\beta_1 \frac{\partial A}{\partial t} - i\frac{\beta_2}{2}\frac{\partial^2 A}{\partial t^2} + i\gamma_0 |A|^2 A - \frac{\alpha}{2}A, \tag{2.20}$$

where β_i is the i^{th} derivative of $\beta(\omega)$ with respect to ω taken at $\omega = \omega_0$, and the nonlinearity coefficient γ_0 is defined by

$$\gamma_0 \equiv \frac{n_2\omega_0}{cA_{eff}}, \tag{2.21}$$

with the effective core area $A_{eff} = \left(\int_{-\infty}^{\infty}\int_{-\infty}^{\infty} |F(x,y)|^2 dxdy\right)^2 \Big/ \int_{-\infty}^{\infty}\int_{-\infty}^{\infty} |F(x,y)|^4 dxdy$. For a single-mode fiber, if the fundamental mode is approximated by a Gaussian shape as $F(x,y) = \exp[-(x^2+y^2)/w^2]$, A_{eff} is evaluated to be $A_{eff} = \pi w^2$ [25].

We note that if the units of m^2/W are used for n_2 in Eq. (2.21), then the pulse amplitude A in this equation is assumed to be normalized so that $|A|^2$ represents the optical power.

Equation (2.20) is the final equation that is generally used to describe propagation of optical pulses in single-mode fibers. It is often referred as the NLS equation since it can be reduced to that equation under certain conditions [25]. In the way it is presented in Eq. (2.20), it includes the effects of fiber losses through α, of fiber nonlinearity through γ_0, and of chromatic dispersion through β_1 and β_2. Describing in short the physical significance of β_1 and β_2, we say that the

pulse envelope moves at the group velocity $v_g = 1/\beta_1$, while GVD is accounted for by β_2. The effects of higher-order dispersion can be included in the equation by keeping the higher-order terms in the Taylor expansion of $\beta(\omega)$, keeping in mind that the condition of narrow spectral width should be satisfied.

2.4 Variational Analysis

As discussed in the previous section, pulse propagation in a DM lightwave system can be described by the following NLS equation:

$$i\frac{\partial A}{\partial z} - \frac{\beta_2}{2}\frac{\partial^2 A}{\partial t^2} + \gamma_0 |A|^2 A = \frac{i}{2}(g - \alpha) A, \tag{2.22}$$

where we performed a change of variables $t \to t - z/v_g$ to eliminate the β_1 term in Eq. (2.20), which is equivalent to working in a coordinate frame propagating with the pulse. We also assume that, besides the loss α, the system possesses a gain g, which may be either distributed or lumped. All the parameters A, β_2, γ_0, g, and α are periodic functions of z for a DM system.

Several approaches exist to find the input pulse parameters that provide periodical pulse propagation in the system. One is to solve the NLS equation (2.22) approximately using a Hermite-Gaussian expansion of pulse amplitude $A(z, t)$ [80]. Another approach solves the equation in the spectral domain using perturbation theory [133]– [135]. A common technique implements the variational method [94]–[99], described below.

With a change of variable $A \equiv V\sqrt{G}$, where G represents the cumulative net gain from 0 to z and is given by

$$G(z) \equiv \exp\left(\int_0^z [g(z') - \alpha(z')]\, dz'\right), \tag{2.23}$$

Eq. (2.22) can be rewritten as

$$i\frac{\partial V}{\partial z} - \frac{\beta_2}{2}\frac{\partial^2 V}{\partial t^2} + \gamma(z)\,|V|^2\, V = 0, \tag{2.24}$$

where $\gamma(z) \equiv \gamma_0 G(z)$. The variational method solves Eq. (2.24) using the Lagrangian density of the form

$$\mathfrak{L} = \frac{i}{2}\left[V\frac{\partial V^*}{\partial z} - V^*\frac{\partial V}{\partial z}\right] - \frac{\beta_2}{2}\left|\frac{\partial V}{\partial t}\right|^2 - \frac{\gamma(z)}{2}|V|^4 \tag{2.25}$$

with the following Gaussian ansatz:

$$V(z,t) = \sqrt{\frac{E_0}{\sqrt{\pi}T}}\exp\left[-(1+iC)\frac{(t-t_p)^2}{2T^2} - i\Omega(t-t_p) + i\phi\right], \tag{2.26}$$

where E_0 is the input energy of the pulse, t_p is peak position, T is the width, C is the chirp, Ω is the frequency shift, and ϕ is the phase of the pulse. The latter five parameters are periodic functions of z. In practice, Ω and ϕ can be chosen to be zero at $z = 0$. However, the input values E_0, T_0, and C_0 of the remaining three parameters need to be specified to ensure periodic propagation of the input pulse through the dispersion map.

The variational approach makes use of the fact that the NLS equation (2.24) is equivalent to the following Euler-Lagrange equation

$$\frac{\partial \mathfrak{L}}{\partial V} - \frac{d}{dt}\left(\frac{\partial \mathfrak{L}}{\partial V_t}\right) - \frac{d}{dz}\left(\frac{\partial \mathfrak{L}}{\partial V_z}\right) \tag{2.27}$$

which, in turn, results from the variational principle

$$\delta \int \int \mathfrak{L}\left(V, V^*, V_z, V_z^*, V_t, V_t^*\right) dzdt \equiv \delta\Lambda = 0, \tag{2.28}$$

where $\mathfrak{L}$ in Eqs. (2.27) and (2.28) is given by Eq. (2.25) and a variable in a subscript denotes a partial derivative with respect to that variable [94,95]. In other words, the function $V(z,t)$ that is a solution of the NLS equation (2.24) is the one that provides a possible extremum to the Lagrangian Λ.

Using Eq. (2.26) for $V(z,t)$ in Lagrangian density (2.25), we can accomplish the integration over time in Eq. (2.28) and calculate the reduced Lagrangian

$$\mathcal{R} \equiv \int_{-\infty}^{\infty} \mathfrak{L}_G dt, \tag{2.29}$$

where $\mathfrak{L}_G$ denotes the result of inserting the Gaussian ansatz (2.26) in the Lagrangian density (2.25). The detailed derivation of $\mathcal{R}$ is provided in Appednix A and results in the following expression:

$$\mathcal{R} = \frac{\sqrt{\pi}}{2} p^2 \left\{ 2\Omega \frac{dt_p}{dz} + 2T\varphi_z - \frac{C_z T}{2} + CT_z - \frac{\gamma}{\sqrt{2}} p^2 T - \frac{\beta_2}{2} \frac{1+C^2}{T} - \beta_2 \Omega^2 T \right\}, \tag{2.30}$$

where $p\left(z\right) \equiv \sqrt{E_0/\sqrt{\pi}T\left(z\right)}$ is the peak amplitude of the pulse.

The variational principle (2.28) converts then to the reduced variational problem

$$\delta \int \mathcal{R} dz = 0, \tag{2.31}$$

where the reduced lagrangian $\mathcal{R}$, after using the Gaussian ansatz in Lagrangian density, is a function of pulse amplitude p, width T, chirp C, phase φ, frequency

shift Ω, position t_p, and their derivatives with respect to z, as it is seen from Eq. (2.30).

As it can be shown from the theory of variational analysis [95], the reduced variational principle (2.31) is equivalent to the set of following ordinary differential equations:

$$\frac{\partial \mathcal{R}}{\partial \eta} - \frac{d}{dz}\left(\frac{\partial \mathcal{R}}{\partial \eta_z}\right) = 0, \tag{2.32}$$

where parameter η takes values p, T, C, φ, t_p, and Ω. While the equation for $\eta = \varphi$ leads to the energy conservation law

$$\sqrt{\pi} T p^2 = \text{const}, \tag{2.33}$$

the rest of the equations (2.32) can be used to obtain the following equations describing the evolution of the pulse width $T(z)$, chirp $C(z)$, and phase $\varphi(z)$ in each fiber section of a DM system:

$$\frac{dT}{dz} = \frac{\beta_2 C}{T}, \tag{2.34}$$

$$\frac{dC}{dz} = \frac{\gamma_0 E_0 G}{\sqrt{2\pi} T} + \frac{\beta_2 \left(1 + C^2\right)}{T^2}, \tag{2.35}$$

$$\frac{d\varphi}{dz} = \frac{5\gamma_0 E_0 G}{4\sqrt{2\pi} T} + \frac{\beta_2}{2T^2} - \frac{\beta_2}{2}\Omega^2. \tag{2.36}$$

$$\frac{dt_p}{dz} = \beta_2 \Omega, \tag{2.37}$$

$$\frac{d\Omega}{dz} = 0. \tag{2.38}$$

The detailed derivation of the Eqs. (2.33) – (2.38) is given in Appendix B.

Equation (2.36) for the phase ϕ is decoupled from Eqs. (2.34) and (2.35). We can ignore it if we are not interested in the phase of the optical pulse. Also,

Ω and t_p remain zero, if they vanish initially, in the absence of noise, as seen from Eqs. (2.37) and (2.38). Thus, solving Eqs. (2.34) and (2.35) for pulse width and chirp is enough for finding the input parameters that ensure periodical pulse propagation in the system. The DM soliton corresponds to a solution of Eqs. (2.34) and (2.35) with the periodic boundary conditions: $T(0) = T(L_A)$ and $C(0) = C(L_A)$, L_A being the amplification period in the system.

2.5 Numerical Results

Solving the variational equations (2.34) and (2.35) numerically, we find periodic solutions over a relatively large range of input energy E_0. For illustration purposes, we focus on two kinds of maps that are used commonly in practice. Each map is made of two types of fibers with dispersions β_{21} and β_{22} and lengths l_1 and l_2. The map A consists of dispersion-shifted and reverse-dispersion fibers of nearly equal length ($l_1 \approx l_2 = 5$ km) with $\beta_{21} = -\beta_{22} = -4$ ps^2/km. We focus on the case of dense dispersion management [126]– [129] in the case of map A and assume that the amplification period L_A includes 8 map periods L_m: $L_A = 8L_m = 80$ km. The map B employs ordinary dispersion management and is made using standard (SMF) fiber of 65-km length ($\beta_{21} = -22$ ps^2/km) and dispersion-compensating fiber of about 14.3 km length ($\beta_{22} = 100$ ps^2/km). We adjust the average dispersion of both maps in the range -0.005 ps^2/km to -0.15 ps^2/km by changing the length l_2. Although the nonlinear parameter γ_0 is generally different for different

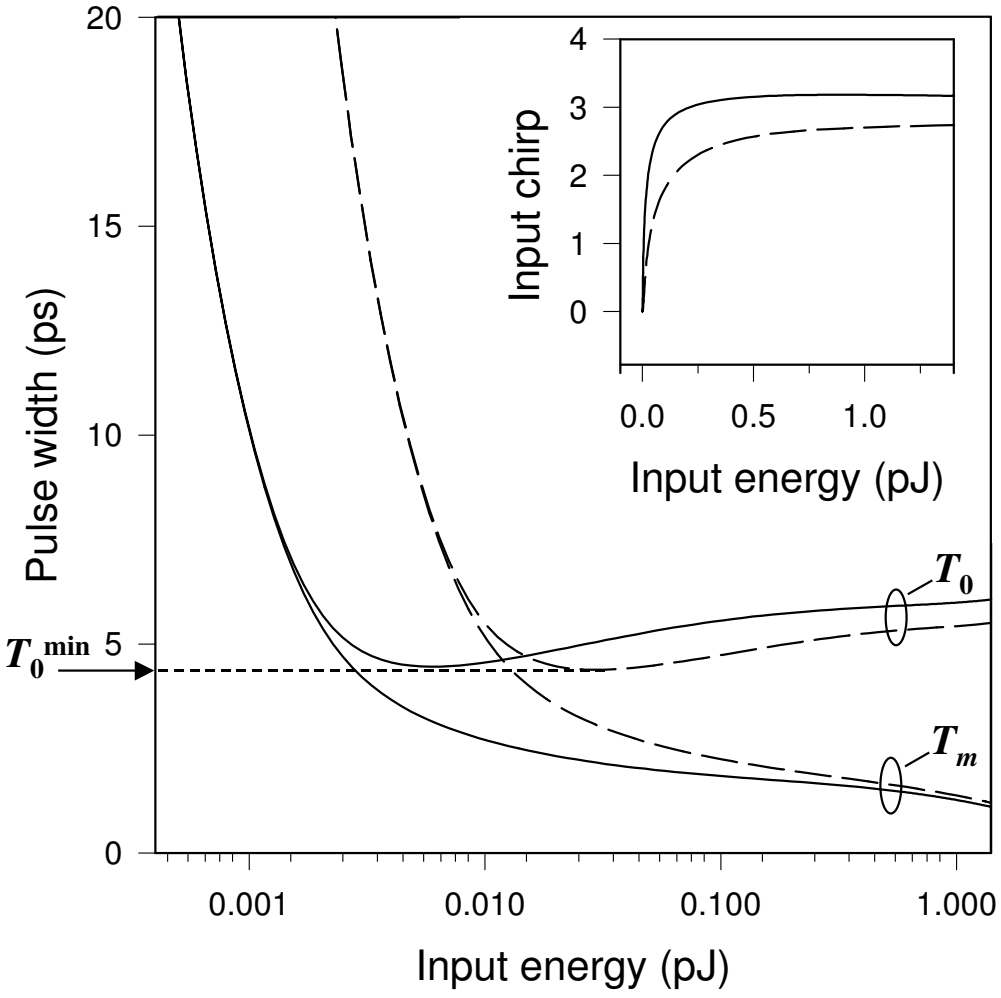

Figure 2.3: Input pulse width T_0 and corresponding minimum pulse width T_m as a function of input energy E_0 for the map A with $\bar{\beta}_2 = -0.01$ ps^2/km. Solid curves are for the loss-less case ($\alpha = 0$), while $\alpha = 0.25$ dB/km for dashed. The inset shows the input chirp in the two cases.

types of fibers, in this work we use $\gamma_0 = 2.5$ W^{-1}km^{-1} unless stated otherwise. This choice does not affect our conclusions.

Figure 2.3 shows the values of input pulse width as a function of E_0 for the dispersion map A with average dispersion $\bar{\beta}_2 = -0.01$ ps^2/km. The curves marked "T_0" represent the input width while the curves "T_m" correspond to the minimum pulse width occurring in the fiber section with anomalous GVD. The

inset shows the input chirp C_0 as a function of E_0. Solid curves in Fig. 2.3 represent the lossless case ($\alpha = 0$) and dashed curves correspond to a loss of 0.25 dB/km in each fiber section. We have verified that the input parameters shown on Fig. 2.3 lead to stable propagation of solitons over more that 10^5 km (in the absence of noise) when Eq. 2.22 is solved numerically by using the split-step method. Examples of pulse peak power oscillations during single pulse propagation (in the absence of noise) is shown on Fig. 2.4. Figure represents pulse propagation in maps A and B, with $\bar{\beta}_2 = -0.01$ ps^2/km and -0.05 ps^2/km and with the input energy $E_0 = 0.032$ pJ and 0.016 pJ for maps A and B, respectively. We see that peak power variations for both maps A and B do not exceed few percent of its mean value for distances up to 40000 km. From Fig. 2.3 we can see that, for low pulse energies, both T_0 and T_m decrease rapidly. Moreover, T_0 and T_m values nearly coincide, indicating that in this region pulse width does not oscillate and remains nearly equal to T_0. An important feature is that at some value of $E_0 = E_c$ the curve $T_0(E_0)$ has a minimum value T_0^{min}. When E_0 exceeds E_c, T_0 and T_m curves diverge from each other, and pulse width starts to oscillate more and more within each fiber section. The qualitative character of the curve $T_m(E_0)$ also changes around E_c from a rapid to a relatively slow decrease, while T_0 slowly increases. The qualitative features shown in Fig. 2.3 hold for any two-section dispersion map having a negative value of average dispersion.

Two parameters are especially important for DM solitons — the ratio

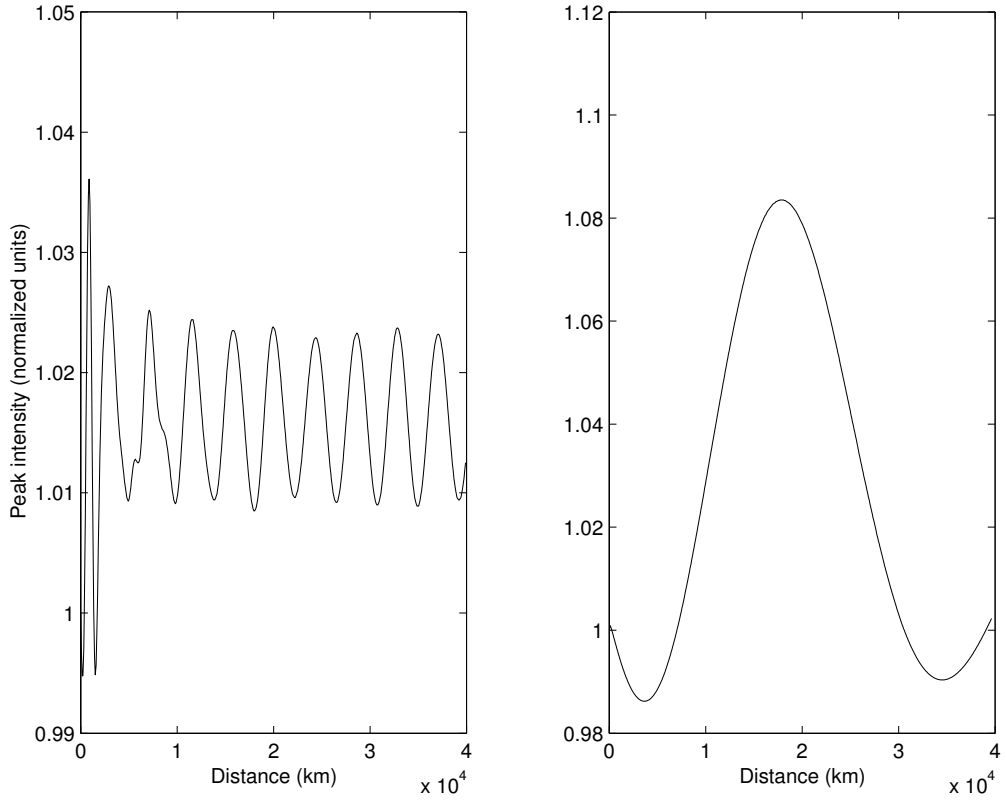

Figure 2.4: Peak power variations during pulse propagation for maps A and B with $\bar{\beta}_2 = -0.01$ ps^2/km. Input energy $E_0 = 0.032$ pJ and 0.016 pJ for maps A and B, respectively.

$\bar{\beta}_2/\gamma_0$ [128] and the stretching factor S_t [130]. In place of the stretching factor we introduce a new parameter

$$T_{map} \equiv \left| \frac{\beta_{21}\beta_{22}l_1 l_2}{\beta_{21}l_1 - \beta_{22}l_2} \right|^{1/2}, \tag{2.39}$$

which depends only on the map parameters β_{2i} and l_i and has units of time. The use of this parameter is justified later. Figure 2.5 shows variations of $T_0(E_0)$ and $T_m(E_0)$ for two values of the ratio $\bar{\beta}_2/\gamma_0$ and two values of T_{map}. Dispersion maps A, for which $T_{map} = 3.16$ ps (solid curves), and B, with $T_{map} = 26.9$ ps (dashed curves), each with two different values of average dispersion ($\bar{\beta}_2 = -0.01$

and -0.15 ps^2/km) are used in this calculation. We see from the figure that the solutions for both maps look similarly, only the whole set of curves for system with $T_{map} = 26.9$ ps is shifted up from the case of system with $T_{map} = 3.16$ ps. As we also see from the figure, the $\bar{\beta}_2/\gamma$ ratio affects dramatically the energy, at which T_0 takes its minimum value T_0^{min} (in agreement with the result of [128]), but it does not affect much the minimum value itself, or the range of pulse stretching from T_0 to T_m. In contrast, the value of T_0^{min}, as well as the asymptotic value of T_m at large energies, depends only on the parameter T_{map}. These results show that for a given two-section map configuration, there exists a limiting bit rate that depends on the value of T_{map}, which will be discussed in details in section 2.8.2.

Considering a wide variety of dispersion maps with different values of $\bar{\beta}_2/\gamma_0$ and T_{map}, we find that for the lossless case, the value of T_0^{min} always corresponds to $C_0 = \pm 1$ (the choice of sign depends on whether β_{21} is negative or positive, respectively). An important feature is that, in a large range of $\bar{\beta}_2$ values, not only the value of T_0^{min}, but also the whole curve $T_0(C_0)$ is invariant with respect to the ratio $\bar{\beta}_2/\gamma_0$. In the next section we use this result and the qualitative features of Fig. 2.5 to find the dependence of T_0 on C_0 in an approximate analytic form.

2.6 Analytical Estimate of T_0

We obtain an approximate analytic formula for the input pulse width in the lossless case, setting $\alpha = 0$ in Eq. (2.35). This approach is justified because, as one

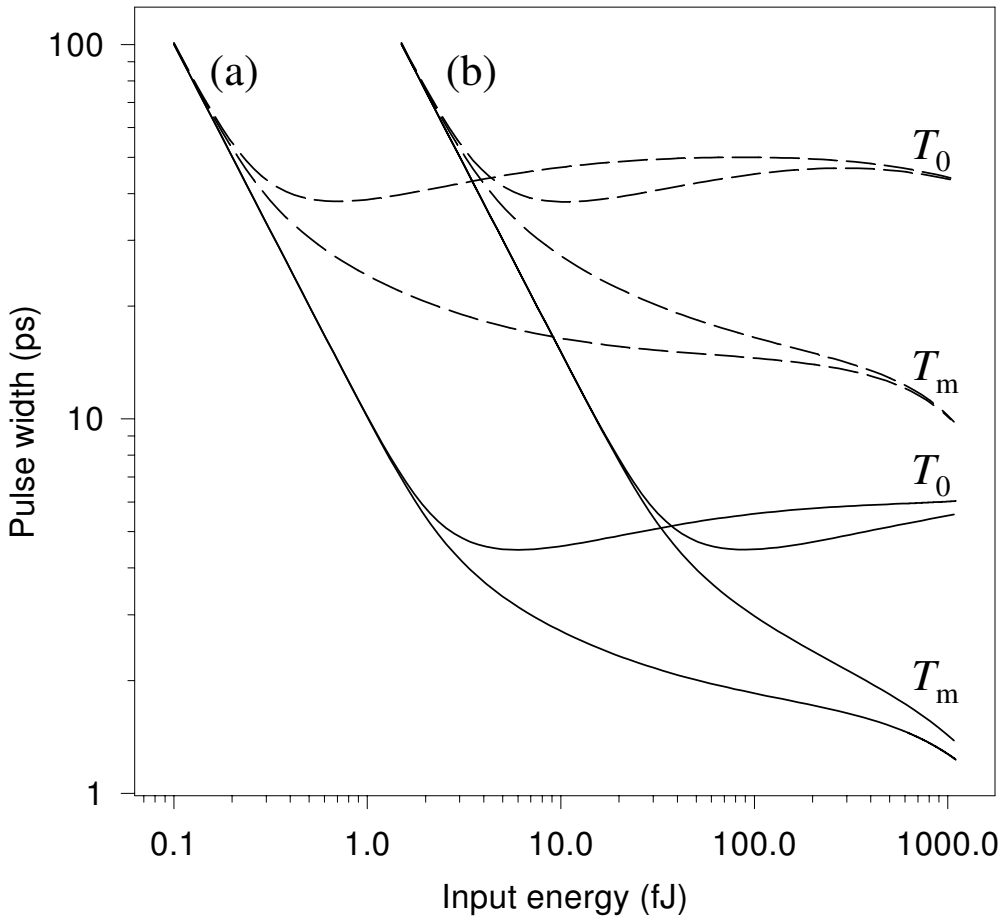

Figure 2.5: Same as Fig. 2.3 except that two different values of $\bar{b}_2/\gamma_0$ are shown for two different maps. (a)$\bar{\beta}_2/\gamma_0 = 0.004$ (ps^{2}W), (b)$\bar{\beta}_2/\gamma_0 = 0.06$ (ps^{2}W). Solid curves are for map A ($T_{map} =$ 3.16 ps) while dashed curves are for map B ($T_{map} = 26.9$ ps). Loss $\alpha = 0$ in all cases.

can see from Fig. 2.3, T_0^{min} value and the range of pulse oscillations are almost the same in a DM system with no loss and in a DM system having 0.25 dB/km loss in each fiber section. This observation remains valid for systems with short-period dispersion maps, having any number of map periods within the amplification period. In such systems, T_0^{min} also corresponds to $|C_0| \approx 1$ even in the presence of loss. This is the consequence of the fact that in short-period maps the chirp-free

point is close to the middle of fiber segments even in the presence of losses (in the loss-less case it is exactly in the middle [131]). The importance of this observation will become clear from what follows. Equation (2.34) can be integrated formally to find

$$T^2(z) = T_0^2(z) + 2\int_0^z \beta_2(z')\, C(z')\, dz'. \tag{2.40}$$

Thus, $T(z)$ can be determined if $C(z)$ is known. Since a closed form expression for $C(z)$ is not available, we follow an empirical method. Numerical simulations show that the chirp C can be represented, with an accuracy better than 0.1%, as a linear function of z in each fiber section for energy values in the range from 0 to about $5E_c$. Examples of chirp and pulse width variation within one map period, obtained by solving variational equations (2.34) and (2.35) numerically for the maps used in the previous section are shown on Figs. 2.6 and 2.7. Fig. 2.6 represents chirp and pulse width variation in maps A and B in the lossless case, with different values of input energy, while Fig. 2.7 assumes 0.25 dB/km losses in each fiber section. We see that chirp varies practically linearly in all cases, so that linear approximation is justified up to quite large values of energy. One can also note that a chirp-free point is located exactly in the middle of each section for all maps in the lossless case [131], as it was mentioned before, while in the presence of loss it is close to the middle of the section only in a dense dispersion map. Using the fact that chirp-free points are located in the middle of each section for $\alpha = 0$,

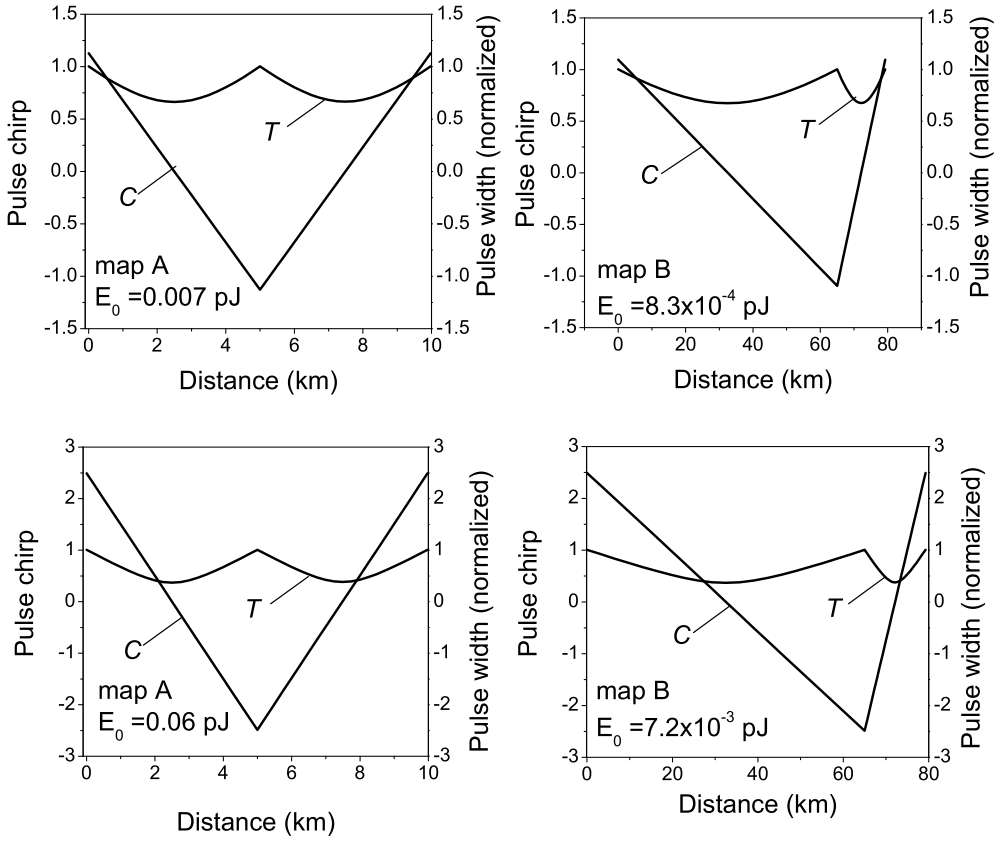

Figure 2.6: Variation of input chirp C_0 and input pulse width T_0 within one map period for maps A and B in the lossless case, with two different values of input energy.

we approximate the chirp in each map period as

$$C(z) = \begin{cases} C_0 \left(1 - \frac{2}{l_1} z\right), & \text{if } 0 \leq z \leq l_1, \\ -C_0 \left(1 - \frac{2}{l_2} \left(z - l_1\right)\right), & \text{if } l_1 \leq z \leq L_m. \end{cases} \tag{2.41}$$

Using Eq. (2.41) in Eq. (2.40), we obtain the following approximate expression for pulse width:

$$T^2(z) = \begin{cases} T_0^2 + 2\beta_{21} C_0 \left(1 - \frac{z}{l_1}\right) z, & \text{if } 0 \leq z \leq l_1 \\ T_0^2 - 2\beta_{22} C_0 \left(1 - \frac{(z-l_1)}{l_2}\right) (z - l_1), & \text{if } l_1 \leq z \leq L_m. \end{cases} \tag{2.42}$$

In order to connect T_0 and C_0 values, we consider the ratio $(1 + C^2)/T^2$ because

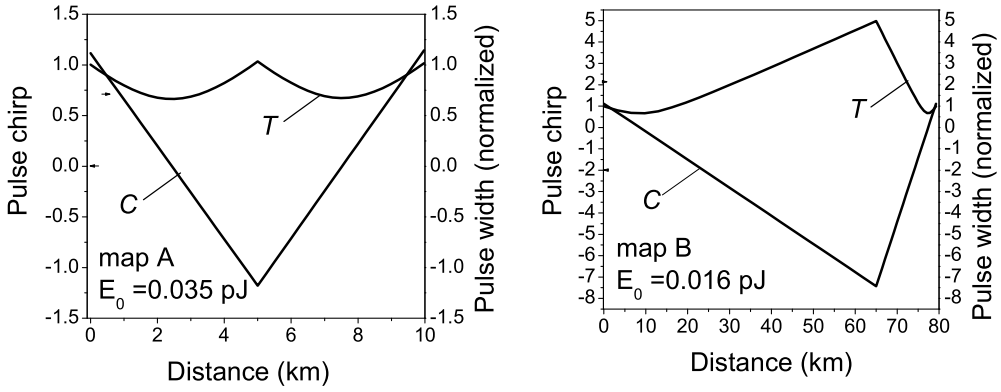

Figure 2.7: Variation of input chirp C_0 and input pulse width T_0 within one map period for maps A and B. Loss $\alpha = 0.25$ dB/km in each fiber section.

it represents the spectral width of a chirped pulse. In a linear system, this ratio remains constant and is equal to $1/T_m^2$. Numerical simulation show, that this ratio does not change much with propagation even in a DM system when the nonlinear length [25] is much larger than the local dispersion length. More specifically, it oscillates within each map period around its average value $(1 + C_0^2)/T_0^2$ by less than 1%. Since the ratio $(1 + C^2)/T^2$ is almost constant during the propagation, the integral

$$I(z) \equiv \int_0^z \frac{1 + C^2(z')}{T^2(z')} dz' \approx \frac{1 + C_0^2}{T_0^2} z \tag{2.43}$$

grows almost linearly with z. We can estimate the error by calculating I using Eqs. (2.41) and (2.42). we show a few steps in deriving the result. Consider first the interval $z \in [0, l_1]$. Making a change of variables $\xi \equiv l_1 - 2z$, noticing that ξ changes from l_1 to $-l_1$ when $z \in [0, l_1]$, and using Eqs. (2.41) and (2.42), the ratio

$(1+C^2)/T^2$ can be rewritten as

$$\begin{aligned}\frac{1+C^2}{T^2} &= \frac{1+(l_1-2z)^2 C_0^2/l_1^2}{T_0^2-(2l_1-2z)\,z\,|\beta_{21}C_0|/l_1} \\ &= \frac{1+\xi^2 C_0^2/l_1^2}{T_0^2-(l_1+\xi)(l_1-\xi)\,|\beta_{21}C_0|/2l_1} \\ &= \frac{1+a_1\xi^2}{p_1+q_1\xi^2},\end{aligned} \tag{2.44}$$

where

$$a_1 \equiv \frac{C_0^2}{l_1}, \quad p_1 \equiv T_0^2 - \frac{|\beta_{21}C_0|\,l_1}{2}, \quad q_1 \equiv \frac{|\beta_{21}C_0|}{2l_1}. \tag{2.45}$$

In deriving Eq. (2.44), we used the fact that the sign of input chirp $\mathrm{sgn}(C_0)$ in a DM soliton system is always opposite to the sign of second-order dispersion in the first segment $\mathrm{sgn}(\beta_{21})$, since the pulse is supposed to be compressed in each fiber section, i.e. $\beta_{21}C_0 = -|\beta_{21}C_0|$. Using Eq. (2.44), the integral $I(z)$ in the first fiber segment can be found as

$$\begin{aligned}I(z) &\equiv \beta_{21}\int_0^{z\le l_1}\frac{1+C^2(z')}{T^2(z')}dz' \\ &= \frac{\beta_{21}}{2}\int_{\xi\ge -l_1}^{l_1}\frac{1+a_1\xi'^2}{p_1+q_1\xi'^2}d\xi' \\ &= 0.5\beta_{21}\left\{(p_1q_1)^{-0.5}\tan^{-1}\left(\xi\sqrt{q_1/p_1}\right)\Big|_{\xi\ge -l_1}^{l_1}\right. \\ &\quad \left. + \left[a_1\xi\Big/q_1 - a_1\sqrt{p_1/q_1^3}\tan^{-1}\left(\xi\sqrt{q_1/p_1}\right)\right]\Big|_{\xi\ge -l_1}^{l_1}\right\} \\ &= \frac{\beta_{21}}{2}\left(\frac{a_1l_1}{q_1}-\frac{a_1\xi}{q_1}\right) \\ &+ \frac{\beta_{21}}{2}\frac{q_1-a_1p_1}{\sqrt{p_1q_1^3}}\left[\tan^{-1}\left(\sqrt{\frac{q_1}{p_1}}l_1\right)-\tan^{-1}\left(\sqrt{\frac{q_1}{p_1}}\xi\right)\right]\end{aligned} \tag{2.46}$$

Going back to the z variable and using again the relation $\beta_{21}C_0 = -|\beta_{21}C_0|$, the

integral $I(z)$ in the first fiber segment is found to be

$$\begin{aligned} I(z) &= \frac{1}{2}\frac{a_1}{q_1}\left(l_1-(l_1-2z)\right) \\ &\quad +\frac{1}{2}\frac{q_1-a_1p_1}{\sqrt{p_1q_1^3}}\left[\tan^{-1}\left(\sqrt{\frac{q_1}{p_1}}l_1\right)-\tan^{-1}\left(\sqrt{\frac{q_1}{p_1}}\left(l_1-2z\right)\right)\right] \\ &= \frac{a_1}{q_1}z+\frac{1}{2}\frac{q_1-a_1p_1}{\sqrt{p_1q_1^3}}\left[\tan^{-1}\left(\sqrt{\frac{q_1}{p_1}}l_1\right)-\tan^{-1}\left(\sqrt{\frac{q_1}{p_1}}\left(l_1-2z\right)\right)\right] \\ &= \frac{2C_0^2z}{|\beta_{21}C_0|\,l_1}+\frac{1}{2}\frac{q_1-a_1p_1}{\sqrt{p_1q_1^3}}\left[\tan^{-1}\left(\sqrt{\frac{q_1}{p_1}}l_1\right)-\tan^{-1}\left(\sqrt{\frac{q_1}{p_1}}\left(l_1-2z\right)\right)\right] \\ &= -\frac{2C_0}{\beta_{21}l_1}z+\frac{1}{2}\frac{q_1-a_1p_1}{\sqrt{p_1q_1^3}}\left[\tan^{-1}\left(\sqrt{\frac{q_1}{p_1}}l_1\right)-\tan^{-1}\left(\sqrt{\frac{q_1}{p_1}}\left(l_1-2z\right)\right)\right], \end{aligned} \tag{2.47}$$

where $z\in[0,l_1]$.

Similarly, considering the second fiber section $z\in[l_1,L_m=l_1+l_2]$, using the change of variables $\zeta\equiv l_2-2\left(z-l_1\right)$, and noticing that in this section $\beta_{22}C_0=|\beta_{22}C_0|$, the ratio $(1+C^2)/T^2$ can be rewritten as

$$\frac{1+C^2}{T^2}=\frac{1+a_2\zeta^2}{p_2+q_2\zeta^2}, \tag{2.48}$$

where

$$a_2\equiv\frac{C_0^2}{l_2},\quad p_2\equiv T_0^2-\frac{|\beta_{22}C_0|\,l_2}{2},\quad q_2\equiv\frac{|\beta_{22}C_0|}{2l_2}. \tag{2.49}$$

The integral $I(z)$ in the second fiber section is then equal to

$$\begin{aligned} I(z) &= I(l_1)+\int_{l_1}^{z\le l_1+l_2}\frac{1+C^2\left(z'\right)}{T^2\left(z'\right)}dz' \\ &= I(l_1)+\frac{2C_0}{\beta_{22}l_2}\left(z-l_1\right) \\ &\quad +\frac{1}{2}\frac{q_2-a_2p_2}{\sqrt{p_2q_2^3}}\left[\tan^{-1}\left(\sqrt{\frac{q_2}{p_2}}l_2\right)-\tan^{-1}\left(\sqrt{\frac{q_2}{p_2}}\left[l_2-2\left(z-l_1\right)\right]\right)\right]. \end{aligned} \tag{2.50}$$

Summarizing the result, the integral over one map period is found to be

$$I(z) = \begin{cases} -\frac{2C_0}{\beta_{21} l_1} z + \varepsilon_1(z), & 0 \le z \le l_1, \\ I(l_1) + \frac{2C_0}{\beta_{22} l_2}(z - l_1) + \varepsilon_2(z - l_1), & l_1 \le z \le L_m, \end{cases} \tag{2.51}$$

where $\varepsilon_i(z)$ $(i = 1,2)$ is defined as

$$\varepsilon_i(z) \equiv \frac{1}{2} \frac{q_i - a_i p_i}{\sqrt{q_i^3 p_i}} \left[\tan^{-1}\left(\sqrt{\frac{q_i}{p_i}}(l_i) \right) - \tan^{-1}\left(\sqrt{\frac{q_i}{p_i}}(l_i - 2z) \right) \right], \tag{2.52}$$

and a_i, p_i, q_i are given by

$$a_i \equiv \frac{C_0^2}{l_i^2}, \quad p_i \equiv T_0^2 - \frac{|\beta_{2i} C_0| l_i}{2}, \quad q_i \equiv \frac{|\beta_{2i} C_0|}{2 l_i}. \tag{2.53}$$

For all practical maps, ε_1 and ε_2 are found to be negligible. Numerical simulations also confirm that the error in Eq. (2.43) does not exceed 0.2 %. Neglecting ε_1 and ε_2 in Eq. (2.51), we notice that $I(z)$ varies linearly with z but with different slopes. Assuming that the average dispersion is relatively small, we find the average slope and equate it to $(1 + C_0^2)/T_0^2$ from Eq. (2.43):

$$\frac{1}{2}\left[-\frac{2C_0}{\beta_{21} l_1} + \frac{2C_0}{\beta_{22} l_2} \right] = \frac{1 + C_0^2}{T_0^2}. \tag{2.54}$$

We then obtain the following expression for the input pulse width in terms of C_0 and dispersion map parameters:

$$T_0 = T_{map} \sqrt{\frac{1 + C_0^2}{|C_0|}}. \tag{2.55}$$

Note the appearance of a single map parameter T_{map} defined as in Eq. (2.39). This parameter has units of time and plays an important role in the following discussion.

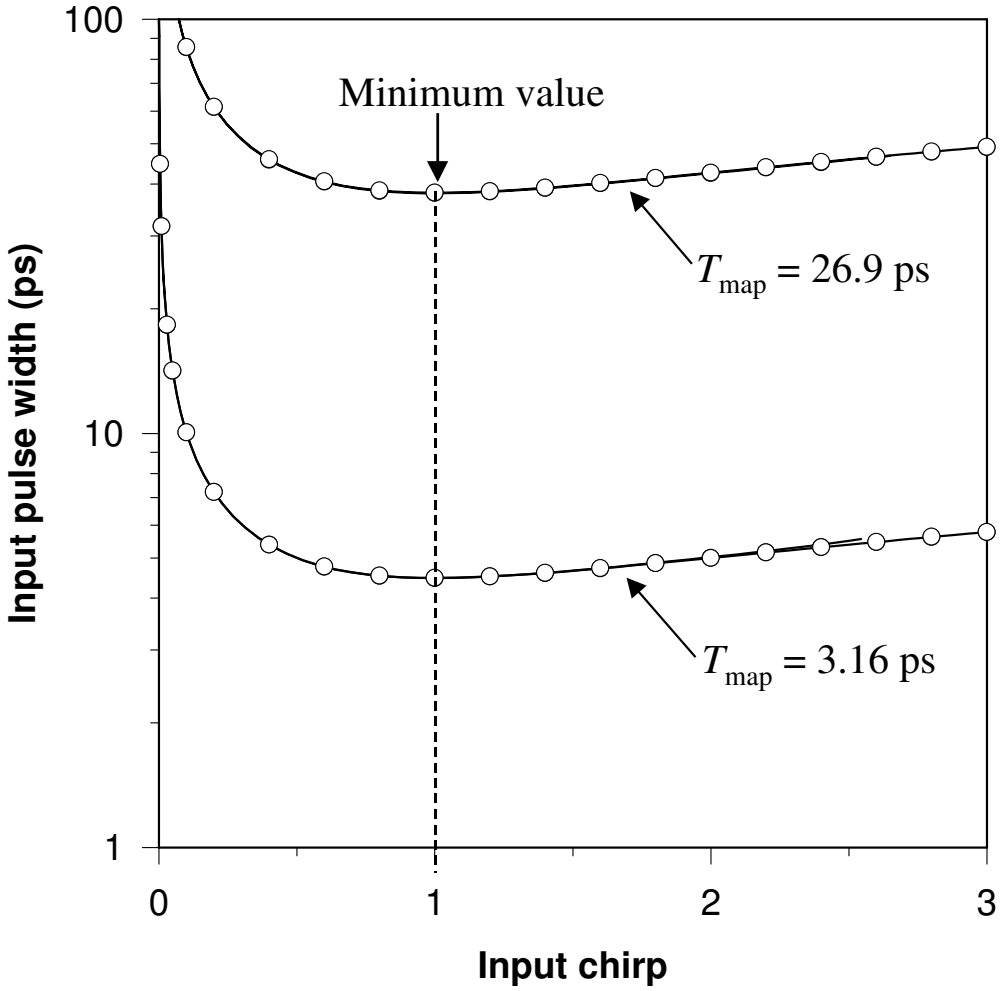

Figure 2.8: Comparison of the input pulse width predicted by Eq. (2.55) (circles) with the numerically calculated values (solid curves) as a function of input chirp for the four maps of Fig. 2.5. Only two curves appear since results are nearly independent of the ratio $\bar{\beta}_2/\gamma$.

The dependence of input pulse width on the input chirp C_0 for the four DM systems of Fig. 2.5 is shown in Fig. 2.8. Open circles represent the values of input pulse width T_0 calculated using Eq. (2.55), while solid lines show the results obtained by solving variational equations (2.34) and (2.35) numerically. We find a very good agreement up to chirp values of $|C_0| = 3$. Although four dispersion maps are used for in Fig. 2.8, only two curves appear on this figure because, as was

mentioned before, the dependence of $T_0(C_0)$ curve on the ratio $\bar{\beta}_2/\gamma$ is negligible when the average dispersion is much smaller than the local dispersion value. For that reason, the curves for $\bar{\beta}_2/\gamma = -0.004$ and -0.06 ps^{2}W are indistinguishable in Fig. 2.8.

Equation (2.55) can be used to find the minimum pulse width. Noticing that the chirp is zero at the location of the minimum pulse width point and using the fact that $(1 + C_0^2)/T_0^2 \approx 1/T_m^2$, the minimum pulse width is given by

$$T_m = \frac{T_{map}}{\sqrt{|C_0|}}. \tag{2.56}$$

Equation (2.56) provides the average value of minimum pulse width in sections with positive and negative dispersions, but these values do not differ much in the region around $|C_0| \approx 1$. A comparison with numerical solutions shows that Eq. (2.56) is accurate to within 2% up to the values of input chirp $|C_0| \approx 3$. The examples of the comparison of numerical and analytical results will be shown in the next section.

Several interesting conclusions can be drawn from Eq. (2.55) and (2.56). First, Eq. (2.56) shows that the qualitative change of the $T_m(E_0)$ curve in Figs. 2.3 and 2.5 from a very rapid to a very slow decrease is due to $1/|C_0|$ dependence of the minimum pulse width. This results from the fact that, as seen in the inset of Fig. 2.3, the value of $|C_0|$ increases rapidly with increased energies. Second, the minimum value of the input pulse width from Eq. (2.55) indeed occurs for $|C_0| = 1$, as also found numerically. Third, when $|C_0| = 1$, T_m is just equal to

the map parameter T_{map}. The input pulse width in this case is $T_0 = \sqrt{2}T_{map}$, showing that pulse width is stretched by the factor of $\sqrt{2}$ within each fiber link when input pulse width corresponds to its minimum width allowed for a given dispersion map. This indicates that the map parameter T_{map} is an important design parameter for system characterization, since$\sqrt{2}T_{map}$ and T_{map} describe, respectively, the minimum possible input width and the corresponding shortest pulse width in the fiber link for a given dispersion map.

2.7 Input energy estimation

Equation (2.55) provides the input pulse width corresponding to a given input chirp, while the full set of input parameters also includes the value of input energy E_0. In this section we estimate E_0 with the help of the approximate solution given in Eqs. (2.41) and (2.42). Setting $\alpha = 0$ in Eq. (2.35), integrating it over one map period and using the periodicity condition $C(0) = C(L_m)$ we obtain

$$\int_0^{L_m} \frac{\gamma_0 E_0}{\sqrt{2\pi}T} + \int_0^{L_m} \beta_2 \frac{1+C^2}{T^2} dz = 0. \tag{2.57}$$

From Eq. (2.57) the input energy can be found as

$$E_0 = \sqrt{2\pi}\frac{I_1 + I_2}{I_3 + I_4}, \tag{2.58}$$

where

$$I_1 \equiv -\beta_{21} \int_0^{l_1} \frac{1+C^2(z)}{T^2(z)} dz, \tag{2.59}$$

$$I_2 \equiv -\beta_{22}\int_{l_1}^{L_m}\frac{1+C^2(z)}{T^2(z)}dz, \tag{2.60}$$

$$I_3 \equiv \gamma_{01}\int_{0}^{l_1}\frac{dz}{T(z)}, \tag{2.61}$$

$$I_4 \equiv \gamma_{02}\int_{l_2}^{L_{m1}}\frac{dz}{T(z)}, \tag{2.62}$$

and γ_{0i} is the nonlinear coefficient in the i^{th} fiber section.

Using the result of Eq. (2.51), we can calculate the first two integrals in Eq. (2.58) as

$$I_1 = -\beta_{21}I(l_1) = 2C_0 - \beta_{21}\varepsilon_1(l_1), \tag{2.63}$$

and

$$I_2 = -\beta_{22}\left[I(l_1+l_2) - I(l_1)\right] = -2C_0 - \beta_{22}\varepsilon_2(l_2). \tag{2.64}$$

Using Eq. (2.42) with the change of variables $\xi \equiv l_2 - 2z$ for $z \in [0, l_1]$ and $\zeta \equiv l_2 - 2(z - l_1)$ for $z \in [l_1, L_m = l_1 + l_2]$, the rest of the integrals in Eq. (2.58) can be found as follows:

$$\begin{aligned}
I_3 &\equiv \frac{\gamma_{01}}{2}\int_{-l_1}^{l_1}\left[T_0^2 + \frac{\beta_{21}C_0}{2l_1}\left(l_1^2 - \xi^2\right)\right]^{-1/2}d\xi \\
&= \frac{\gamma_{01}}{2}\int_{-l_1}^{l_1}\frac{d\xi}{\sqrt{p_1 + q_1\xi^2}} \\
&= \frac{\gamma_{01}}{2}\frac{1}{\sqrt{q_1}}\ln\frac{\sqrt{p_1+q_1l_1^2}+\sqrt{q_1}l_1}{\sqrt{p_1+q_1l_1^2}-\sqrt{q_1}l_1} \\
&= \frac{\gamma_{01}}{2\sqrt{q_1}}\ln\frac{T_0+l_1\sqrt{q_1}}{T_0-l_1\sqrt{q_1}} \\
&= \frac{\gamma_{01}}{2\sqrt{q_1}}\ln\frac{T_0+\sqrt{|\beta_{21}C_0|\,l_1/2}}{T_0-\sqrt{|\beta_{21}C_0|\,l_1/2}},
\end{aligned} \tag{2.65}$$

where Eq. (2.53) is used for q_i and p_i and the relation $\beta_{21}C_0 = -|\beta_{21}C_0|$ was employed. Similarly,

$$\begin{aligned} I_4 &\equiv \frac{\gamma_{02}}{2}\int_{-l_2}^{l_2}\left[T_0^2 - \frac{\beta_{22}C_0}{2l_2}\left(l_2^2-\zeta^2\right)\right]^{-1/2} d\zeta \\ &= \frac{\gamma_{02}}{2\sqrt{q_2}}\ln\frac{T_0+l_2\sqrt{q_2}}{T_0-l_2\sqrt{q_2}} \\ &= \frac{\gamma_{02}}{2\sqrt{q_2}}\ln\frac{T_0+\sqrt{|\beta_{22}C_0|\,l_2/2}}{T_0-\sqrt{|\beta_{22}C_0|\,l_2/2}}. \end{aligned} \tag{2.66}$$

Using Eqs. (2.63)-(2.66) in Eq. (2.58), we arrive at the following expression for the input energy:

$$E_0 = 2\sqrt{2\pi}\frac{\beta_{21}\varepsilon_1(l_1)+\beta_{22}\varepsilon_2(l_2)}{\left(\gamma_{01}\big/\sqrt{q_1}\right)\ln r_1+\left(\gamma_{02}\big/\sqrt{q_2}\right)\ln r_2}, \tag{2.67}$$

where

$$\begin{aligned} r_i &\equiv \frac{T_0-l_i\sqrt{q_i}}{T_0+l_i\sqrt{q_i}} \\ &= \frac{T_0-\sqrt{|\beta_{2i}C_0|\,l_i/2}}{T_0+\sqrt{|\beta_{2i}C_0|\,l_i/2}}, \end{aligned} \tag{2.68}$$

and ε_i and q_i are given by Eqs. (2.52) and (2.53), respectively. Note that, from Eq. (2.52), $\varepsilon_i(l_i)$ are equal to:

$$\begin{aligned} \varepsilon_1(l_1) &= \frac{q_1-a_1p_1}{\sqrt{p_1q_1^3}}\tan^{-1}\left(\sqrt{\frac{q_1}{p_1}}l_1\right), \\ \varepsilon_2(l_2) &= \frac{q_2-a_2p_2}{\sqrt{p_2q_2^3}}\tan^{-1}\left(\sqrt{\frac{q_2}{p_2}}l_2\right), \end{aligned} \tag{2.69}$$

so that Eq. (2.67) can be expressed as

$$E_0 = 2\sqrt{2\pi}\frac{\beta_{21}\frac{q_1-a_1p_1}{\sqrt{p_1q_1^3}}\tan^{-1}\left(l_1\sqrt{\frac{q_1}{p_1}}\right)+\beta_{22}\frac{q_2-a_2p_2}{\sqrt{p_2q_2^3}}\tan^{-1}\left(l_2\sqrt{\frac{q_2}{p_2}}\right)}{\left(\gamma_{01}\big/\sqrt{q_1}\right)\ln r_1+\left(\gamma_{02}\big/\sqrt{q_2}\right)\ln r_2}. \tag{2.70}$$

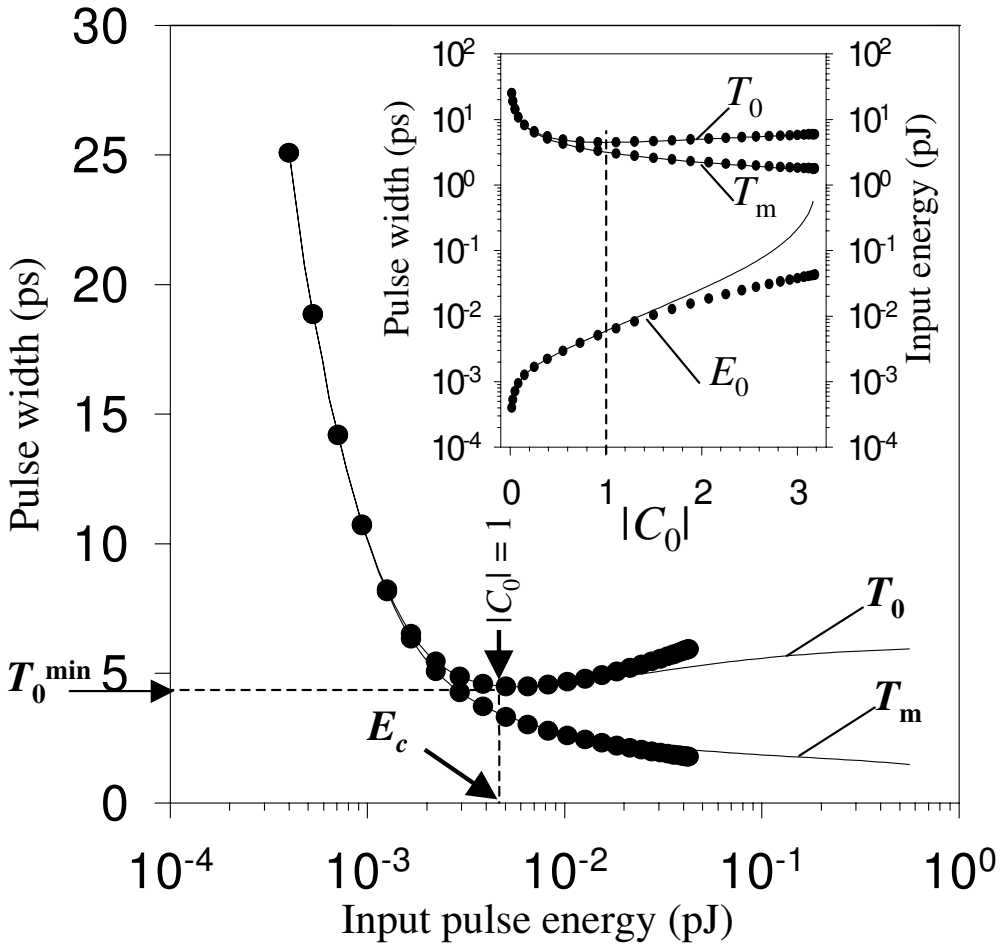

Figure 2.9: Comparison of numerical and analytical results for dense DM system with no loss and with $T_{map} = 3.16$ ps.

A comparison of numerical and analytical results is represented in Figs. 2.9–2.11. Figs. 2.9 and 2.10 show the comparison in the case of no loss for two of the systems used in Fig. 2.5: for the dense DM system with $T_{map} = 3.16\ ps$ (map A) and for ordinary DM system with $T_{map} = 26.9\ ps$ (map B). Solid lines represent the numerical solution while circles show analytical results. The inserts show pulse width and energy as functions of input chirp, as suggested by the analytical solution (2.55),(2.56), and (2.67), while the larger graphs are the same kind of

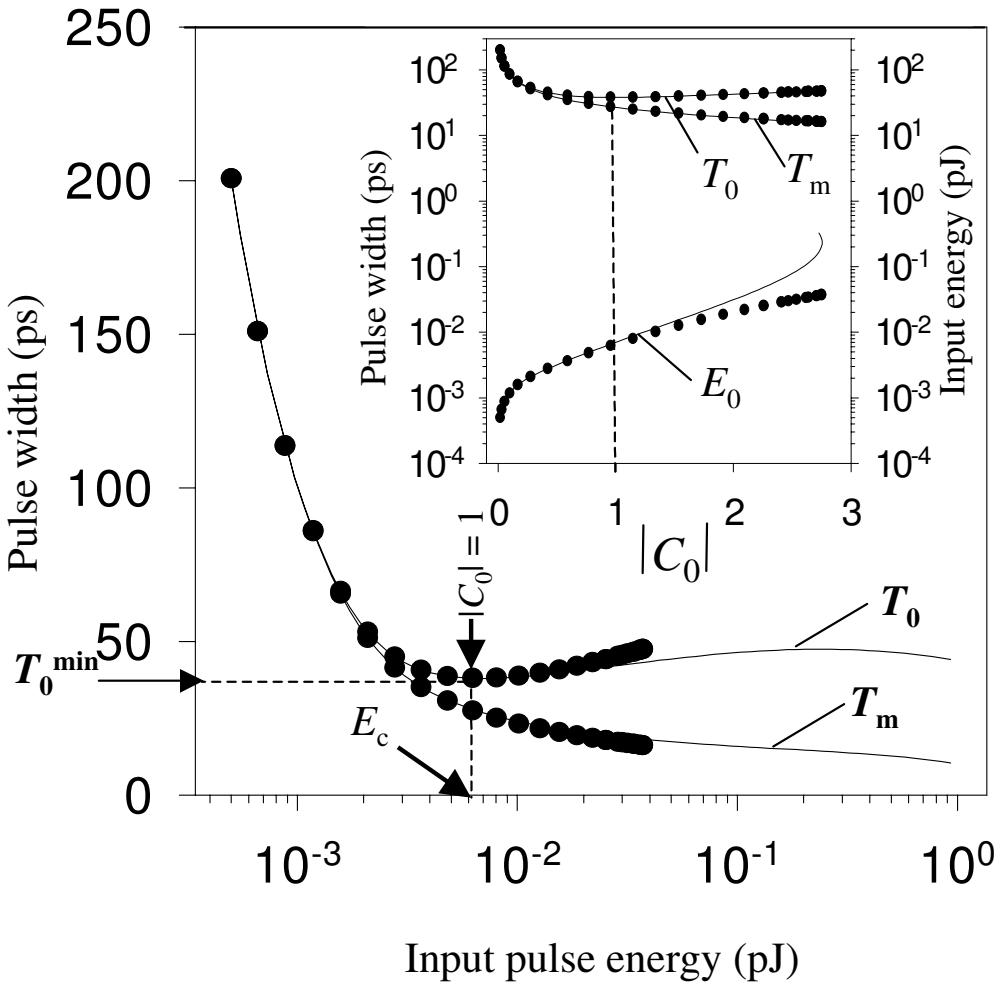

Figure 2.10: Comparison of numerical and analytical results for ordinary DM system with no loss and with $T_{map} = 26.9$ ps.

curves considered in Figs. 2.3 and 2.5. In all cases we see an excellent agreement for input and minimum pulse width results, for all values of input chirp, and we see a good agreement for the energy up to chirp values of about 1.5. The energy values obtained from Eqs. (2.67) or (2.70) differ by at most 5% from numerically obtained values in the region around $|C_0| = 1$, while the difference becomes about 10% for $|C_0| \approx 1.25$.

Note that Eqs. (2.67) and (2.70) are derived for a lossless system or for systems with distributed amplification. The effect of periodic gain/loss variation can be included by increasing E_0 by a factor of

$$\begin{aligned} k &= \left\{ (1/L_A) \int_0^{L_A} \exp\left[\int_0^z (g(z') - \alpha_s(z'))\, dz' \right] dz \right\}^{-1} \\ &= \begin{cases} 1, & \text{no loss} \\ \mathrm{GlnG}/(G-1)\,, & \text{lumped amplification} \\ \left\{ (1/L_A) \int_0^{L_A} \exp\left[\int_0^z (g(z') - \alpha_s(z'))\, dz' \right] dz \right\}^{-1}, & \text{Raman} \end{cases} \end{aligned} \tag{2.71}$$

where G represents the cumulative net gain from 0 to L_A and $g(z)$ is the local gain in the case of distributed amplification. This is the same factor as it is required for a classical soliton to maintain itself over long fiber length (satisfying $L \ll L_{NL}$) in the average sense in the presence of loss and lumped amplification [25]. This scaling is valid for values of S_m up to 4 for DM systems with short fiber sections. The comparison of the results for system with losses is shown in Fig. 2.11. The same dense DM system with $T_{map} = 3.16$ ps as in Fig. 2.9 is considered here, except that 0.25 - dB/km losses are included. Dashed lines and open circles show the results from Fig. 2.9 for the lossless case. We see again an excellent agreement for input and minimum pulse width for all values of input chirp, and a good agreement for energy for chirp values up to 1.5. We see also that the set of curves for system with losses is shifted from the lossless case to the larger values of energy in accordance with the scaling factor (2.71). We have verified that energy values obtained using Eq. (2.67) give a stable pulse propagation up to

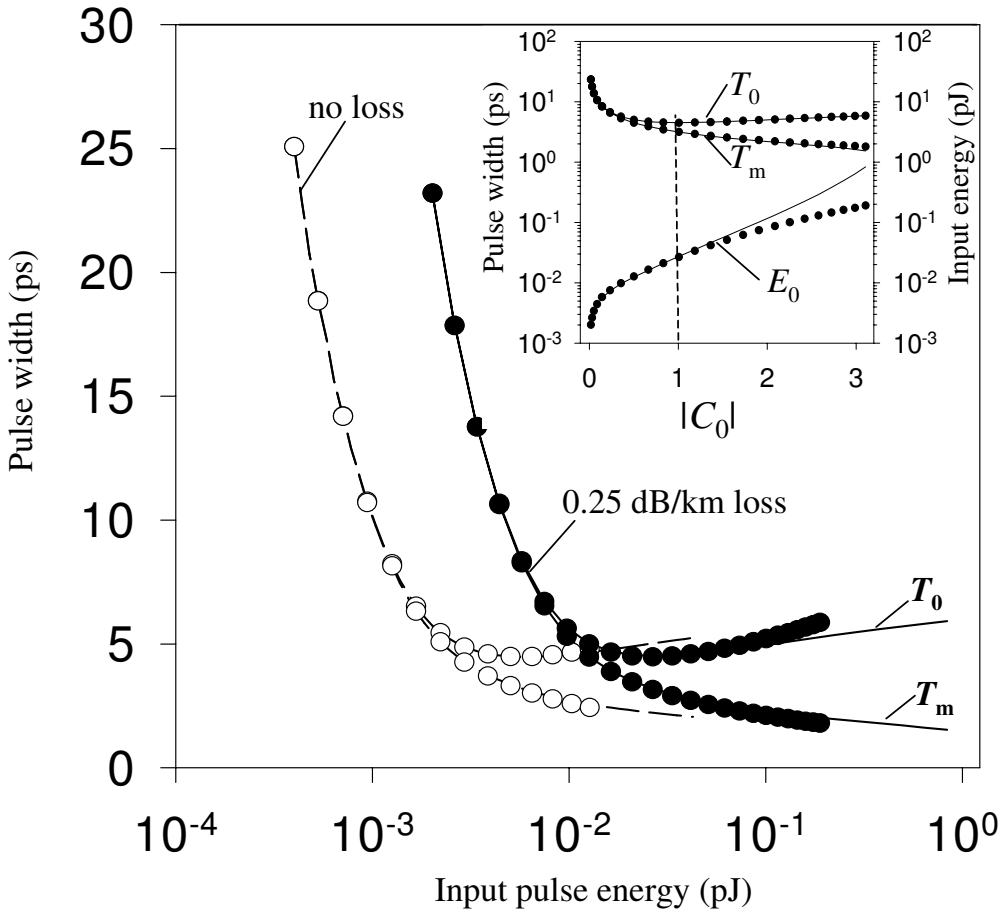

Figure 2.11: Comparison of numerical and analytical results for dense DM system with 0.25 dB/km loss in each fiber section ($T_{map} = 3.16$ ps.)

about 40,000 km. Although the error in E_0 leads to larger peak power oscillations during propagation, the amplitude of such oscillations does not exceed $\pm$ 5% of the average peak power.

Summarizing the results of Figs. 2.9 – 2.11, we can conclude that for ideal distributed amplification which is, basically, the lossless case, there is a good agreement of results for arbitrary DM system and for system with losses and lumped amplification, there is a good agreement in the case of dense dispersion

management. The reason that, in the case of lumped amplification, Eqs. (2.55), (2.56), and (2.67) work only for dense DM system comes from the fact that the assumption of chirp free point location to be in the center of fiber section, used in the derivation [see Eq. (2.41)], is strictly valid only for a lossless system, and is approximately valid in system with losses only in the case of short map periods, as it was mentioned in the beginning of section 2.6.

We can also see from Eqs. (2.67) and (2.70), that the input energy increases for larger value of the ratio β_2/γ_0, in accordance with Fig. 2.5 and with the results of [130], and in analogy with the classical soliton behavior.

2.8 Design Rules

2.8.1 Optimum chirp values

Eqs. (2.55) and (2.67) provide the values of input pulse width and energy as functions of input chirp. We now consider which range of input chirp values should be used to obtain the best pulse sequence propagation. From Figs. 2.3, 2.5, and 2.9-2.11 we note that just after T_0 takes its minimum value, T_m continues to decrease while T_0 is relatively constant. We expect the longest propagation distance, as well as a highest bit rate for a given distance, to occur in this region ($|C_0| \approx 1$, $E_0 \approx E_c$). For energies smaller than E_c, the bit rate is limited by the large values of T_0 and T_m and for energies much larger than E_c it would be

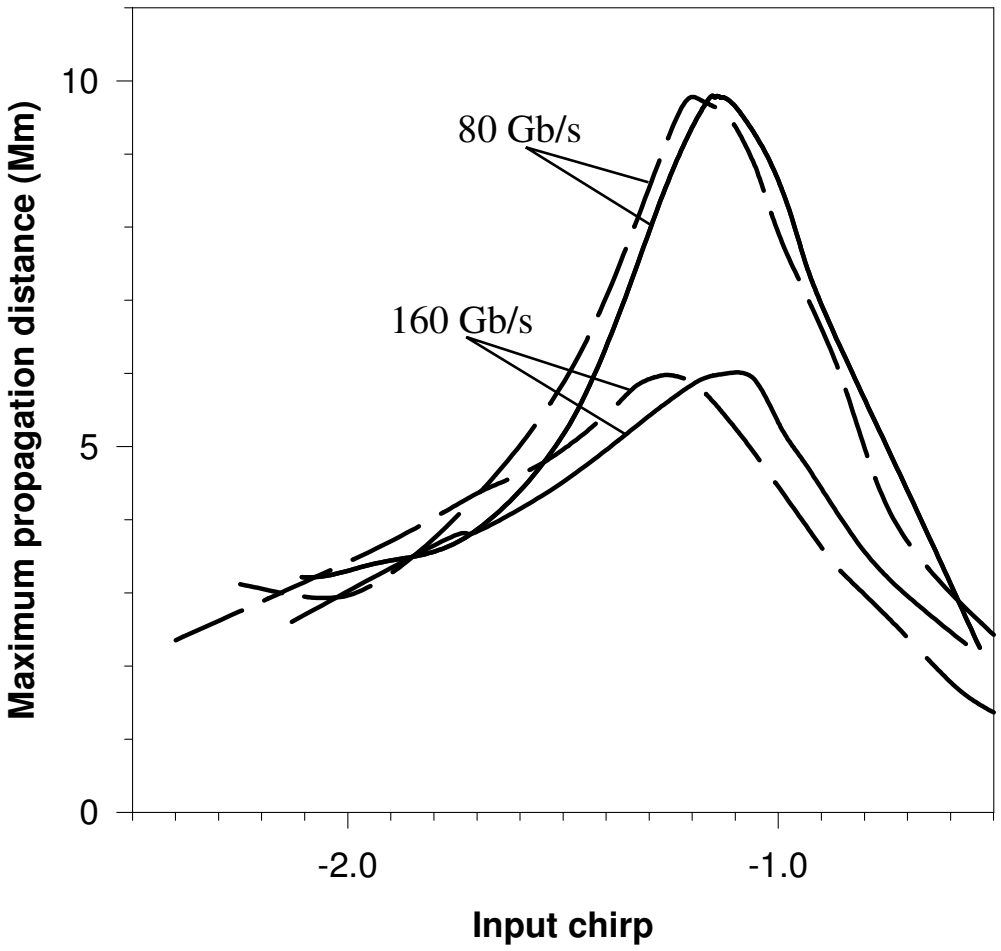

Figure 2.12: Maximum propagation distance as function of input chirp for systems operating at 80 and 160 Gb/s bit rates. Loss parameter $\alpha = 0$ for solid curves but $\alpha = 0.25$ dB/km for dashed curves.

limited by pulse interactions because of increased pulse stretching and higher pulse energies. This is confirmed in Fig. 2.12, where we show the maximum propagation length as a function of input chirp C_0 for pseudorandom bit sequence at 80 and 160 Gb/s. The figure represents the results of numerical simulations, not including noise in the system, so that propagation was limited only by pulse interactions. As the criterion for figure construction, the requirement was used that timing jitter

because of pulse interactions is less than 8% of the bit slot and an eye closing is not more than 5%. The map with $\beta_{21} = 4$ ps^2/km and $\beta_{22} = -4$ ps^2/km is used in this calculation by choosing $\bar{\beta}_2 = -0.01$ and -0.005 ps^2/km for 80 and 160 Gb/s systems, respectively. We also reduce the section length to $l_1 = 0.6$ km, for 160 Gb/s system, and use $l_1 = 3$ km for 80 Gb/s systems. The solid curves represent the results when losses are neglected and the dashed curves include 0.25 dB/km loss in each fiber section and assume 80 km amplifier spacing. Two points are noteworthy. First, maximum distance can exceed 6000 km even at a bit rate of 160-Gb/s when dense DM is used [132]. Second, in all cases the maximum occurs in the region $1.1 < |C_0| < 1.2$.

2.8.2 Limiting bit rate

Using this optimum region of chirp values, we can estimate, from Eq. (2.55) and (2.56), the maximum possible bit rate for a given map configuration. For example, consider a dispersion map made using 70 km of standard fiber ($\beta_{21} = -22$ ps^2/km) and 15.3 km of DCF ($\beta_{22} = 100$ ps^2/km). The average dispersion for this map is $\bar{\beta}_2 \approx -0.1$ ps^2/km, while $T_{map} = 27.7$ ps. From Eqs. (2.55) and (2.56), T_0 is about 39.3 ps and $T_m \approx 26.4$ ps for $|C_0| = 1.1$, the chirp value within the optimum range. Since the shortest pulse width that can propagate as a DM soliton is 26.4 ps, such a map configuration can never provide a bit rate of 40 Gb/s for which the bit slot is only 25 ps.

To increase the bit rate, according to Eqs (2.55) and (2.56), one needs to reduce the value of the map parameter T_{map}. From Eq. (2.39) this is possible by reducing either the dispersion or the length of fiber segments. Consider the design of a 160 Gb/s system. Since the bit slot is only 6.25 ps wide, the map parameter T_{map} should not exceed 1.06 ps to avoid soliton interaction. For $(\beta_{2i} - \bar{\beta}_2) = \pm 1$ ps^2/km ($i = 1$ and 2 in the first and second fiber sections, respectively), according to Eq. (2.39), we need to take $l_i \approx 2.24$ km. Moreover, the section lengths reduce to only $l_i \approx 0.6$ km if it is necessary to use larger local dispersion values of ± 4 ps^2/km to avoid four-wave mixing in WDM applications. This result explains why dense dispersion management is a necessity for designing systems at bit rates > 40 Gb/s [126]– [129].

2.8.3 Optimum map strength values

We now discuss the range of map strength [130] S_m corresponding to the values of input chirp $1.1 < |C_0| < 1.2$. The map strength parameter in our notation can be written as

$$S_m = \frac{\left|\left(\beta_{21} - \bar{\beta}_2\right) l_1 - \left(\beta_{22} - \bar{\beta}_2\right) l_2\right|}{\left(1.665 T_{map}\right)^2} |C_0| \,, \tag{2.72}$$

where the factor of 1.665 results from using the full width at half maximum. For small average dispersion values, $|\beta_{21} l_1| \approx |\beta_{22} l_2|$, and Eq. (2.72) can be approximated as $S_m \approx 1.443\,|C_0|$. As discussed above, pulse interactions are minimized for value of input chirp $|C_0|$ between 1.1 and 1.2. Using those values,

we find that using chirp values from the optimum region is equivalent to having a system with map strength of $1.59 < S_m < 1.73$. This explains the previously known empirical result that the least interactions occur for S_m values around 1.65 [125].

2.8.4 Optimum fiber section length

Eq. (2.55) together with the fact that optimum chirp values are around 1.1 also suggests that an optimum fiber section length exists. For a small average dispersion value, we can approximate Eq. (2.55) as $T_0^2 \approx |\beta_{21} l_1| (1 + C_0^2)/(2|C_0|)$. Using $C_0 \approx 1.1$ and $L_D \equiv T_0^2/|\beta_{21}|$, the configuration giving the map strength of about 1.65 corresponds to the map for which the length of each fiber segment is approximately equal to the local dispersion length L_D.

Although Eq. (2.55) and 2.56) appear similar to those obtained for a linear system, the presence of nonlinearity is critical for DM solitons. In fact, a periodic solution of Eqs. (2.34) and (2.35) does not exist in the linear case ($\gamma_0 = 0$) unless the average dispersion $\bar{\beta}_2$ is zero. We have verified through numerical simulations that Eq. (2.55) remains valid in the region $1 < |C_0| < 1.5$ with an accuracy better than 1% as long as the value of $\bar{\beta}_2 L_m$ does not exceed $\approx 12\%$ of $(\beta_{2i} - \bar{\beta}_2) l_i$ in the i^{th} section ($i = 1, 2$). This relation gives, for example, average dispersion as large as $\bar{\beta}_2 = -0.5$ ps^2/km for $(\beta_{2i} - \bar{\beta}_2) l_i = 20$ ps^2 and $\bar{\beta}_2 \approx -2$ ps^2/km for $(\beta_{2i} - \bar{\beta}_2) l_i = 1500$ ps^2.

2.9 Conclusions

In this chapter, using the approximate analytic solutions of the variational equations (2.35) and (2.34), we derived analytical expressions for input pulse parameters that ensure a periodical pulse propagation in a two-fiber-section dispersion map. The expressions are explicit and relatively simple. We compared the approximate values of the input chirp, width, and energy with numerical solutions of the variational equations and found a very good agreement with the numerical results. The derived analytical expressions also show several interesting facts about a DM soliton system design; these which can be summarized as follow.

- There exists a minimum input pulse width T_0^{min}, and this value limits the bit rate for a given map configuration.
- A new map parameter is introduced that allows the estimation of the limiting bit rate and explains the need of dense DM at high bit rates.
- The expressions provide simple suggestions on how to design a system so that intrachannel pulse interactions are minimized.
- The optimal input chirp value is around 1.1. This optimum explains the previously known empirical result that pulse interactions are minimized for the map strength of 1.65 [125].
- Expressions also show that this optimal design corresponds to the case when fiber section length is approximately equal to the local dispersion length.

Chapter 3

Impact of dispersion fluctuations

3.1 Introduction

In this chapter we present the results of extensive numerical simulations performed to identify the impact of dispersion fluctuations on the performance of 40-Gb/s dispersion-managed lightwave systems with several different modulation formats. The emphasis in this analysis is on identifying how the nonlinear effects degrade the system performance in the presence of dispersion fluctuations. The chapter is organized as follow. In Section 3.2 we discuss the numerical approach. Section 3.3 focuses on non-soliton systems based on the CRZ format and employing backward-pumped distributed Raman amplification. We start by considering a perfectly linear system and study how the presence of nonlinearity aggravates the extent of system degradation induced by dispersion fluctuations. We then discuss the ways to improve system tolerance to dispersion fluctuations. In Section 3.4, we consider DM soliton systems. We first address the questions of the

optimization of input parameters for a given dispersion map and then investigate the influence of dispersion fluctuations on the system performance. The main conclusions of the paper are summarized in Section 3.5.

3.2 Numerical approach

Accounting for the presence of noise and dispersion fluctuations, the NLS equation (2.22), describing propagation of pulses on optical fiber, can be modified as follow:

$$\frac{\partial A}{\partial z} = -i\frac{\tilde{\beta}_2}{2}\frac{\partial^2 A}{\partial t^2} + i\gamma_0 |A|^2 A + \frac{1}{2}(g-\alpha)A + f_n(z,t), \tag{3.1}$$

where $\tilde{\beta}_2(z)$ is a fluctuating second-order dispersion parameter and $f_n(z,t)$ represents the contribution of noise along the fiber length.

In this section, we assume that distributed Raman amplification is employed for the gain $g(z)$ in Eq. (3.1). This technique of amplification is used for simulations because it provides a better SNR compared with lumped EDFAs and is rapidly being adopted in practice.

We solve Eq. (3.1) numerically using the split-step Fourier method [25]. This method obtains an approximate solution of the NLS equation (3.1) by assuming that in propagating the optical field over a small distance h, the dispersive and nonlinear effects can be pretended to act independently. In short, propagation from z to $z+h$ is carried out in two steps. In the first step, fiber is assumed to be nondispersive, so that nonlinearity acts alone and a pulse just acquires a nonlinear

phase shift during propagation. In the second step, the system is assumed to be linear, so that the equation can be solved in the Fourier domain. Mathematically, Eq. (3.1) can be formally written in the form [25]

$$\frac{\partial A}{\partial z} = (\hat{D} + \hat{N})A, \tag{3.2}$$

where $\hat{D}$ is a differential operator that accounts for dispersion, absorption, and noise in a linear medium and $\hat{N}$ is a nonlinear operator that governs the effect of fiber nonlinearities on pulse propagation. Propagation from z to $z + h$ is then calculated as

$$A(z + h, T) \approx \exp(h\hat{D}) \exp(h\hat{N})A(z, T), \tag{3.3}$$

where the execution of the exponential operator $\exp(h\hat{D})$ is carried out in the Fourier domain by using the prescription

$$\exp(h\hat{D})B(z, T) = F^{-1} \exp[h\hat{D}(i\omega)]FB(z, T). \tag{3.4}$$

In the last equation, F denotes the Fourier-transform operation and $\hat{D}(i\omega)$ is obtained from $\hat{D}$ by replacing the differential operator $\frac{\partial}{\partial z}$ by $i\omega$, ω being the frequency in the Fourier domain. The discussion of the accuracy of this method and the ways to achieve the best accuracy can be found in [25].

We model dispersion fluctuations as

$$\tilde{\beta}_2 (z) = \beta_2 (z) + \delta\beta_2 (z), \tag{3.5}$$

where $\beta_2(z)$ is the average value of local dispersion and $\delta\beta_2(z)$ is a small random variable assumed to have a Gaussian distribution with zero mean. In numerical

simulations, $\delta\beta_2$ is changed every step (0.3 km) along the fiber length using a Gaussian random variable with zero mean and with standard deviation of up to $0.2\beta_2(z)$. We use 15 different realizations of this stochastic Gaussian process, representing 15 different fiber links.

To account for the ASE noise for each of the 15 links, the Q parameter (defined later) is evaluated by averaging over an ensemble of 1280 pulses, realized by repeated propagation of a 64-bit pseudorandom bit sequence with 20 different ASE noise realizations. As it was mentioned in chapter 1, there are two main sources of dispersion fluctuations. One of them is the variation of the material and waveguide portions of the refractive index along the fiber length. Such variation introduces static dispersion fluctuations. Another source comes from environmental changes and leads to varying in time, or dynamic, dispersion fluctuations. Since time-dependent dispersion fluctuations happen on quite a long time scale ($>$ 1 ms), there are no dynamic fluctuations during a single run for a bit stream of 128 bits or less. Assuming static and dynamic dispersion fluctuations to be independent events, the impact of both types of fluctuations can be treated by considering the results of propagation of the same bit stream over multiple fiber links with different realizations of dispersion fluctuations.

For numerical simulations, we use two dispersion maps. Each map consists of two fiber sections of nearly equal length (5 km) with opposite signs of the dispersion parameter (but the same absolute value). For map 1, $\beta_2 = \pm 4$ ps^2/km,

while for map 2 $\beta_2 = \pm 8$ ps^2/km. In both cases, the average dispersion $\bar{\beta}_2$ is -0.01 ps^2/km and $L_A = 8L_m = 80$ km, L_A and L_m being the amplification and the map periods, respectively. We adopt the dense DM technique ($L_m \ll L_A$) because, according to the results of Chapter 2, its use improves the performance of 40-Gb/s systems especially when DM solitons are used. Fiber losses are included using $\alpha_s = 0.2$ and $\alpha_p = 0.27$ dB/km in each fiber section, α_p being pump power losses at the pump wavelength. We employ the technique of Raman distributed amplification with backward pumping for compensating fiber losses. The gain profile $g(z)$ is obtained by solving the appropriate equations for the Raman amplification process [3]. In particular, in the case of distributed Raman amplification, gain $g(z)$ in Eq. (3.1) can be shown to be expressed as [25]

$$g(z) = g_s \left|A_p(z)\right|^2, \tag{3.6}$$

where g_s is related to the peak Raman gain g_R as $g_s = g_R/A_{eff}$. Raman gain g_R is, in turn, related to the cross section of spontaneous Raman scattering [121,120] and is a measurable quantity [25,136,137]. In the expression for $g(z)$, $\left|A_p(z)\right|^2$ is the pump power. In the case of continuous-wave backward pumping and with the undepleted pump approximation, pump power $I_p \equiv \left|A_p(z)\right|^2$ can be approximated as $I_p = I_{p0} \exp[-\alpha_p(L_A - z)]$, where $I_{p0} \equiv \left|A_p(L)\right|^2$ is the peak pump power at $z = L_A$ and pump power losses are assumed to be constant throughout the fiber link. We choose the input peak power I_{p0} at $z = L_A$ from the condition of complete loss compensation, such that $\int_0^{L_A} g(z)dz = \alpha_s L_A$. Using the expression (3.6) for

$g(z)$, we find $I_{p0} = \alpha_p \sum_{i=1}^{N} \alpha_{si} l_i \Big/ (g_s \left[1 - \exp^{-\alpha_p L_A}\right])$, where N is the number of fiber sections within the amplification period. At the input, we use 6-ps input pulses with the input chirp $C_0 = 0.3$. We also use optical filters with 400 GHz bandwidth separated by L_A.

The system performance is quantified by the well-known Q parameter that is related to the bit-error rate in a simple way [1]. We calculate the Q parameter in two ways. The first measure Q_1 uses the detector current filtered with a Butterworth filter of 35 GHz ($\Delta f = 0.875$ B) bandwidth at the receiver. More specifically, Q_1 is calculated using [1]

$$Q_1 = \frac{I_1 - I_0}{\sigma_1 + \sigma_0}, \tag{3.7}$$

where I_1 and I_0 are the average values for 1 and 0 bits at the center of the bit slot, and σ_1 and σ_0 are the corresponding standard deviations. In this approach, I_1 and I_0 correspond to the peak power of the optical pulse (assuming that the timing jitter introduced by Raman amplification is negligible).

In the second approach we calculate the optical Q parameter by using the pulse energy obtained by integrating over the entire bit slot and define Q as

$$Q_2 = \frac{E_1 - E_0}{\sigma_1 + \sigma_0}, \tag{3.8}$$

where E_1 and E_0 are the average energies for 1 and 0 bits and σ_1 and σ_0 are the corresponding standard deviations.

3.3 CRZ systems

We start by considering a perfectly linear 40-Gb/s system. For this case, nonlinearity is set to zero ($\gamma_0 = 0$) temporarily in Eq. (3.1). For the 15 fiber

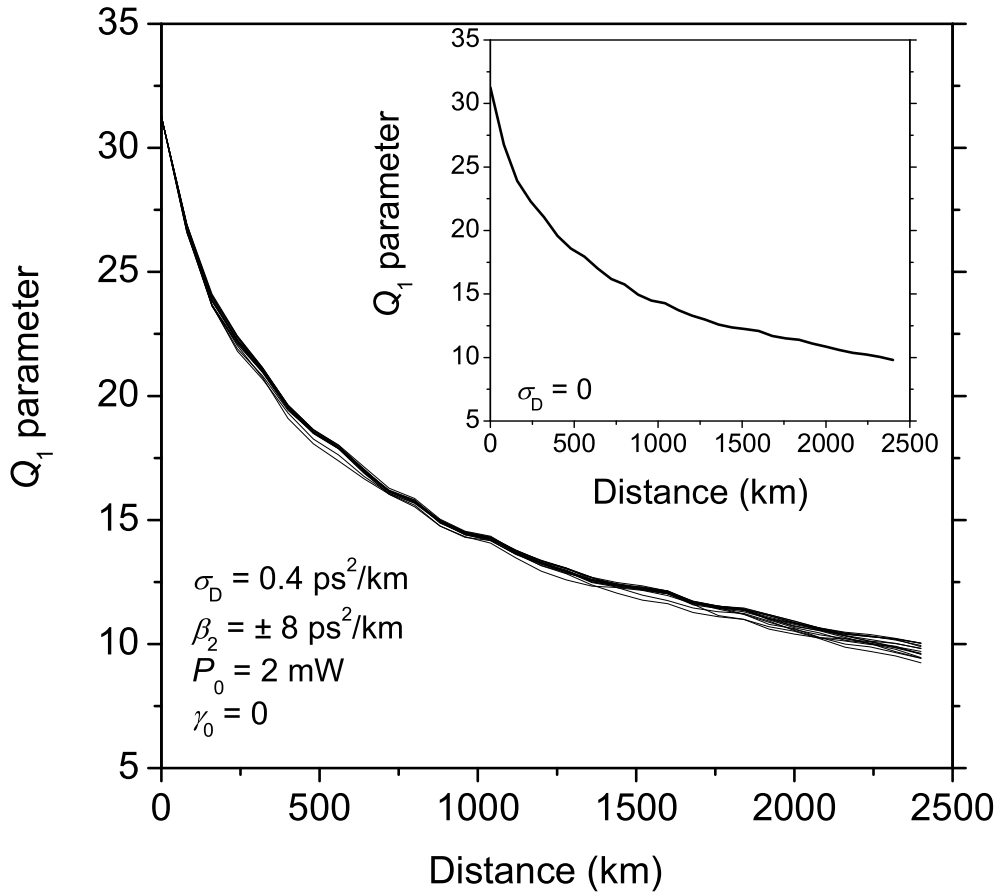

Figure 3.1: Influence of dispersion fluctuations in a linear 40-Gb/s CRZ DM system with $\beta_2 = \pm 8$ ps^2/km. The Q_1 parameter is shown as a function of distance for 15 fiber links with 5% dispersion fluctuations (standard deviation $\sigma_D = 0.4$ ps^2/km). The insert shows Q_1 in the absence of fluctuations.

links, we find the Q parameter (averaged over 1280 pulses for each fiber link) as a function of propagation distance for several values of the standard deviation of local dispersion. As an example, Figure 3.1 shows the Q_1 parameter for all 15 fiber links for the map with $\beta_2 = \pm 8$ ps^2/km with 5% of dispersion fluctuations, which

corresponds to the standard deviation σ_D of local dispersion of 0.4 ps^2/km for this map. The input peak power of each pulse is $P_0 = 2$ mW, which corresponds to an average power of 0.42 mW for the pseudorandom bit sequence. The insert shows the Q_1 parameter in the absence of fluctuations.

We see that, in the linear case, the Q parameter does not change much in the presence of fluctuations for all 15 fiber links used. The reason for small difference in Q along the distance for 15 fiber links comes from additional accumulated dispersion $d_r = \int_0^L \delta\beta_2\,(z)dz$ that varies randomly for different fibers. This additional contribution broadens the pulse even more during signal propagation [114,115]. The value and the sign of this additional broadening depend on d_r [115]. This random broadening leads to a change in the Q value. For the 15 fiber links used, d_r at 2400 km ranged from -12.6 ps^2 to 22.8 ps^2 when 5% of dispersion fluctuations were introduced, while the deterministic value of accumulated dispersion at this distance is -24 ps^2.

We consider now the worst-case Q-parameter at 2400 km. Figure 3.2 shows the dependence of the worst-case Q for the two maps on the standard deviation of dispersion fluctuations. The levels of fluctuations used correspond to the standard deviation σ_D ranging from 0 to 20% of the local dispersion value. For each value of standard deviation, the same 15 sequences of random numbers, scaled accordingly, were used, and the fiber link with the worst value of Q at 2400 km was then considered.

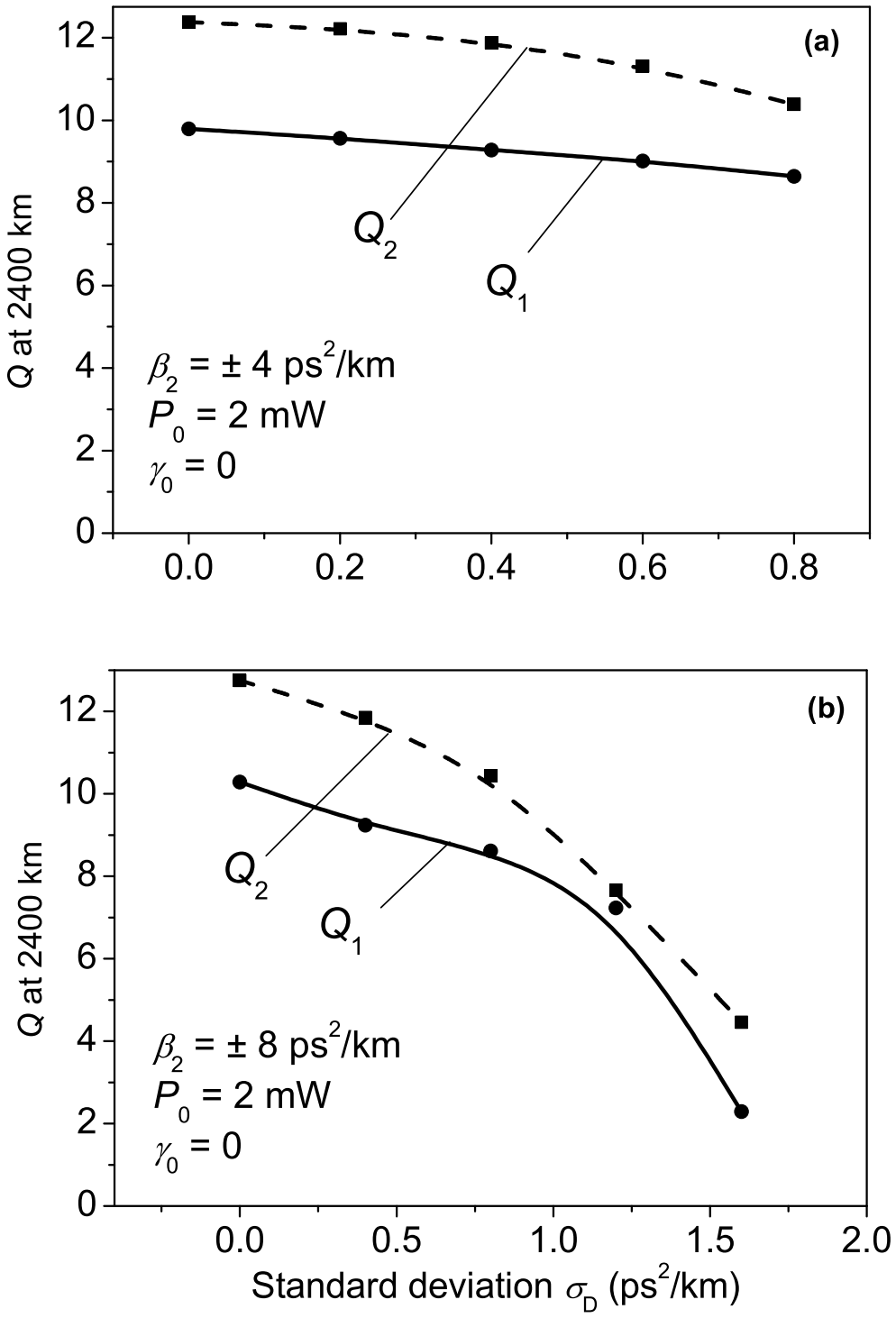

Figure 3.2: The worst-case Q parameter at 2400 km for two linear 40-Gb/s CRZ DM systems. Dispersion map is such that (a) $\beta_2 = \pm 4$ ps^2/km and (b) $\beta_2 = \pm 8$ ps^2/km. Solid and dashed lines show Q_1 and Q_2 calculated using peak powers and pulse energies, respectively.

As seen in Fig. 3.2, the Q parameter decreases in all cases even in a purely linear system as the standard deviation of dispersion fluctuations increases. Although this decrease is relatively slow, eventually Q becomes small enough that the system will be limited by dispersion fluctuations. The decrease of Q parameter with increased β_2 fluctuations even for a linear system is due to the larger values of d_r for larger amounts of fluctuations. The results indicate that, for a given fiber link, Q can be improved by post-compensating or periodically compensating the accumulated random dispersion.

We note from Fig. 3.2 that Q_1 is up to 1.1 dB larger than Q_2. The reason is related to the fact that Q_1 samples the pulse power at the bit center while Q_2 measures the pulse energy spread over the entire bit. As a result, Q_1 parameter is much more sensitive to timing jitter than Q_2. This result suggests that the use of a receiver that integrates the signal over the bit slot rather than makes a measurement at one point would improve the system performance. Since most receivers currently sample the signal at the bit center, we use the Q_1 parameter for system characterization in this thesis.

The results shown in Fig. 3.2 were obtained by turning off the nonlinear term in Eq. (3.1) by setting $\gamma_0 = 0$. However, the nonlinearity is inherent in any real system. In the presence of nonlinearity, the pulse propagation is affected by the interplay between the local dispersion and nonlinearity (rather than been dependent only on the total accumulated dispersion). We consider next how the

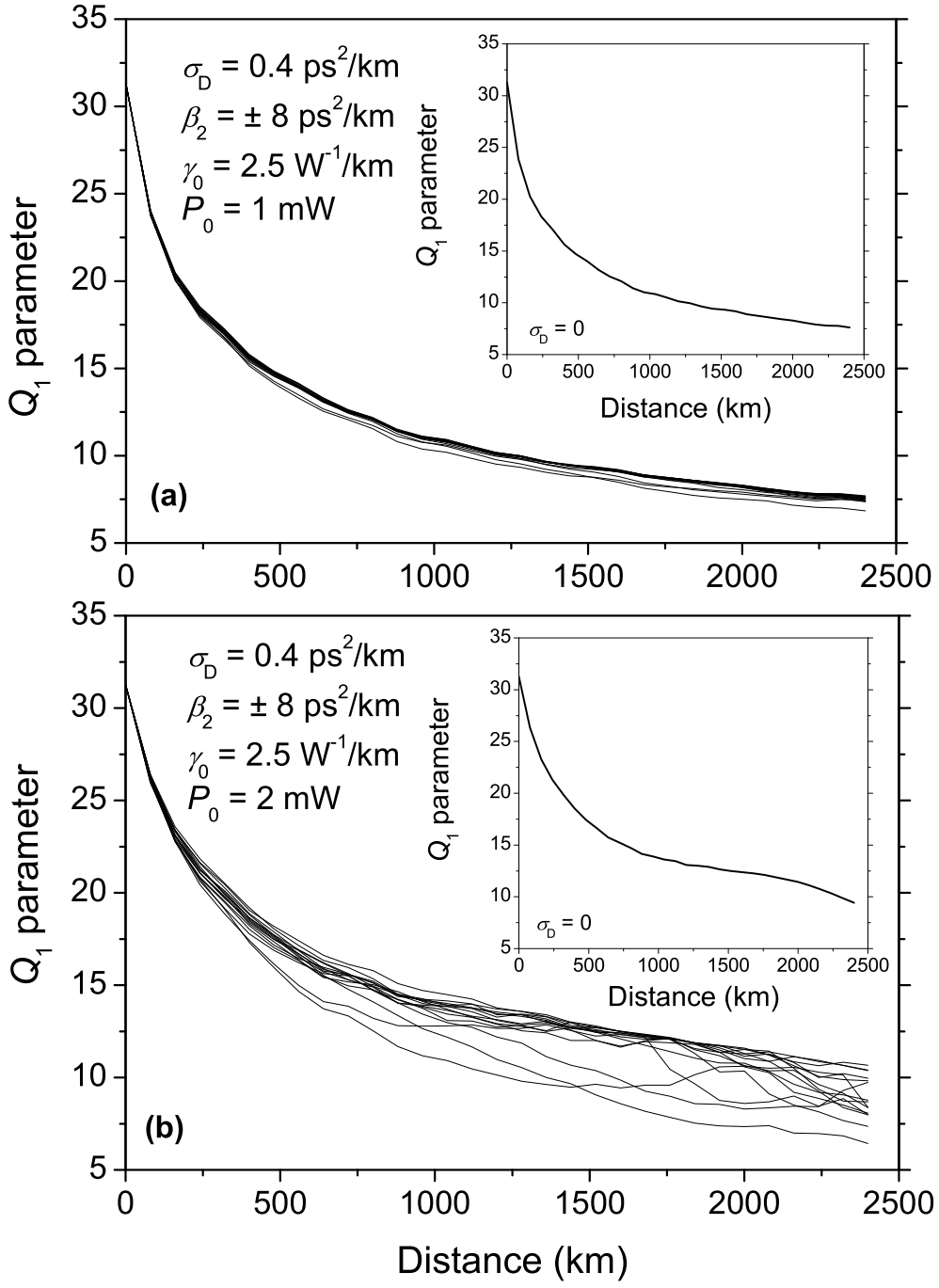

Figure 3.3: Influence of dispersion fluctuations in the presence of nonlinearity for the same 40-Gb/s CRZ system shown in Fig. 3.1. The inserts show Q_1 in the absence of fluctuations. The input peak powers are (a) 1 mW and (b) 2 mW.

impact of dispersion fluctuations is changed when the nonlinear effects are taken into account by choosing $\gamma_0 = 2.5$ W^{-1}/km in all fiber sections.

Figure 3.3 shows the Q_1 parameter as a function of distance for the 15 fiber links for the DM system with $\beta_2 = \pm 8$ ps^2/km using $P_0 = 1$ and 2 mW. For both peak power levels the standard deviation of local dispersion is 5% (0.4 ps^2/km). The inserts show Q_1 in the absence of fluctuations. We see that, as nonlinear effects become stronger, the impact of dispersion fluctuations on system performance becomes much more noticeable. While the decrease in Q_1 at 2400 km is at most 0.46 dB for 1 mW peak power, it becomes 1.8 dB at 2 mW.

For any peak power, larger fluctuations lead to more degradation. As an example, the worst-case Q_1 parameter at a peak power of 1.5 mW is shown on Fig. 3.4 for several levels of σ_D. We see that fluctuations with $\sigma_D = 1.6$ ps^2/km can lead to about 6.5 dB degradation of the Q parameter. We note also that, for all fiber links considered, the worst case Q at 2400 km for CRZ systems is usually obtained in the fiber which has the largest random accumulated dispersion d_r at 2400 km.

The results of Figs. 3.3 and 3.4 are summarized in Fig. 3.5 which shows the worst-case Q_1 at 2400 km for several values of input peak power as a function of σ_D. Comparing to Fig.3.2, we see that in all cases the Q parameter degrades much faster with increasing dispersion fluctuations than in a linear system. The rate of

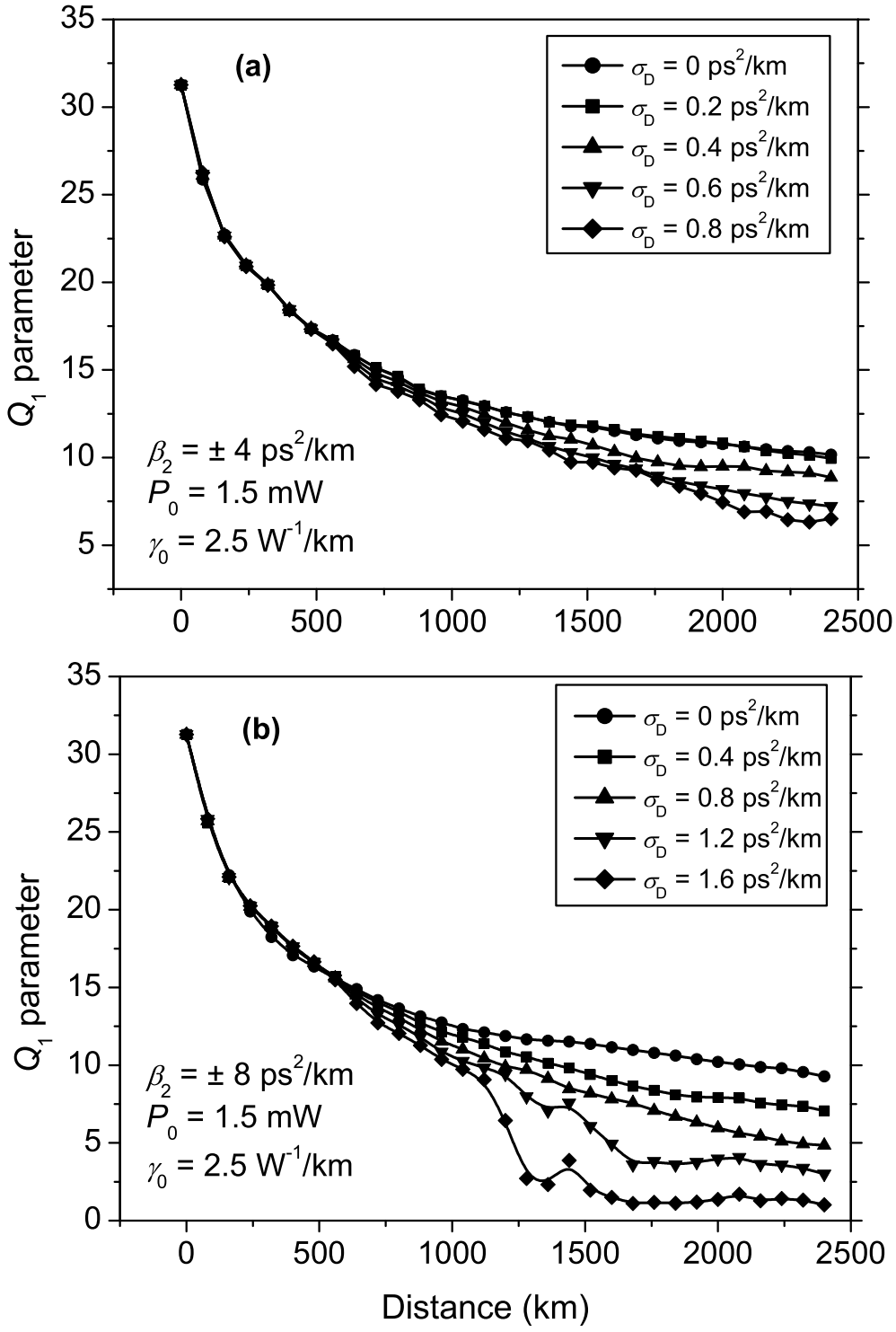

Figure 3.4: Dependence of the worst-case Q_1 parameter on transmission distance for several values of σ_D. Dispersion maps are such that (a) $\beta_2 = \pm 4$ ps^2/km and (b) $\beta_2 = \pm 8$ ps^2/km.

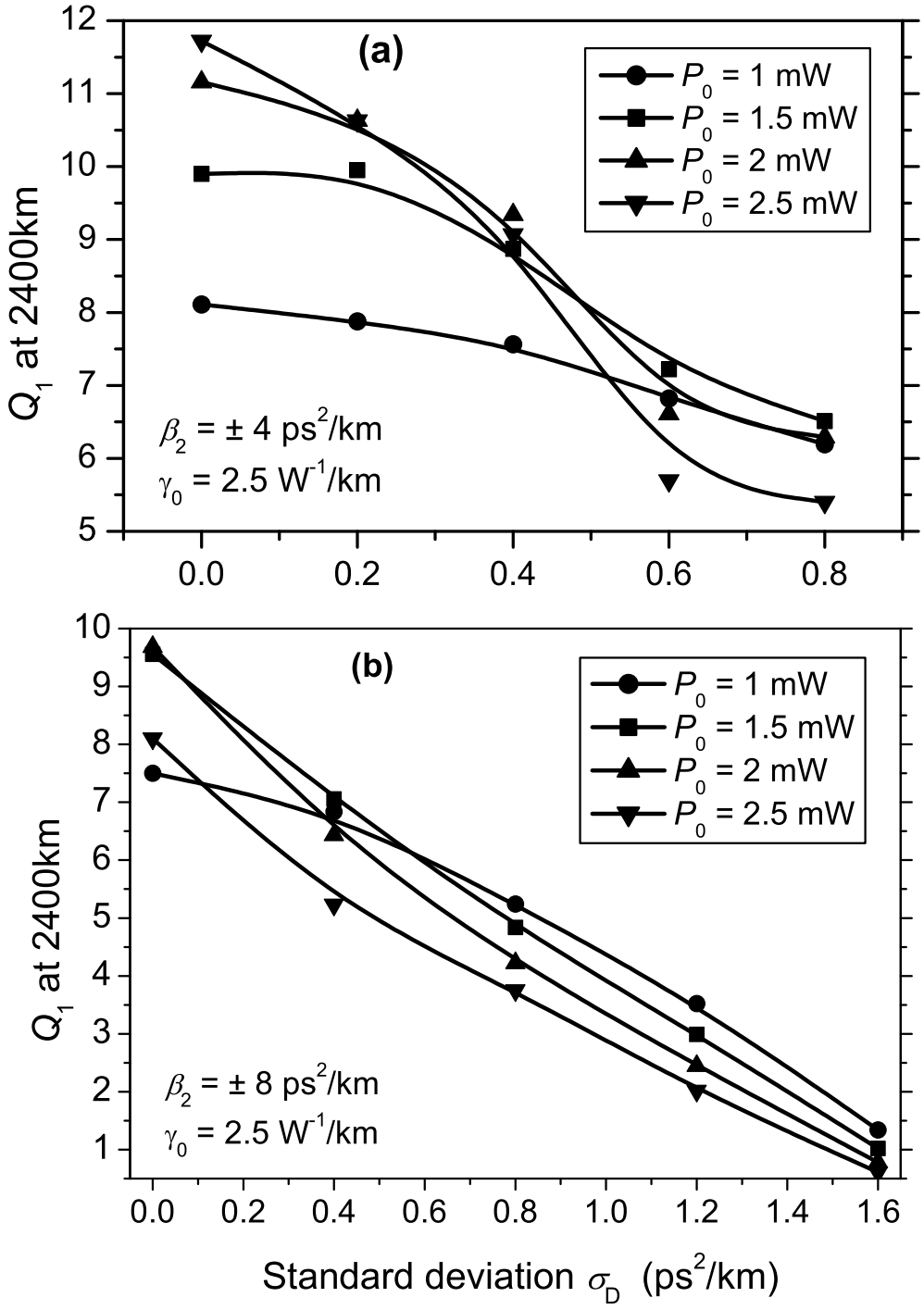

Figure 3.5: Effect of dispersion fluctuations on Q_1 at several peak power levels for the same two systems shown in Fig. 3.2 except that the nonlinear effects are turned on by setting $\gamma_0 = 2.5$ W^{-1}/km.

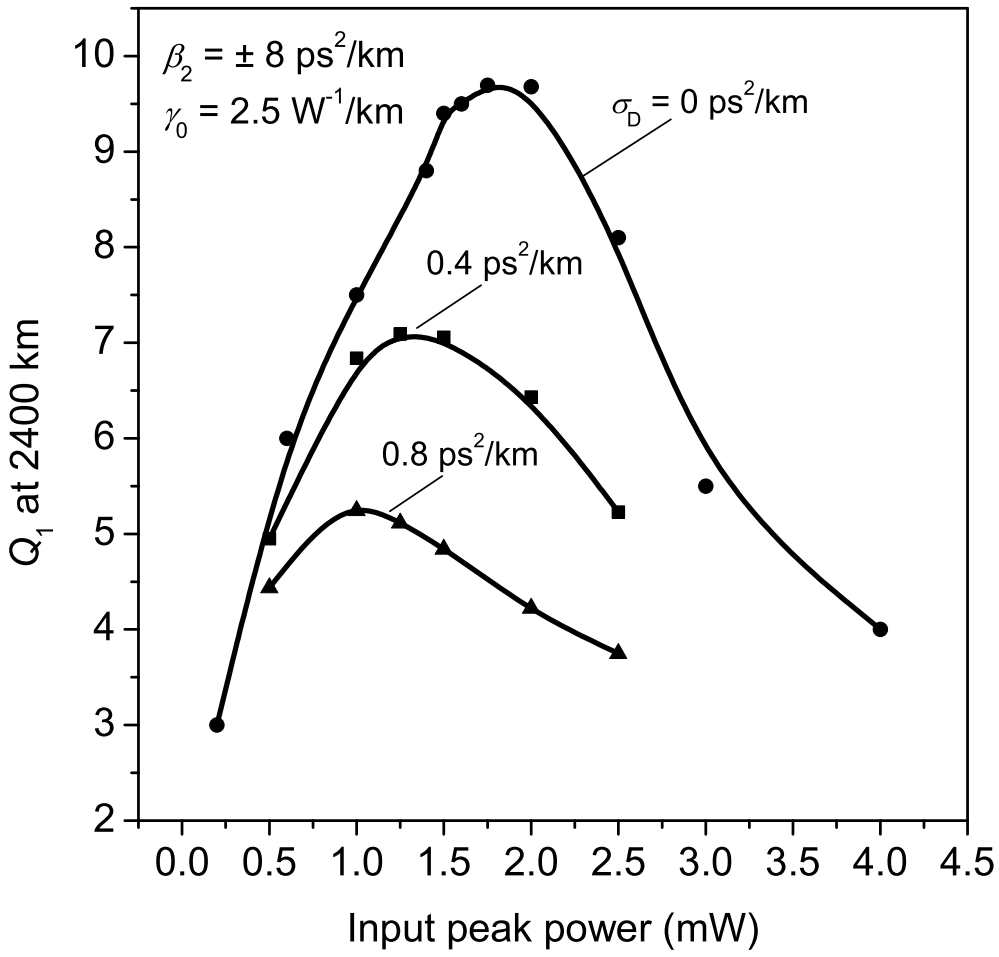

Figure 3.6: Dependence of the worst-case Q_1 parameter on the input peak power for the same 40-Gb/s system shown in Fig. 3.5(b) for several levels of dispersion fluctuations.

degradation increases when the nonlinear effects are intensified using larger input powers.

For any CRZ system, an optimum input power exists that provides the best system performance for a certain propagation distance [138]. For input powers smaller than the optimum, the CRZ system becomes limited by noise added by amplifiers, while for larger input powers it is limited by the increased nonlinear

effects. An example of such a behavior at a distance of 2400 km for the 40 Gb/s system designed with $\beta_2 = \pm 8$ ps^2/km, is shown on Fig. 3.6, where we plot Q_1 as a function of input power. The optimum peak power in the absence of dispersion fluctuations is about 2 mW. Even 5% dispersion fluctuations (standard deviation 0.4 ps^2/km) reduce the optimum peak power to near 1.3 mW while lowering the value of Q by about 26%. Larger values of fluctuations make the situation worse. To increase the system tolerance to dispersion fluctuations it may be better, according to figs. 3.5 and 3.6, to use input peak powers slightly less than the optimum value predicted in the absence of fluctuations.

3.4 DM soliton systems

A natural question is how the impact of dispersion fluctuations on system performance is affected when DM solitons are used as bits. In this section we answer this question. Since DM soliton systems require a balance between the dispersive and nonlinear effects, the presence of dispersion fluctuations might break this balance and degrade the system performance even more. We study how much the rate of degradation increases when the input power and, hence, the nonlinear effects in DM soliton system become larger.

The new feature of DM solitons is that the system is designed such that the pulse in each bit slot recovers its width, chirp, and energy after each amplification period. Thus, all pulse parameters vary periodically during the propagation with

a period equal to L_A. As discussed in Chapter II, the periodicity can be ensured only if the input pulse parameters have specific values for a given dispersion map. As shown in the previous chapter, the input width of a chirped pulse T_0 and the input energy E_0 can be found as functions of input chirp using Eqs. (2.55) and (2.67). The input parameters for chirp values ranging from 0.03 to 3 is shown in Fig. 3.7 for the same two maps used in CRZ case.

As it is shown in Chapter 2, in the absence of noise but accounting for intrachannel pulse interactions, the best pulse propagation occurs near this region $|C_0| \approx 1$, $E_0 \approx E_c$, E_c being the value of input energy corresponding to $|C_0| = 1$. In this section we consider several input parameters sets, with the energies ranging from E_c to $\approx \ 5E_c$, where the nonlinear effects become quite strong. The sets of input parameters used are shown with arrows in Fig. 3.7. For comparison purposes, we employ same two dispersion maps used earlier for CRZ systems. We note from Eq.(2.39) that reducing the length of fiber segments decreases the T_{map} parameter, which helps to increase the possible bit rate of a DM soliton system. For that reason, dense dispersion management is used in this chapter. The map parameter is $T_{map} = 3.17$ ps and $T_{map} = 4.47$ ps for systems with $\beta_2 = \pm 4$ and $\pm$ 8 ps^2/km, respectively.

We consider the same 15 fiber links with random dispersion fluctuations as in the CRZ case. Figure 3.8 shows the Q_1 parameter as a function of distance for the map $\beta_2 = \pm 8$ ps^2/km for input parameters sets corresponding to $C_0 = -1.2$

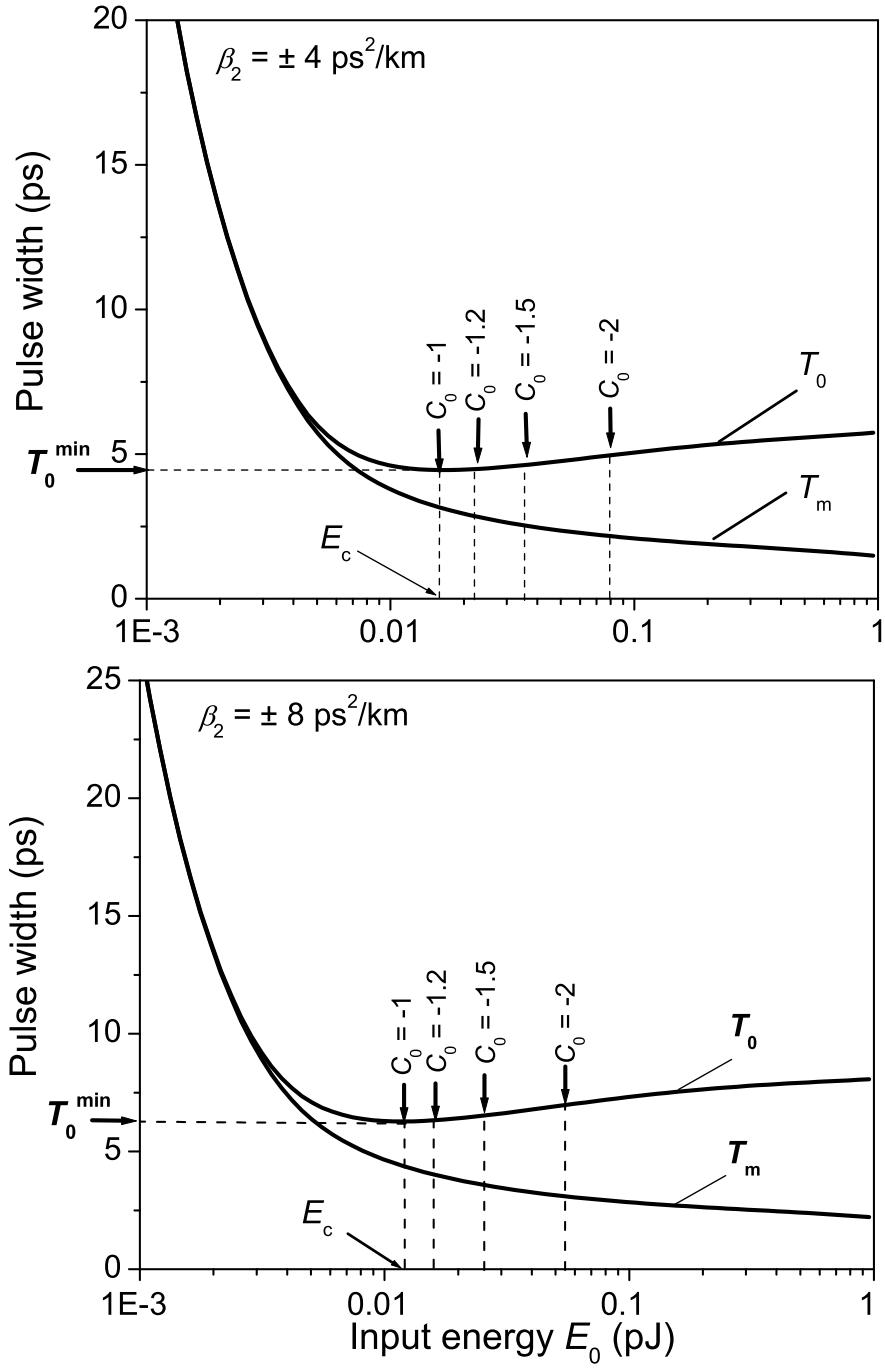

Figure 3.7: Input pulse width T_0 and corresponding minimum pulse width T_m at the chirp-free point for a DM soliton system plotted as functions of the input pulse energy. The arrows indicate the input pulse parameters used in Figs. 3.8 and 3.9 simulations.

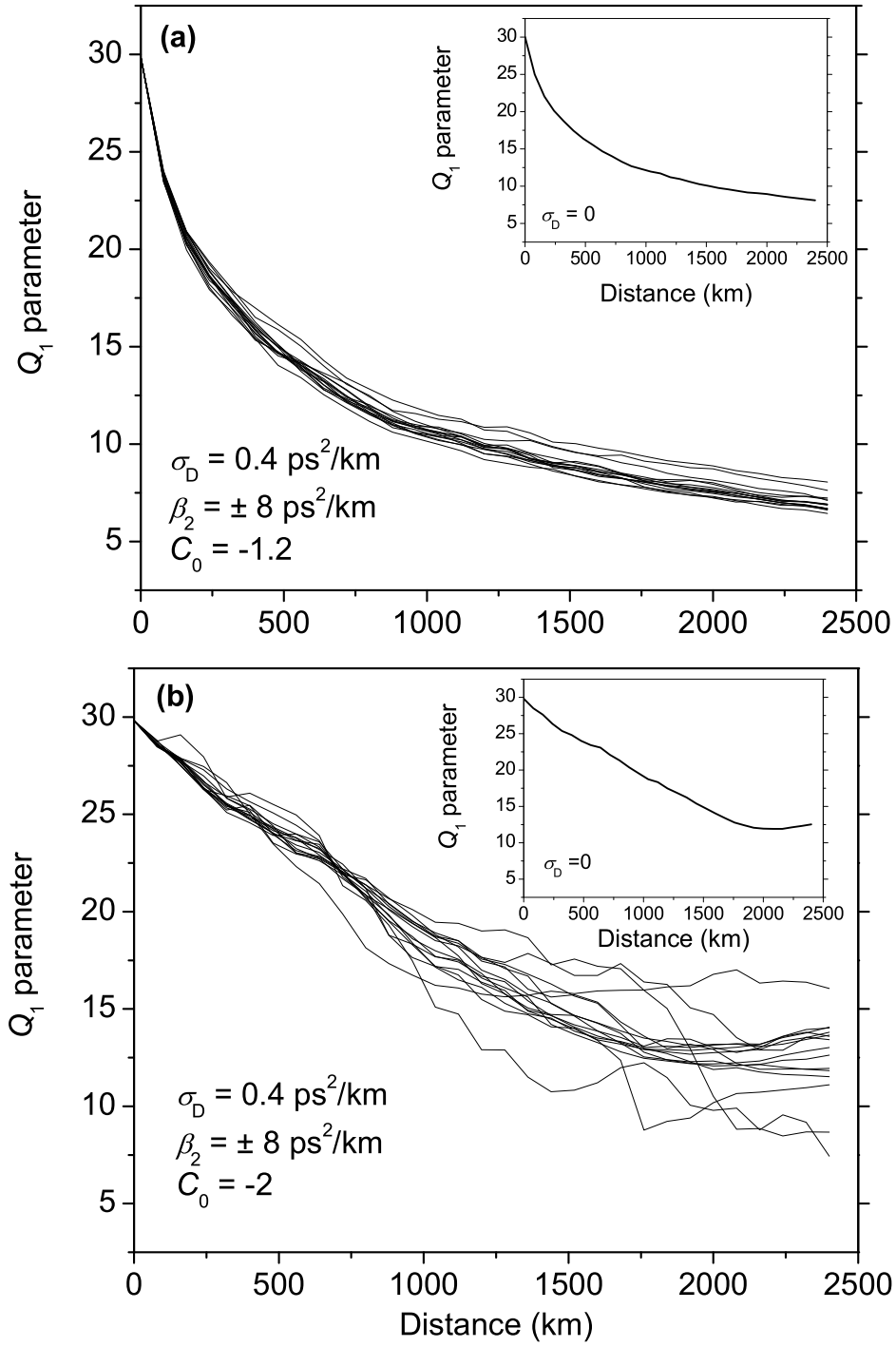

Figure 3.8: Effect of dispersion fluctuations on Q_1 parameter for a DM soliton system for the same map used in Fig. 3.3. The input parameters are obtained from Fig. 3.7 for (a) $C_0 = -1.2$ and (b) $C_0 = -2.0$

and -2. The level of fluctuations is 5% ($\sigma_D = 0.4$ ps^2/km) for both sets of input parameters. The inserts show Q_1 in the absence of fluctuations.

Since the input energy is increased for $C_0 = -2$, the nonlinear effects are much stronger in this case and the Q parameter is affected much more by dispersion fluctuations than in system with $C_0 = -1.2$. We have chosen to label the graphs with the input chirp C_0 because, as described before, the optimization of this parameter will apply to almost any dispersion map while the optimum value of pulse energy is map dependent.

The dependence of the worst case Q_1 parameter on the standard deviation of β_2 at a distance of 2400 km is shown on Fig. 3.9 for several input parameters sets. The σ_D values are in the range from 0 to 20% of the local dispersion for each map. Similarly to the CRZ case, the use of higher energy pulses (and higher average power at the input end) decreases the system tolerance to dispersion fluctuations. This behavior is the same for both maps. In the absence of both noise and dispersion fluctuations ($\langle \delta\beta_2^2 \rangle = 0$) the optimum value of the Q parameter is obtained for input chirp values near 1.1, as discussed in Chapter 2. According to Fig. 3.9, in the presence of noise but without dispersion fluctuations, Q increases for larger values of C_0 because the use of higher-energy pulses improves the SNR while the nonlinear effects are balanced by the use of DM solitons. However, dispersion fluctuations change this behavior because they perturb the balance between the dispersive and nonlinear effects. For example, in the presence of

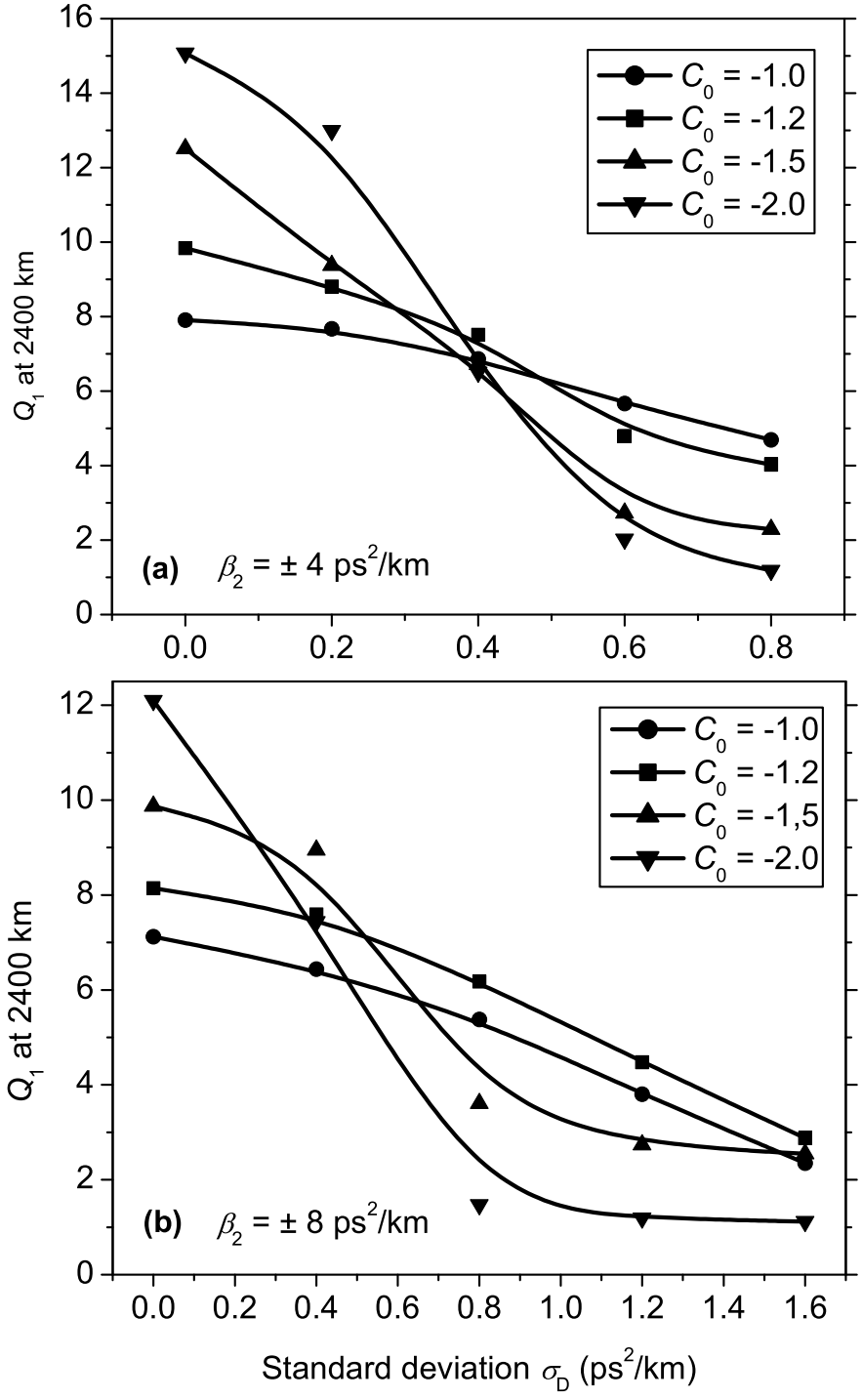

Figure 3.9: Effect of dispersion fluctuations on Q_1 parameter in DM soliton systems for the same two dispersion maps used in Fig. 3.5.

10% dispersion fluctuations, it is better to reduce the pulse energy by lowering the chirp in the neighborhood of $C_0 = 1.2$. We conclude that while accounting for both noise and dispersion fluctuations, the optimum input parameters should remain in the region around $C_0 \approx 1.2$. Comparing DM solitons with the CRZ case, we note that Q_1 decreases with increasing β_2 fluctuations in nearly the same manner, suggesting that the impact of dispersion fluctuations does not depend on the use of solitons as long as the RZ format is employed.

3.5 Conclusions

In this chapter we investigated numerically the influence of second-order dispersion fluctuations on the performance of 40 Gb/s systems designed with distributed Raman amplification. We have considered both the CRZ and DM soliton formats and used the Q parameter for judging the system performance.

We have shown that dispersion fluctuations can lead to performance degradation even in a linear system when the change in the total accumulated dispersion, introduced by fluctuations, is not completely compensated. The presence of nonlinearity aggravates the extent of system degradation induced by dispersion fluctuations for both CRZ and DM soliton systems. We show that this degradation increases fast when the nonlinear effects in the system are made stronger by using higher-energy pulses. The system tolerance to dispersion fluctuations can be improved by employing a receiver that integrates the signal over some portion

of the bit slot, rather than making a measurement at the center of the bit slot. We discuss the impact of dispersion fluctuations on the optimum input parameters and show that, for CRZ systems, one should use the input peak powers slightly smaller than the optimum values predicted in the absence of fluctuations.

For DM soliton systems, accounting for both noise and the presence of dispersion fluctuations, the optimum input pulse width and pulse energy should be calculated from Eqs. (2.55) and (2.67) by choosing $|C_0| \approx 1.2$. For such values of C_0 , the map strength is about 1.65, and the effects of intrapulse interaction are also minimized, as it is discussed in Section 2.8. Although we have focused here on a single-channel system, the preceding discussion should apply even for WDM systems.

In our simulations, dispersion values were changed after every step, in effect making the correlation length of dispersion fluctuations equal to the step size (0.3 km). The correlation length l_c in actual fibers may vary over a considerable range and is not often known precisely. Our results can be used for other values of l_c by noting that the product $\sigma_D^2 l_c$ determines the extent of pulse broadening for long link lengths [115], where σ_D^2 is the variance of dispersion fluctuations. Thus, one should scale σ_D with l_c such that $\sigma_D^2 l_c$ remains constant.

Finally, we note that the fluctuations of the second-order dispersion β_2 result from the static or dynamic fluctuations in the frequency-dependent refractive index. This implies that fluctuations are present in all orders of dispersion. When

the refractive index fluctuations are dynamic, including the first-order dispersion fluctuations results in the presence of one more fluctuating term in the nonlinear Schrdinger equation that depends on fluctuations in the group velocity and can lead to a new source of timing jitter. However, if dynamic fluctuations happen on a sufficiently long time scale, the effect of fluctuations in the group velocity may be compensated electronically.

Chapter 4

Timing jitter

4.1 Introduction

In this chapter, we use the approach developed in Ref [108] to compare the ASE-induced timing jitter in DM systems for the cases of lumped, distributed, and hybrid Raman amplification. In Section 4.2 we extend the theory of [108] to the case of distributed amplification. In Section 4.3 we derive an analytic expression for the timing jitter at any position within the fiber link in the case of ideal distributed amplification for which losses are compensated by gain perfectly at every point. We also derive an analytical expression for the timing jitter induced by lumped amplifiers and compare the two cases. In Section 4.4 we investigate timing jitter in DM systems for the case of erbium-based distributed amplification, realized when the transmission fiber itself is lightly doped with erbium ions. We show that timing jitter can be reduced by about 40% with proper system design and is quite close to the ideal case. In Section 4.5 we consider timing jitter in DM

soliton systems making use of Raman amplification. We show that considerable timing reduction occurs when bidirectional, backward, or even partial Raman amplification is employed. We also investigate timing jitter dependence on other system parameters such as the bit rate and the map strength.

4.2 General formalism

We give in this section a short description of the moment method for calculating timing jitter [108] and extend the method for the case of distributed amplification. Optical pulse propagation in any lightwave system, accounting for the presence of noise and neglecting for now dispersion fluctuations, is governed by the NLS equation, similar to the one used in Chapter 3 [25]

$$\frac{\partial A}{\partial z} = -i\frac{\beta_2}{2}\frac{\partial^2 A}{\partial t^2} + i\gamma_0 \left|A^2\right| A + \frac{1}{2}(g-\alpha)A + f_n(z,t), \tag{4.1}$$

where β_2 is now a fixed quantity within each fiber section and $f_n(z,t)$ represents the contribution of noise (distributed or lumped) along the fiber length. The ASE noise contribution vanishes on average, i.e. $\langle f_n(z,t)\rangle = 0$, but has a correlation function of the form [3,106]

$$\langle f_n(z,t) f_n^*(z',t')\rangle = g(z) n_{sp}(z) h\nu_0 \delta(z-z')\delta(t-t'), \tag{4.2}$$

where $n_{sp}(z)$ is the spontaneous emission factor, $h\nu_0$ is the photon energy at the central frequency ν_0, and δ represents Dirac's delta function. Both $n_{sp}(z)$ and

$g(z)$ are nonzero only within the amplifier in the case of lumped amplification, but vary with z continuously in the case of distributed amplification

As in Chapter 2, with a change of variables $A \equiv V\sqrt{G}$, where G represents the cumulative net gain from 0 to z and is given by Eq. (2.23), Eq. (4.1) can be rewritten as

$$\frac{\partial V}{\partial z} = -i\frac{\beta_2}{2}\frac{\partial^2 V}{\partial t^2} + i\gamma_0 \left|V^2\right| V + f_n(z,t)\Big/\sqrt{G}, \tag{4.3}$$

In the moment method [122], the central position t_p and the central frequency Ω of an optical pulse are defined as

$$t_p(z) = \frac{1}{E_0}\int_{-\infty}^{\infty} t\left|V^2\right| dt, \tag{4.4}$$

$$\Omega(z) = \frac{1}{2iE_0}\int_{-\infty}^{\infty} (V_t^* V - V_t V^*) dt, \tag{4.5}$$

where V_t stands for the time derivative of V and

$$E_0 \equiv \int_{-\infty}^{\infty} \left|V^2(z,t)\right| dt \tag{4.6}$$

is the input energy of the pulse.

In order to calculate the timing jitter, it is necessary to know how t_p and Ω evolve with z. Following [108], Eqs. (4.4) and (4.5) for t_p and Ω are differentiated with respect to z and Eq. (4.3) is used to eliminate $V(z)$. We then obtain the following two differential equations:

$$\frac{dt_p}{dz} = \beta_2\Omega + \frac{i}{E_0\sqrt{G}}\int_{-\infty}^{\infty} (t - t_p)\left[f_n^* V - f_n V^*\right] dt, \tag{4.7}$$

$$\frac{d\Omega}{dz} = \frac{i\Omega}{E_0\sqrt{G}}\int_{-\infty}^{\infty} (f_n V^* - f_n^* V) dt - \frac{1}{E_0\sqrt{G}}\int_{-\infty}^{\infty} (f_n V_t^* - f_n^* V_t) dt. \tag{4.8}$$

Introducing a new variable $q \equiv V \exp i\Omega(t - t_p)$, which has a meaning of eliminating a shift from the carrier frequency, equations (4.7) and (4.8) can be rewritten as

$$\frac{dt_p}{dz} = \beta_2\Omega + \frac{i}{E_0\sqrt{G}} \int_{-\infty}^{\infty} (t - t_p) \left[q f_n^* e^{-i\Omega(t-t_p)} - q^* f_n e^{i\Omega(t-t_p)} \right] dt, \quad (4.9)$$

$$\frac{d\Omega}{dz} = \frac{1}{E_0\sqrt{G}} \int_{-\infty}^{\infty} \left(q_t^* f_n e^{i\Omega(t-t_p)} - q_t f_n^* e^{-i\Omega(t-t_p)} \right) dt. \quad (4.10)$$

One can integrate the Eqs. (4.9) and (4.10) and introduce the random time shift $\delta t_p \equiv t_p - \langle t_p \rangle$, which is found to vary with z as

$$\delta t_p(z) = F(z) + S(z), \quad (4.11)$$

where F and S represent the contributions to δt_p from frequency and position fluctuations, occurring because of ASE noise along the fiber link. Their explicit expressions are

$$F(z) \equiv \int_0^z \beta_2(z')\, \delta\Omega(z')\, dz', \quad (4.12)$$

$$S(z) = i \int_0^z \left\{ \frac{1}{E_0\sqrt{G}} \int_{-\infty}^{\infty} (t - t_p) \left[q f_n^* e^{-i\Omega(t-t_p)} - q^* f_n e^{i\Omega(t-t_p)} \right] dt \right\} dz', \quad (4.13)$$

where $\delta\Omega$ is defined as

$$\delta\Omega(z) \equiv \int_0^z \left\{ \frac{1}{E_0\sqrt{G}} \int_{-\infty}^{\infty} \left[q_t^* f_n e^{-i\Omega(t-t_p)} + q_t f_n^* e^{i\Omega(t-t_p)} \right] dt \right\} dz' \quad (4.14)$$

As discussed in Ref. [108], Eqs. (4.12) and (4.13) are linearized with respect to the noise term f_n, meaning that q and G in those equations correspond to the deterministic solution of Eq. (4.3), obtained after setting $f_n = 0$. Following Ref. [108],

linearized equations (4.11)–(4.14) are used to calculate the timing jitter σ defined as $\sigma^2 = \langle \delta t_p^2 \rangle$ and given by

$$\sigma^2 = \langle F^2 \rangle + 2\langle FS \rangle + \langle S^2 \rangle. \tag{4.15}$$

Since all quantities, except for f_n, are deterministic after linearization of Eqs. (4.12)–(4.14), the correlation $\langle F^2 \rangle$ can be expressed in terms of the correlation of $\delta\Omega$, as it is seen from Eq. (4.12). The correlation $\delta\Omega$, in turn, can be found using noise correlation function (4.2). Similarly, equation (4.2) is used to obtain the expressions for $\langle FS \rangle$ and $\langle S^2 \rangle$ terms. The complete derivation of the $\langle F^2 \rangle$, $\langle FS \rangle$, and $\langle S^2 \rangle$ terms is provided in Appendix C and results in the following expressions, which are valid for arbitrary pulse shape:

$$\left\langle F^2 \right\rangle = \frac{4h\nu_0}{E_0^2} \int_0^z \beta_2(z_1)dz_1 \int_0^{z_1} \beta_2(z_2)dz_2 \int_0^{z_2} g(z')n_{sp}(z')G^{-1}(z') \int_{-\infty}^{\infty} |q_t|^2 \, dtdz', \tag{4.16}$$

$$\langle FS \rangle = \frac{ih\nu_0}{E_0^2} \int_0^z \beta_2(z_1)dz_1 \int_0^{z_1} g(z')n_{sp}(z')G^{-1}(z') \int_{-\infty}^{\infty} (t - t_p) \left[q_t q^* - q_t^* q \right] dz', \tag{4.17}$$

$$\left\langle S^2 \right\rangle = \frac{2h\nu_0}{E_0^2} \int_0^z g(z')n_{sp}(z')G^{-1}(z') \int_{-\infty}^{\infty} (t - t_p)^2 |q|^2 \, dtdz'. \tag{4.18}$$

We apply those expressions to a chirped Gaussian pulse of the form:

$$V(z,t) = V_0 \exp\left(-\frac{(1+iC)(t-t_p)^2}{2T^2} - i\Omega(t-t_p) + i\phi \right), \tag{4.19}$$

or, according to the definition of q,

$$q(z,t) = q_0 \exp\left(-\frac{(1+iC)(t-t_p)^2}{2T^2} + i\phi \right), \tag{4.20}$$

where C is chirp, T is the pulse width at 1/e point, $q_0 = V_0$ is the peak amplitude of the pulse, and φ is the phase, all those variables been functions of z. Using Eq. (4.20) in Eqs. (4.16)–(4.18), we obtain the following expressions:

$$\left\langle F^2 \right\rangle = \frac{2h\nu_0}{E_0} \int_0^z \beta_2(z_1)dz_1 \int_0^{z_1} \beta_2(z_2)dz_2 \int_0^{z_2} g(z')n_{sp}(z')\frac{1+C^2(z')}{G(z')T^2(z')}dz', \quad (4.21)$$

$$\langle FS \rangle = \frac{h\nu_0}{E_0} \int_0^z \beta_2(z_1)dz_1 \int_0^{z_1} g(z')n_{sp}(z')G^{-1}(z')\,C(z')dz', \quad (4.22)$$

$$\left\langle S^2 \right\rangle = \frac{h\nu_0}{E_0} \int_0^z g(z')n_{sp}(z')G^{-1}(z')\,T^2(z')dz'. \quad (4.23)$$

Equations (4.15) and (4.21)–(4.23) provide semi-analytical expressions for the timing jitter. They can be used for any amplification scheme, whether lumped, distributed, or hybrid. The only assumption made is that we use a chirped Gaussian shape for pulses propagating inside a DM system. Analysis based on the variational and Hermite-Gauss-expansion methods have shown [123,124] that numerically calculated pulse shapes are close to Gaussian (except in the pulse wings). In the next section, we justify this approximation by comparing timing jitter calculated using the actual pulse shape (taken from a NLS-based propagation code) and the pulse shape given by Eq. (4.19).

4.3 Analytical treatment

In this section we use Eqs. (4.21)–(4.23) to calculate variances and cross-correlation of F and S for a DM soliton communication system and calculate timing jitter for lumped and distributed amplification scheme. We focus on the

case of ideal distributed amplification first. We consider a DM system in which each map period L_m consists of two fiber sections with dispersion parameters β_{21} and β_{22}, respectively, and the local gain $g(z) \equiv \alpha$ at every point, so that $G(z) = 1$ in (4.21)–(4.23). We assume for simplicity that both fiber sections have the same value of losses α. The results can be generalized later to the case of an arbitrary loss profile. The variables $G(z)$, $g(z)$, and $n_{sp}(z)$ are now constants in Eqs. (4.21)–(4.23). Using the variational equation for the pulse width (2.34) in Eq. (4.22), we can express the variance of S in terms of cross-correlation of F and S as

$$\langle S^2 \rangle = 2\langle FS \rangle + Q_d T_0^2 z / L_m, \tag{4.24}$$

where

$$Q_d \equiv h\nu_0 n_{sp} g L_m / E_0 \tag{4.25}$$

is a dimensionless parameter.

To calculate the variance of F and cross-correlation of F and S, we need to calculate in Eqs. (4.21)–(4.23) the integrals like

$$I_1(z) \equiv \int_0^z \frac{1 + C^2(z)}{T^2(z)} dz, \tag{4.26}$$

$$I_2(z) \equiv \int_0^z C(z)\, dz. \tag{4.27}$$

Performing the first integral numerically, we find that I_1 grows with z almost linearly (with an accuracy of about 0.01%) as $I_1(z) \approx (1 + C_0^2)/T_0^2$, where C_0 and T_0 are the input values of chirp and pulse width, respectively. This result has a physical basis since the ratio represents spectral width of a chirped pulse. The

spectral width remains constant for a linear system and does not change much if the nonlinear length of the system is much larger than the local dispersion length. Even numerical solutions of the nonlinear variational equations show that the ratio oscillates around its input value within each map period with a negligible amplitude. To estimate the integral in Eq. (4.27), we approximate $C(z)$ by a linear function of z in each fiber section as in Eq. (2.41), making use of the fact that, for ideal loss compensation ($g = a$), chirp-free point is located in the middle of each fiber section [131].

Using Eq. (4.24) in Eq. (4.21), we perform the remaining two integrations for calculating $\langle F^2 \rangle$ using a geometrical approach. In short, noting that $\beta_2(z_2)I_1(z_2)$ is a piecewise continuous function, we carry out the integration over z_2. We then repeat the same process for integrating over z_1 and completing the integration in Eqs. (4.22) and (4.23). Using the notation $z = mL_m + x$, where m is the number of complete map periods up to the distance z and x is a fractional distance in the next map period ($0 \leq x \leq Lm$), the final result for timing jitter is given as:

$$\begin{aligned}\sigma_d^2(m,x) &= Q_d \frac{1+C_0^2}{T_0^2}\Big[b_0^2 m(m-1)(2m-1)\big/6 + b_0 b_1 m(m-1)/2 + \Delta_0 m/3 \\ &\quad + b(x)\, b_0 m(m-1) + b^2(x)\, m + b(x)\, b_1 m + \Delta(x)/3\Big] \\ &\quad + Q_d 4C_0\left[\varepsilon_0 m + \varepsilon(x)\right] + Q_d T_0^2\left[m + x/L_m\right], \end{aligned} \tag{4.28}$$

where $b(x)$ is the dispersion accumulated over a distance x:

$$b(x) \equiv \int_0^x \beta_2(x')\, dx', \tag{4.29}$$

so that $b_0 \equiv b(L_m) = \beta_{21} l_1 + \beta_{22} l_2 = \bar{\beta}_2 L_m$, $\bar{\beta}_2$ being the average dispersion of the map. Further, $b_1 \equiv b_0 + (\beta_{22} - \bar{\beta}_2) l_2$, and the functions $\Delta(x)$ and $\varepsilon(x)$ are defined as

$$\Delta(x) \equiv \begin{cases} x b^2(x)/L_m, & \text{if } 0 \le x \le l_1, \\ \left[l_1 b(x) \left[b(x) + \beta_{22}(x - l_1) \right] + \beta_{22}^2 (x - l_1)^2 x \right] \Big/ L_m, & \text{if } l_1 \le x \le L_m, \end{cases} \tag{4.30}$$

where $\Delta_0 \equiv \Delta(L_m)$, $\varepsilon_0 \equiv \varepsilon(L_m)$ in Eq. (4.28).

Before discussing this analytic result, we derive a similar formula for the lumped amplification case, for which both $n_{sp}(z)$ and $g(z)$ are nonzero only within each amplifier whose length is quite short ($\sim$ 10 m). Using $G_l = \exp(\alpha L_A)$ for the amplifier gain, where L_A is the amplifier spacing, the integrals in Eqs. (4.21)–(4.23) can be performed analytically as

$$\frac{h\nu_0}{E_0} \int_0^{z_2} g(z_2') n_{sp}(z_2') \frac{1 + C(z_2')^2}{G(z_2') T(z_2')^2} dz_2' = Q_l \frac{1 + C_0^2}{T_0^2} N_l(z_2), \tag{4.31}$$

$$\frac{h\nu_0}{E_0} \int_0^{z_1} g(z_1') n_{sp}(z_1') G^{-1}(z_1) C(z_1) dz_1' = Q_l C_0 N_l(z_1), \tag{4.32}$$

$$\frac{h\nu_0}{E_0} \int_0^{z} g(z') n_{sp}(z') G^{-1}(z') T_0^2(z') dz' = Q_l T_0^2 N_l(z), \tag{4.33}$$

where $N_l(z_i)$ is a staircase function representing the number of amplifiers up to the coordinate z_i, and

$$Q_l \equiv h\nu_0 n_{sp} (G_l - 1)/E_0. \tag{4.34}$$

Using expressions (4.31)–(4.33) we complete the integrations in Eqs. (4.21)–(4.23), employing the same geometrical approach described earlier. The final result for

the variance of timing jitter at a distance $z = nL_A + x$ in system for an arbitrary dispersion map within each amplification period is given as

$$\begin{aligned}\sigma_l^2(n,x) &= Q_l \frac{1+C_0^2}{T_0^2}\left[b_0^2 n(n-1)(2n-1)/6 + b(x)\, b_0 n(n-1) + b^2(x)\, n\right] \\ &\quad + Q_l C_0\left[b_0 n(n-1) + 2b(x)\, n\right] + Q_l T_0^2 n, \end{aligned} \tag{4.35}$$

where n is the number of amplifiers up to the distance z and x is the fractional distance in the next amplification period ($0 \le x \le L_A$). We keep different notations for amplification period L_A and map period L_m since Eq. (4.35) applies to the case of dense DM in which each amplification period contains several map periods.

From Eqs. (4.28) and (4.35) we note that the largest contribution to timing jitter comes from the first term resulting from frequency fluctuations and increasing with distance as z^3. If we use Eq. (4.14), the variance of frequency fluctuations $\langle \delta\Omega^2 \rangle$, accumulated within one map period (or amplification period in the case of lumped amplifiers) is given by:

$$\left\langle \delta\Omega^2 \right\rangle_{d,l} = Q_{d,l} \frac{1+C_0^2}{T_0^2}, \tag{4.36}$$

where the subscripts "d" and "l" stand for distributed and lumped amplification, respectively. In (4.28) and (4.35), the term in the first square brackets represents the variance $\langle F^2 \rangle$. For constant-dispersion fibers ($\beta_{21} = \beta_{22} \equiv \beta_2$) and for lumped amplification, $\langle F^2 \rangle$ term with $x = 0$ converts to the standard Gordon-Haus formula [105,107] $\langle F^2 \rangle = \langle \delta\Omega^2 \rangle_l \beta_2^2 L_A^2 \sum_{i=1}^{n} (n-i)^2$. We have also verified that, for

constant dispersion, $\langle \delta\Omega^2 \rangle_l$ reduces to the equivalent expression in Refs. [105,107] when a hyperbolic secant pulse shape is used instead of a Gaussian shape in Eq. (4.1).

We now focus on the effect of distributed amplification on timing jitter. Consider first the timing jitter at the end of a map period by setting $x = 0$. Several differences are apparent from Eqs.(4.28) and (4.35). In the case of lumped amplification, the $\langle F^2 \rangle$ term depends only on the average dispersion irrespective of the actual map configuration, while this is not the case for ideal distributed amplification. The $\langle F^S \rangle$ term grows as z^2 for lumped amplification, but only linearly with z in Eq. (4.28), indicating that cross-correlation is less important in the case of distributed amplification. For lumped amplification, the variance $\langle S^2 \rangle$, representing direct temporal shift of a soliton by ASE, does not depend on dispersion, but this is not so for distributed amplification, as seen from Eq. (4.24). This is the consequence of the fact that such position fluctuations happen only when noise is added. For lumped amplification, noise is not added outside amplifiers, while noise is added all along the fiber length in the case of distributed amplification.

Consider now the timing jitter inside a map period so that $x \neq 0$. As seen from Eqs. (4.28) and (4.35), the x-dependent terms provide additional contribution to timing jitter within each map period, which depends on the accumulated dispersion $b(x)$ over the fractional distance x within each map period L_m (or the amplification period L_A). Since $b(x)$ is periodic, we expect timing jitter to exhibit

oscillatory behavior. As seen from Eqs. (4.28) and (4.35), the amplitude of such oscillations grows as z^2 with distance, while the first term in Eq. (4.28) and in Eq. (4.35) grows as z^3. This means that jitter never oscillates down to zero as z increases and the relative contribution of the oscillating terms to the total timing jitter decreases as $1/z$. For long distances such that $L \gg L_m$, taking the limit $m \gg 1$ and $n \gg 1$ in x-dependent terms in Eqs. (4.28) and (4.35), we note that this additional contribution is positive or negative depending on the sign of the product $b(x)b_0$. For example, for the system with even number of fiber sections within the map period, this contribution is negative if the sign of β_{21} is opposite to the sign of average dispersion $\bar{\beta}_2$.

An important question is how much timing jitter can be reduced by using distributed amplification. To answer this question, we consider a long-haul lightwave system such that the number of map periods L_m (or amplifies in the case of lumped amplification) is very large. Taking the limit $m \gg 1$ and $n \gg 1$ in Eqs. (4.28) and (4.35), the timing jitter is reduced for distributed amplification by the factor

$$f_r \equiv \frac{\sigma_d^2}{\sigma_l^2} \approx \frac{\langle \delta\Omega^2 \rangle_d}{\langle \delta\Omega^2 \rangle_l} = \frac{\alpha L_A}{(G_l - 1)} \frac{n_{sp}^d}{n_{sp}^l} \frac{E_0^l}{E_0^d} \frac{[(1 + C_0^2)/T_0^2]_d}{[(1 + C_0^2)/T_0^2]_l}. \tag{4.37}$$

In the most cases of practical interest $[(1 + C_0^2)/T_0^2]_l \gg [(1 + C_0^2)/T_0^2]_d$ when the system is designed to have the same value of the minimum pulse width. The energy ratio $E_0^l/E_0^d > 1$ under such conditions, increasing f_r. However, this increase, being of the order of $G_l \ln G_l/(G_l - 1)$, does not overcome the reduction

in timing jitter due to the ratio $\alpha L_A/(G_l - 1)$. The net result is that timing jitter can be reduced by using distributed amplification. Physically, the possibility of timing jitter reduction with distributed amplification comes from the fact of the smaller power spectral density of noise in the case of distributed amplification.

Figure 4.1 shows timing jitter for lumped and distributed amplification schemes calculated at the end of each amplifier (each map period in the distributed case) using Eqs. (4.28) and (4.35) based on the Gaussian shape ansatz (solid curves). To estimate the error introduced by this ansatz, circles show the results when the exact pulse shape obtained by solving the NLS equation is used in Eqs. (4.16)–(4.18). In the lumped case, we consider a dense DM system with an amplifier spacing of 80 km and assume 8 map periods within one amplifier period. Each map period has 5 km of fiber with $\beta_{21} = 3.9$ ps^2/km and 5 km of fiber with $\beta_{22} = -4.1$ ps^2/km, resulting in the average dispersion of -0.1 ps^2/km. Losses in each fiber section are 0.2 dB/km, and the value of nonlinearity is $\gamma_0 = 2.5$ W^{-1}km^{-1}. The input pulse parameters (width T, chirp C, and energy E_0) are obtained by solving the variational equations (2.35) and (2.34) numerically. The minimum value T_{min} of pulse width is kept fixed at 3.11 ps [FWHM 5.18 ps] in all cases to ensure a 40 Gb/s bit rate. For lumped amplification, the input parameters are $T_0 = 4.94$ ps, $C = -1.2$, $E_0 = 0.22$ pJ, while for ideal distributed amplification $T_0 = 4.47$ ps, $C = -1.0$, and $E_0 = 0.0597$ pJ. The map

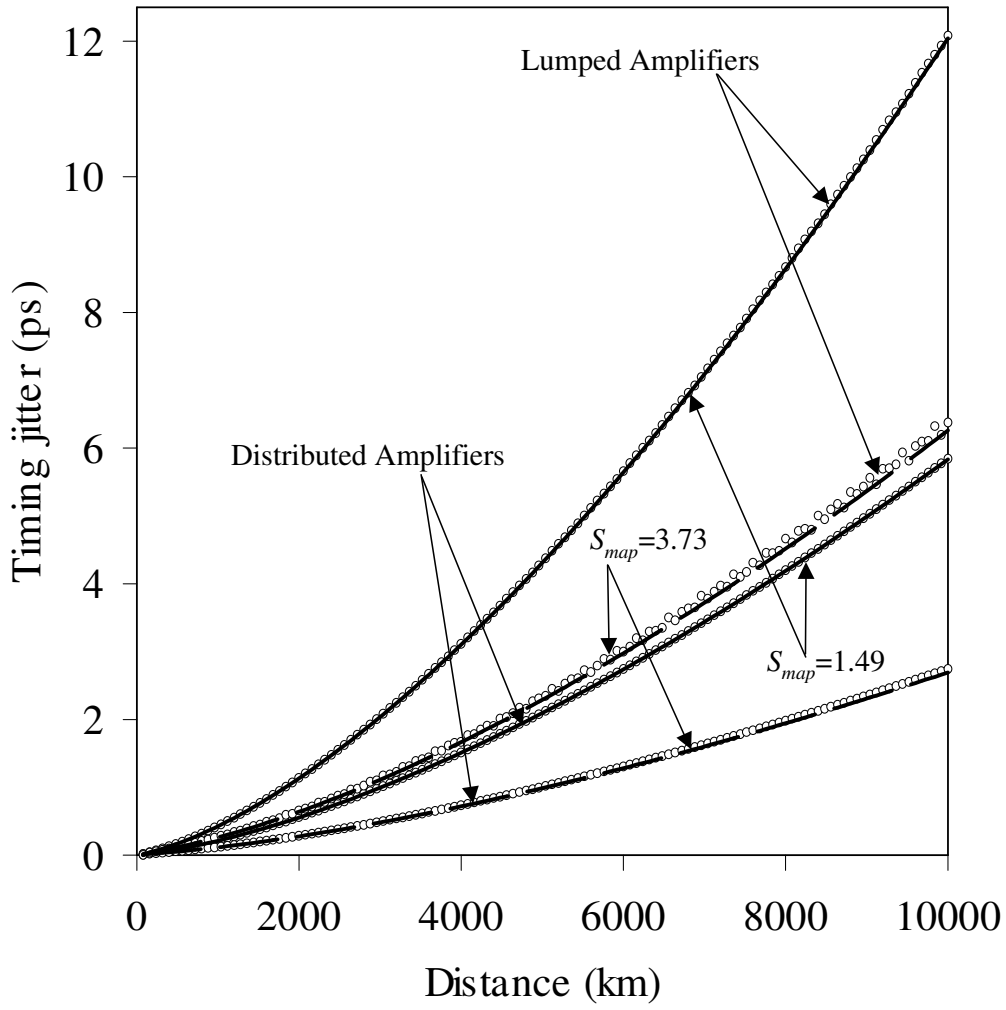

Figure 4.1: Comparison of timing jitter as a function of transmission distance for lumped and ideal distributed amplification schemes for dispersion maps with $S_{map} = 1.49$ (solid lines) and $S_{map} = 3.73$ (dashed lines). Circles represent results obtained using the numerical pulse shape.

strength of this system, defined as in Eq. (2.1), where $T_{FWHM} \approx 1.665 T_{min}$ is the FWHM of the pulse at the minimum pulse width point, is equal to $S_{map} \approx 1.49$.

Since the deviation of pulse shape from Gaussian ansatz increases with map strength, we consider a similar system with a map strength of $S_{map} \approx 3.73$. To increase the map strength we keep same geometry but increase dispersion values

in both fiber sections to $\beta_{21} = 9.9$ ps^2/km, $\beta_{22} = -10.1$ ps^2/km. The input parameters in this case are $T_0 = 8.61$ ps, $C = -2.31$, $E_0 = 0.729$ pJ for lumped amplification and $T_0 = 8.29$ ps, $C = -2.31$, $E_0 = 0.270$ pJ in the ideal distributed amplification case. In all cases we use $n_{sp} = 1.5$ for lumped amplifiers (corresponds to a noise figure of 4.8 dB) and $n_{sp} = 1$ for ideal distributed amplification.

Several conclusions can be drawn from Fig. 4.1. Timing jitter increases with transmission distance L as L^3 in all cases, as expected for the Gordon-Haus jitter. However, it is smaller by about a factor of 2 when distributed amplification is used. The approximations made in deriving Eqs. (4.28) and (4.35) lead to the 0.02% error in comparison with the result of Eqs. (4.21)–(4.23) and are not noticeable at the scale of Figure 4.1. The curves calculated using the exact pulse shape (obtained by solving the NLS equation) show that the error in timing jitter values by using a Gaussian pulse shape is less than 2% and nearly vanish for smaller values of S_{map}.

To see how well Eq. (4.37) for the reduction factor works, we compare its predictions with the results shown in Figure 4.1. We find that the error in the reduction factor given by Eq. (4.37), in comparison with the similar factor calculated using full analytical theory [Eqs. (4.28) and (4.35)] reduces to below 10% after about 7 amplification periods. Moreover, at the distances larger than 14 amplification periods the error becomes less than 5%. We have also verified that these error values do not change much with the map strength.

Figure 4.2 shows how timing jitter oscillates within each map period for lumped and distributed amplification schemes. In the lumped case (Figure 4.2a), no jitter occurs until first amplifier is encountered at a distance of 80 km. Since in the map considered the sign of β_{21} is opposite to the sign of average dispersion, jitter is reduced within each map period in comparison with its values in the ends of the periods. The value in the end of each period increases with distance as L^3. For long distances such that $L \gg L_m$, eventually the oscillations in timing jitter within each period become small in comparison with its average value, so that the oscillations are important at short propagation distances. In the distributed amplification case (Figure 4.2b)), similar behavior occurs, except that jitter starts to grow from $L = 0$ and has overall smaller values.

In the following two sections, we calculate timing jitter accounting for local gain variations which occur invariably in real DM systems. In section 4.4, we consider the case in which gain is provided by erbium ions distributed throughout the fiber link and take into account pump absorption and depletion $[g(z) \neq \alpha]$ for the bidirectional pumping scheme. In section 4.5 we focus on the case of Raman amplification.

4.4 Erbium-based distributed amplification

To calculate the actual variations of the gain $g(z)$ along the fiber, we use the two-level model of Ref. [4]. We solve numerically the multiple rate equations,

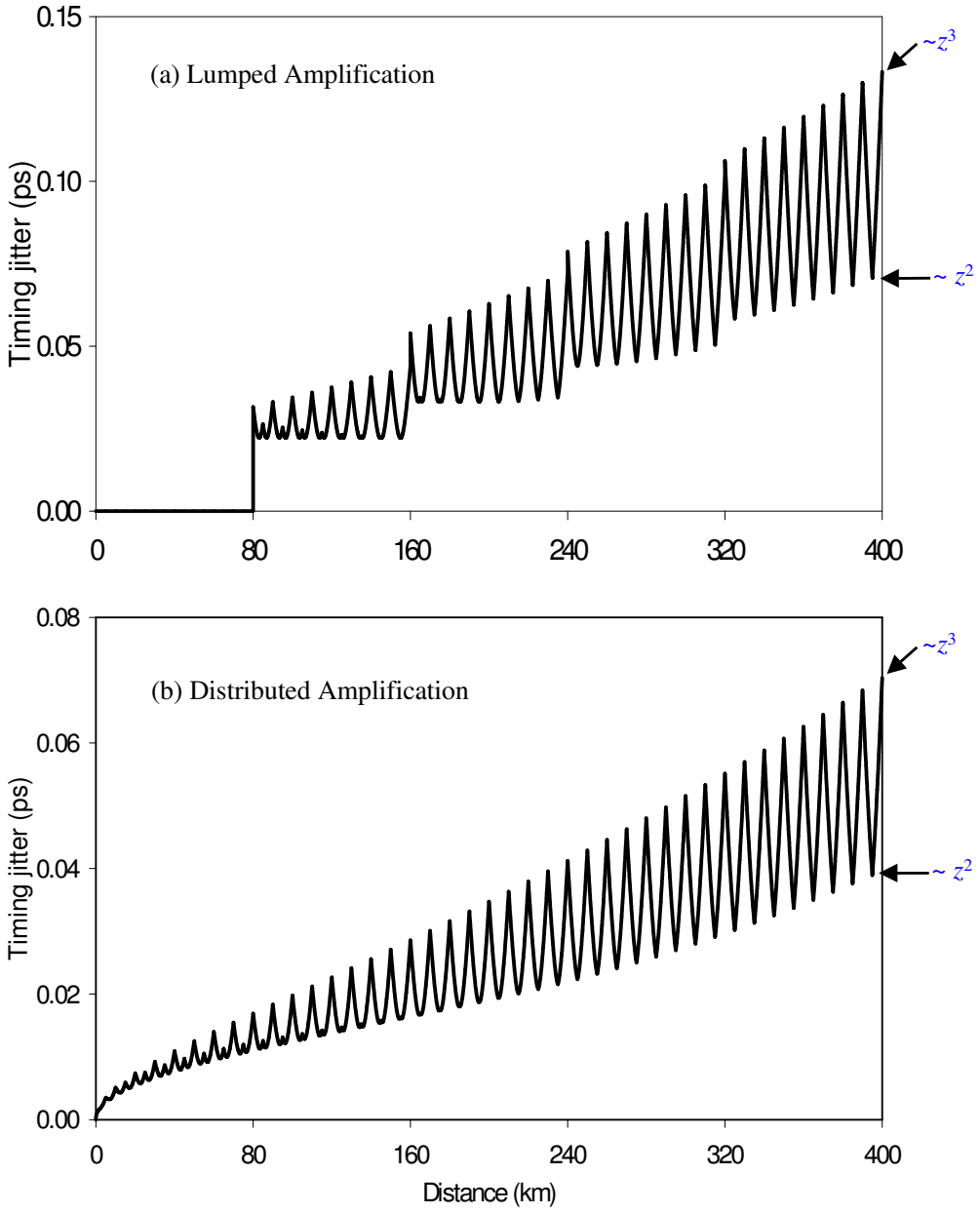

Figure 4.2: Timing jitter variations within each map period for lumped and distributed amplification for the map with $S_{map} = 1.49$.

accounting for gain saturation and pump depletion and assuming a bidirectional pumping scheme at 1480 nm. The inversion factor n_{sp} is obtained using

$$n_{sp} = \sigma_e N_2/(\sigma_e N_2 - \sigma_a N_1), \tag{4.38}$$

where N_2 and N_1 are the ion densities of the upper and lower energy levels participating in stimulated emission, respectively, and σ_e and σ_a are the emission and absorption cross-sections for the signal wavelength, respectively. The distributed gain can be written as $g(z) = \Gamma(\sigma_e N_2 - \sigma_a N_1)$, where Γ is the overlap factor between the doped region and the fiber mode. Neglecting the population N_3 of the third and higher levels, the total dopant density is $N_t = N_1 + N_2$. The parameter n_{sp} is then related to the gain as

$$n_{sp} = \frac{\sigma_e}{\sigma_e + \sigma_a}\left[1 + \frac{\sigma_a \Gamma N_t}{g\,(z)}\right]. \tag{4.39}$$

We take $\sigma_e = 3.9 \times 10^{-21}$ cm^2, $\sigma_a = 3.5 \times 10^{-21}$ cm^2 and $\Gamma = 0.4$, the values appropriate for a Ge-Er-doped silica fiber at 1550 nm [139]. From the noise standpoint of view, N_t should be as small as possible. However, pump power increases as N_t approaches its minimum possible value [140,141]. As a compromise, we choose $N_t = 5.5 \times 10^{14}$ cm^{-3}, a value that requires pump power of about 100 mW for a 80-km pump-station spacing. We also consider a larger density value of $N_t = 9 \times 10^{14}$ cm^{-3} with a reduced pump power of about 50 mW. Such values are normally used for distributed erbium-doped fibers [140]. For each density value, we calculate timing jitter numerically using Eqs. (4.21)–(4.23) with

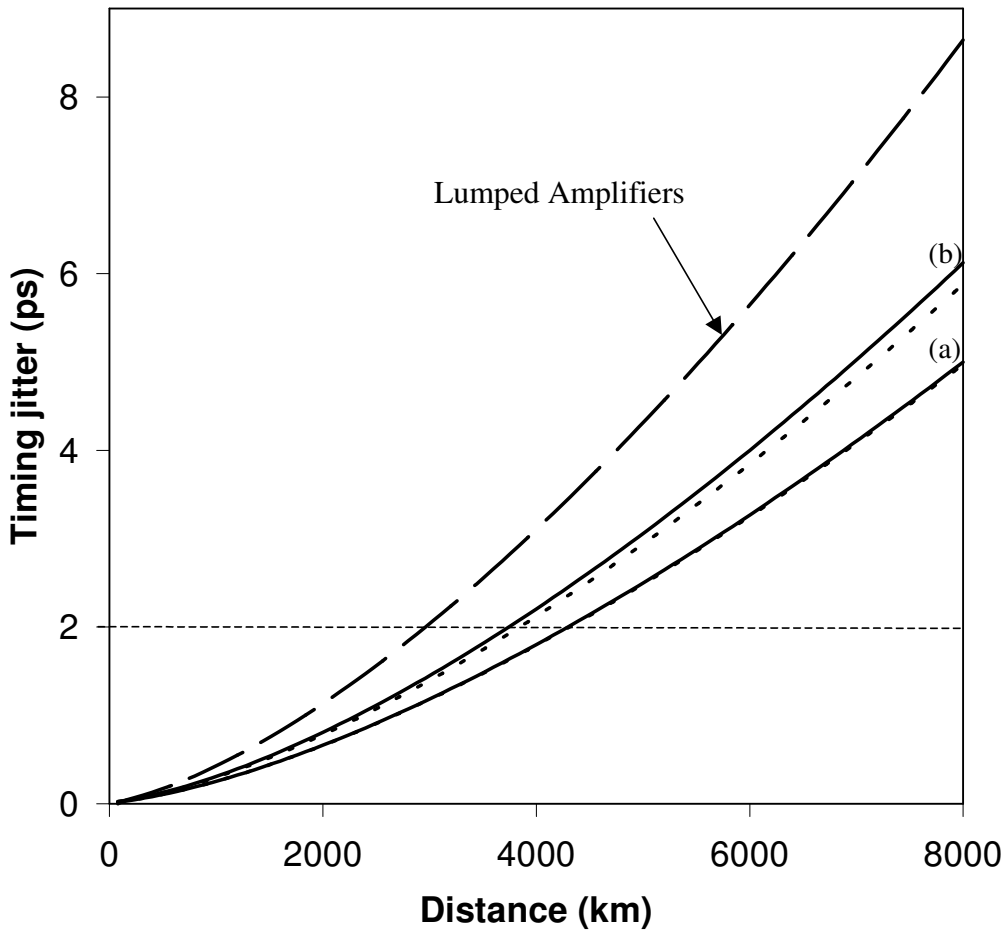

Figure 4.3: Timing jitter at the end of each map period for the systems with erbium-based amplification (solid lines) for the dopant densities of $N_t = 5.5 \times 10^{14} cm^{-3}$ (a) and $N_t = 9 \times 10^{14} cm^{-3}$(b). Dotted lines show the results obtained assuming perfect loss compensation. Dashed line represents timing jitter for the same DM system with lumped amplification.

the actual gain profile and using Eq. (4.28) obtained for ideal loss compensation $[g(z) = \alpha]$. In both cases, inversion parameter n_{sp} is calculated from Eq. (4.39). For perfect loss compensation n_{sp} is constant with values of 1.41 and 1.97 for the N_t values given above.

Figure 4.3 shows the timing jitter calculated at the end of each amplifier. Solid curves represent timing jitter with the actual gain profile and dotted curves

represent timing jitter assuming $g = \alpha$. Timing jitter for the case of lumped amplification with $n_{sp} = 1.5$ is also shown for comparison (dashed curve). The input parameters in each case are calculated by solving the variational equations numerically and are close to the parameters used in section 4.3. In order to verify, how much the soliton interaction itself would limit the transmission distance, the three cases shown in Fig. 4.3 were checked for propagation of a 40 Gb/s pseudorandom pulse train by solving Eq. (4.1) numerically with the split-step method. As an example, we solve Eq. (4.1) using $V(0,t) = \sum b_n V_n(0,t)$, where b_n is a binary random variable with values 0 and 1, and $V_n(0,t)$ is given by Eq. (4.19). In the case of distributed amplification with $N_t = 5.5 \times 10^{14}$ cm^{-3}, using $T_0 = 4.48$ ps, $C = -1.0$, and $E_0 = 0.0593$ pJ (parameters, corresponding to 3.11 ps minimum pulse width, accounting for the actual gainprofile), we obtain the contour map shown in Fig. 4.4. These results were obtained without including amplifier noise and show that interaction among solitons does not affect the pulse train at distances as large as 10,000 km. The results for the other two cases from Figure 4.3 look similarly.

Figure 4.3 shows that it is possible to achieve about 40% jitter reduction using distributed amplification with bidirectional pumping. Assuming Gaussian statistics for timing jitter σ, the bit error rate (BER) can be found as

$$\mathrm{BER} = \frac{2}{\sqrt{2\pi}\sigma} \int_{T_B/2}^{\infty} \exp\left(-\frac{t^2}{2\sigma^2}\right) dt = \mathrm{erfc}\left(\frac{T_B}{2\sqrt{2}\sigma}\right) \approx \frac{4\sigma}{\sqrt{2\pi}T_B} \exp\left(-\frac{T_B^2}{8\sigma^2}\right), \tag{4.40}$$

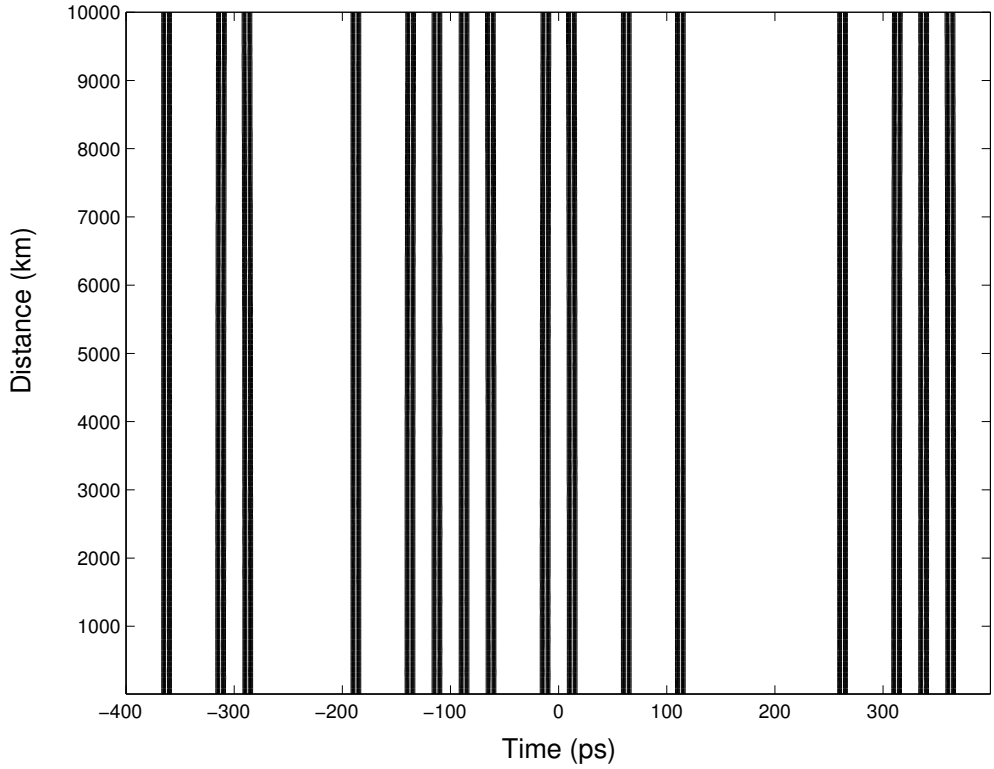

Figure 4.4: Contour map of the bit sequence over 10000 km for the 40-Gb/s system employing erbium-based distributed amplification with bidirectional pumping

where T_B is the bit slot and $\text{erfc}\,(x) \equiv (2/\sqrt{\pi}) \int_x^\infty \exp\,(-y^2)dy$. According to Eq. (4.40), for a BER of less than 10^{-9}, timing jitter should be less than 8% of bit slot [107]. This value can be increased to 12% by using a forward-error correction technique that can tolerate a BER of 10^{-4}. In the following discussion, we use the 8% criteria, which gives a value of 2 ps for the limiting timing jitter at 40 Gb/s. Dashed line in Figure 4.3 shows that transmission distance is limited to about 2900 km in the case of lumped amplification, but can be increased up to 4300 km using the distributed amplification scheme. The dotted lines in Figure 4.3 show that timing jitter is well approximated by the analytical result in Eq. (4.28),

especially for relatively low dopant concentration values. The reason for better agreement for lower N_t values is that gain variations become smaller as N_t is reduced. Note that even for larger values of N_t, Eq. (4.28) is accurate to within a few percent.

4.5 Distributed Raman amplification

In this section we consider the distributed Raman amplification (DRA) scheme for the same dispersion map used earlier. The input parameters, corresponding to the 3.11-ps minimum pulse width, are $T_0 = 4.737$ ps, $C = -1.1$, and $E_0 = 0.0494$ pJ for Raman amplification with bidirectional pumping, and $T_0 = 4.696$ ps, $C = -1.08$, and $E_0 = 0.192$ pJ for backward pumping. These parameters were obtained by solving the variational equations (2.34), (2.35) and were checked numerically for the 40 Gb/s propagation over long distance. For both pumping schemes we use $n_{sp} = [1 - \exp(-h\nu/kT)]^{-1} \approx 1.13$ at room temperature. Gain variations $g(z)$ for Raman amplification are calculated analytically using the condition of full loss compensation and neglecting pump depletion [3].

Figure 4.5 shows timing jitter at the end of each amplifier as a function of transmission distance for bidirectional and backward pumping schemes. The limiting cases of lumped and ideal distributed amplification are shown for comparison. Considerable reduction occurs for both bidirectional and backward pumping schemes although the bidirectional pumping scheme gives smaller jitter values.

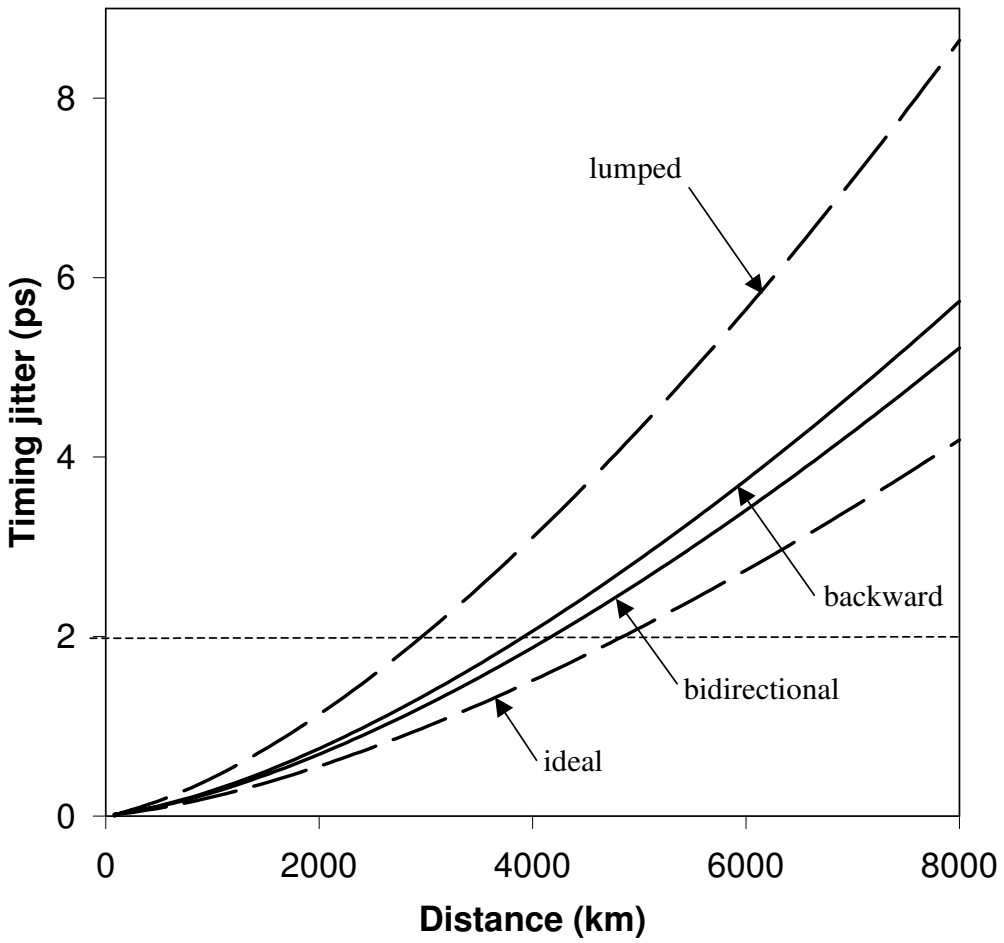

Figure 4.5: Timing jitter at the end of each map period for distributed Raman amplification (solid lines) with bidirectional and backward pumping schemes. For the same DM system, lumped amplification ($n_{sp} = 1.5$) and ideal distributed amplification ($n_{sp} = 1$) are also shown for comparison (dashed lines).

The horizontal dashed line in Figure 4.5 shows that transmission distance can be increased up to about 4200 km using a bidirectional Raman amplification scheme whereas it would be limited to 2900 km for lumped amplifiers. Larger jitter values for a backward pumping scheme result from larger gain variations along the fiber. According to Eqs. (4.21)–(4.23), timing jitter is proportional to n_{sp} and is inversely proportional to the input energy of the pulse. Although the n_{sp} parameter

for Raman amplification is almost the same as for ideal distributed amplification, timing jitter is larger for Raman amplification. This is the consequence of larger gain variations along the fiber when Raman amplification is used. Comparing Figures 4.3 and 4.5 we note that jitter values are within 10% of each other for Raman and erbium-based distributed amplification although gain variations are larger in the Raman case. This is due to larger n_{sp} values for erbium dopants.

We consider now the practical case of hybrid amplification, in which a coded pulse train is amplified periodically using a module consisting of a lumped fiber amplifier and a Raman-pump laser injected backward into the fiber to provide the DRA. In this hybrid scheme, total fiber losses G_{tot} are compensated using the combination of lumped and Raman amplification such that $G_R + G_L = G_{tot}$, or, equivalently,

$$\exp\left(\int_0^{L_A} g_R(z)dz\right) + G_L = \exp\left(\int_0^{L_A} \alpha(z)dz\right), \tag{4.41}$$

where g_R and G_R are, respectively, local and accumulated Raman gain, G_L is the gain of lumped amplifier, and L_A is the amplifier spacing. The same dispersion map is used and input parameters are also comparable to those given earlier. Figure 4.6 shows timing jitter after each amplifier as a function of transmission distance for several values of the Raman gain. While the smallest value of jitter occurs when 100% of losses are compensated using DRA, considerable reduction occurs even when losses are only partially compensated by the Raman gain.

We consider the question whether distributed amplification can allow a longer

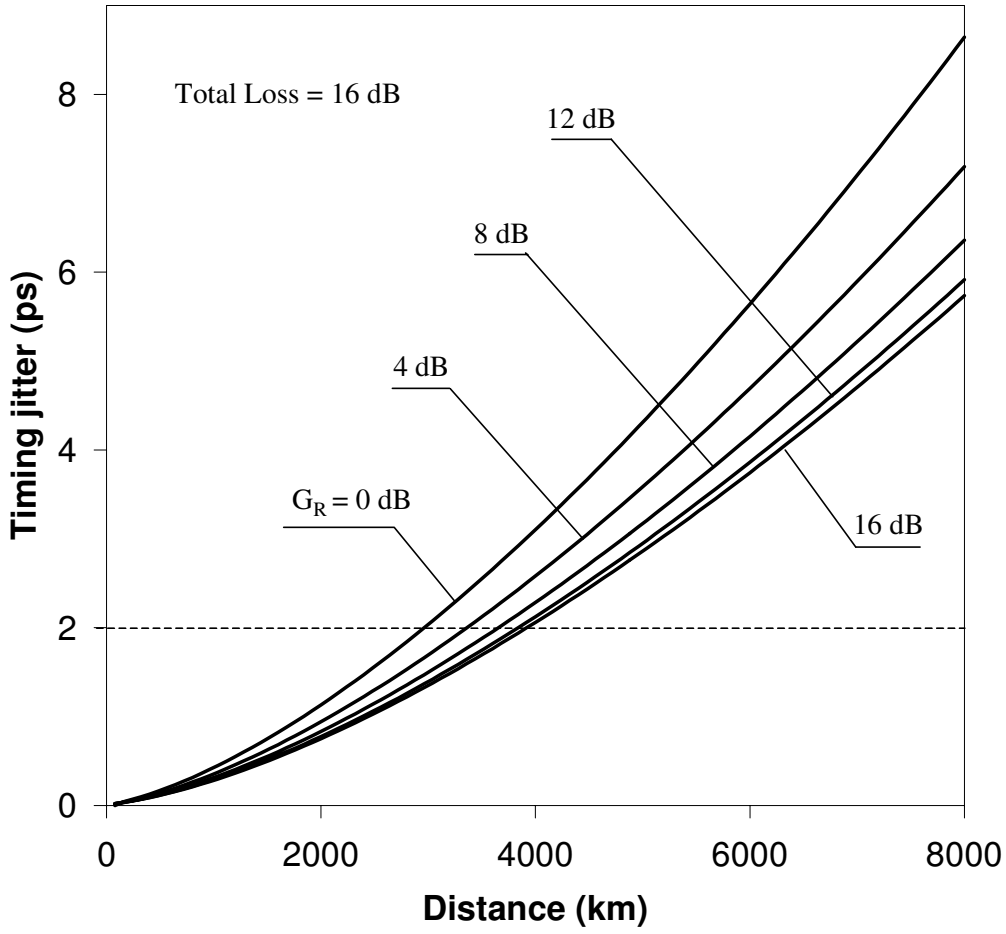

Figure 4.6: Timing jitter after each amplifier as a function of transmission distance for several values of Raman gain. Losses are 16 dB over 80 km of amplifier spacing.

amplifier spacing. Figure 4.7 shows timing jitter after 3100 km as a function of the Raman gain for 40-Gb/s systems employing a hybrid amplification scheme with amplifier spacings of 60, 80, and 100 km. The systems have 6, 8, and 10 map periods within each amplifier spacing, respectively, while the other parameters are the same as before. In each case, jitter is reduced by up to 40% by using DRA. More importantly, the use of lumped amplifiers alone leads to limiting jitter in excess of 2 ps when L_A exceeds 70 km. In contrast, amplifiers can be placed as

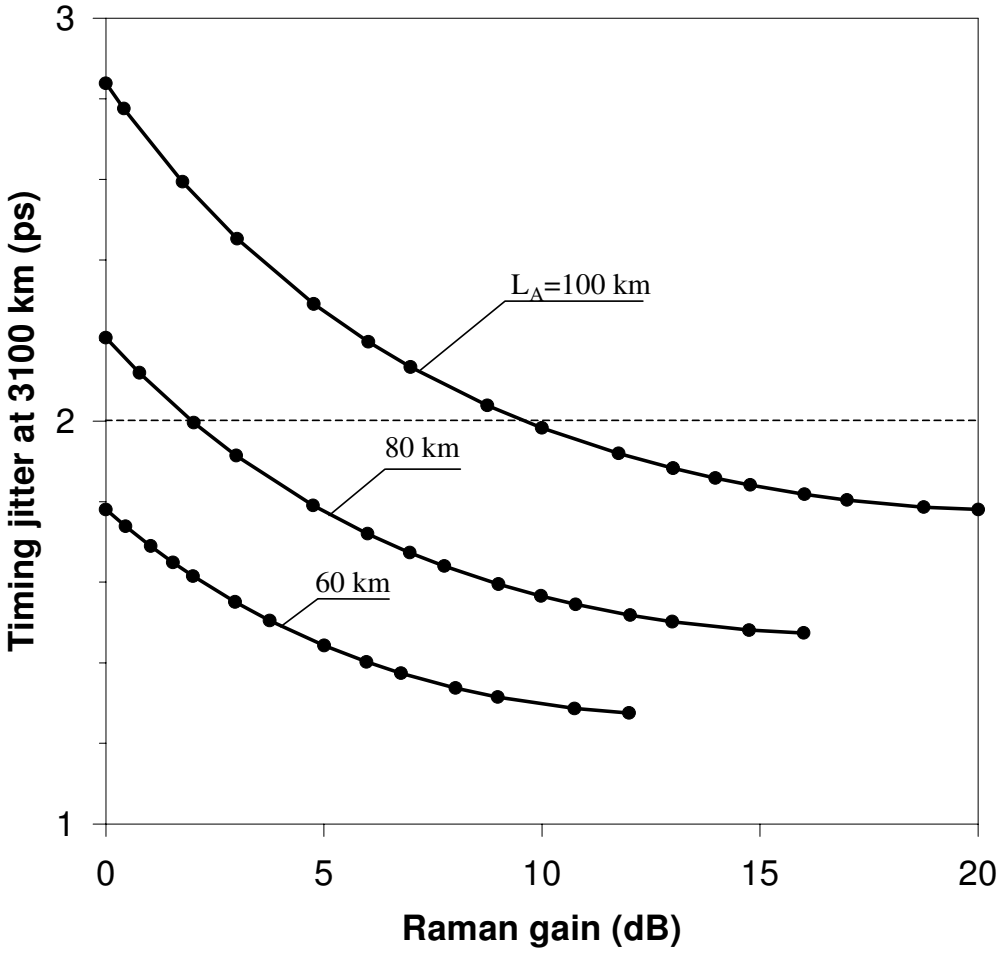

Figure 4.7: Timing jitter after 3100 km as a function of Raman gain for amplifier spacings of 60, 80, and 100 km.

much as 100 km apart when an hybrid amplification scheme is employed. The required Raman gain is only 2 dB for 80-km spacing but becomes 10 dB when amplifiers are 100 km apart.

Finally, we investigate timing jitter dependence on the map strength of the system. To change the map strength, we vary the values of the second order dispersion β_{21} and β_{22} while keeping the average dispersion β_2 and minimum

pulse width T_{min} constant. Figure 4.8(a) shows timing jitter dependence on the map strength at a distance of 4000 km for systems with lumped amplifiers and bidirectionally pumped DRAs. The n_{sp} parameter values used are the same as in Figure 4.5. Solid curves correspond to $T_{min} = 3.11$ ps and are suitable for a 40-Gb/s system while dashed curves with $T_{min} = 8$ ps are appropriate for a 10-15 Gb/s system. In each case, timing jitter decreases as map strength is increased. The reason for this decrease is that larger values of the map strength require higher values of input pulse energy in order to keep the pulse width fixed. Since timing jitter is inversely proportional to the pulse energy, the jitter decreases as map strength increases. Input pulse energies for each value of the map strength are shown on Figure 4.8(b) and support this conclusion. Note, however, that pulse breathing increases significantly for large map strengths, and the system may be limited by soliton interaction.

Figure 4.8a also shows that timing jitter values are larger for shorter pulse widths although shorter pulse widths require larger pulse energies. We have verified that this behavior holds for erbium distributed amplification as well. The reason for this can be understood from Eqs. (4.28) and (4.35), which show that the term growing as z^3 with distance z is proportional to the ratio $(1 + C_0^2)/(T_0^2 E_0)$. Numerical solutions of the variational equations show, that this ratio increases for smaller T_0 values, thus giving rise to a larger timing jitter.

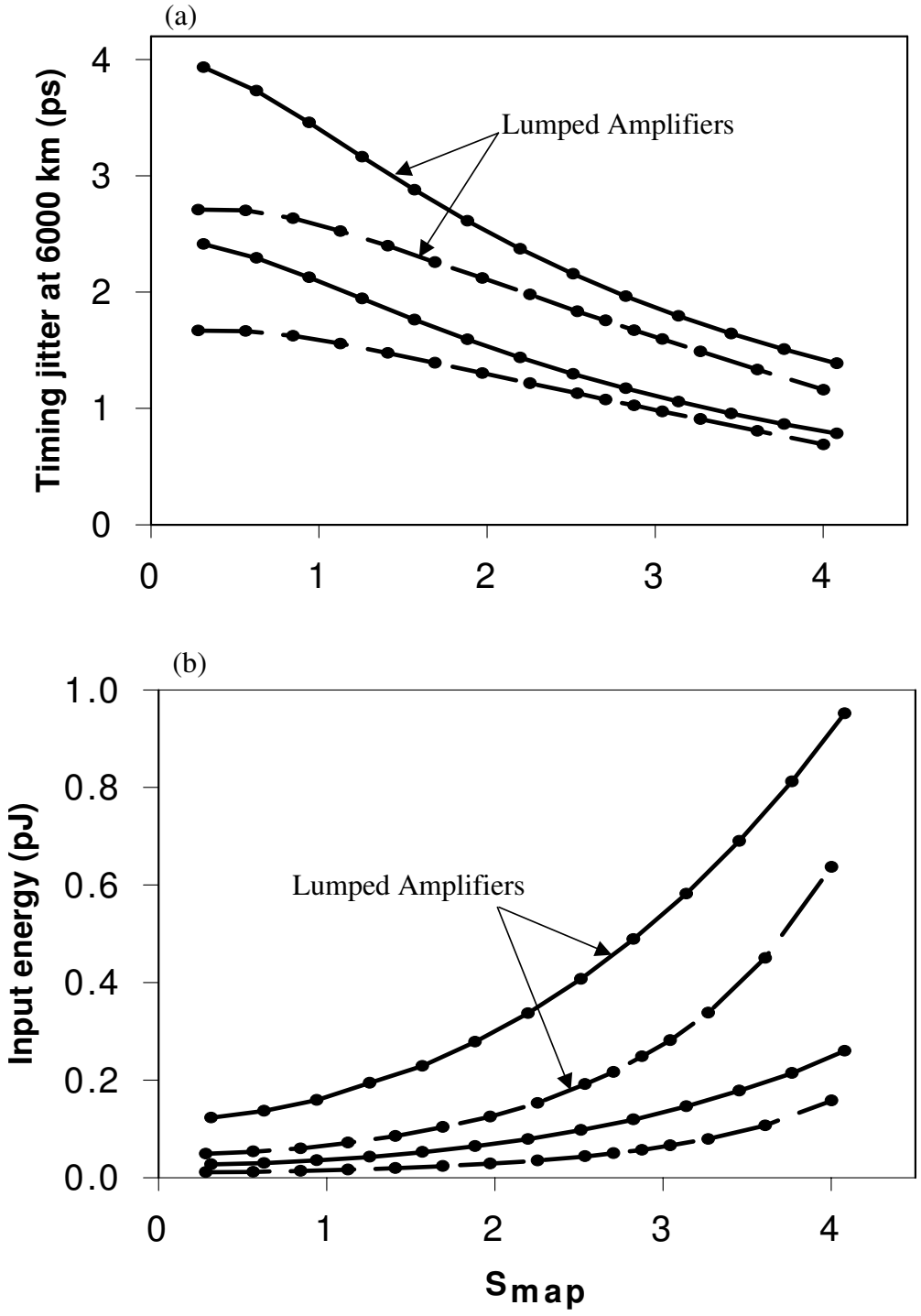

Figure 4.8: (a) Timing jitter after 4000 km as a function of the map strength in DM systems with lumped and bidirectionally pumped Raman amplification. Minimum pulse width remains fixed at 3.11 ps (solid lines) and at 8 ps (dashed lines). Corresponding input energy values are shown in Figure 4.8(b).

4.6 Conclusions

We have compared the ASE-induced timing jitter in dispersion-managed systems for the cases of lumped, distributed, and hybrid Raman amplification schemes. We show that, while the erbium-based distributed amplification gives the smallest timing jitter value, considerable reduction occurs when bidirectional, backward, or even partial Raman amplification is employed. We have derived an analytical expression for the timing jitter at any position within the fiber link in the case of ideal distributed amplification for which losses are exactly compensated by gain at every point. We show that in the case of a low erbium-dopant density timing jitter is well approximated by this formula. We also derive an analytical expression for the timing jitter for lumped amplifiers and compare it to the case of distributed amplification. Finally, we show that timing jitter decreases for stronger maps at a given bit rate (fixed minimum pulse width).

Chapter 5

Conclusions

In this thesis, we have considered different aspects of DM systems design. We started by considering a DM soliton system design and derived approximate analytic expressions for the input pulse parameters that provide periodical pulse propagation in such a system. The expressions showed a good agreement with the numerically found values of input parameters and revealed several interesting features in the DM soliton system design. In particular, they showed that there exists a minimum input pulse width, and this fact limits the bit rate for a given map configuration. We introduced a new map parameter that allowed the estimation of the limiting bit rate. The way in which this parameter depends on the map configuration explains the need of dense DM at high bit rates. The expressions provided also simple suggestions on how to design a system so that intrachannel pulse interactions are minimized. In particular, optimal input chirp values are found to be around ± 1.1. This value was expected based on the expressions and was confirmed by the numerical analysis of pseudorandom bit sequence propaga-

tion in the absence of noise and parameters fluctuations. This optimum explains the previously known empirical result that pulse interactions are minimized for the map strength of 1.65 [125]. Expressions also showed that this optimal design corresponds to the case when fiber section length is approximately equal to the local dispersion length.

In a real system, practically any parameter, designed to have a fixed value, usually deviates more or less from that value in a random fashion. In particular, the dispersion of an optical fiber can vary over a considerable range because of unavoidable variations in the core diameter along the fiber length, as well as because of the environmental changes. We investigated numerically the impact of dispersion fluctuations on the performance of 40-Gb/s DM lightwave systems designed with distributed Raman amplification. We have considered both the CRZ and DM soliton formats and used the Q parameter for judging the system performance. The analysis showed that dispersion fluctuations can lead to performance degradation even in a linear system when the change in the total accumulated dispersion, introduced by fluctuations, is not completely compensated. The presence of nonlinearity aggravates the extent of system degradation induced by dispersion fluctuations for both CRZ and DM soliton systems. We have shown that this degradation increases fast when the nonlinear effects in the system are made stronger by using higher-energy pulses. The system tolerance to dispersion fluctuations can be improved by employing a receiver that integrates the signal

over some portion of the bit slot, rather than making a measurement at the center of the bit slot.

Discussing the impact of dispersion fluctuations on the optimum input parameters we showed that, for CRZ systems, one should use the input peak powers slightly smaller than the optimum values predicted in the absence of fluctuations. For DM soliton systems, in the absence of both noise and dispersion fluctuations the optimum value of the Q parameter is obtained for input chirp values near ± 1.1, as discussed before. In the presence of noise but without dispersion fluctuations, Q increases for larger values of C_0 because the use of higher-energy pulses improves the SNR while the nonlinear effects are balanced by the use of DM solitons. However, dispersion fluctuations change this behavior because they perturb the balance between the dispersive and nonlinear effects. As a result, while accounting for both noise and dispersion fluctuations, the optimum input parameters should remain in the region around $|C_0| \approx 1.2$.

The fluctuations of the second-order dispersion β_2 result from the static or dynamic fluctuations in the frequency-dependent refractive index, which implies that fluctuations are present in all orders of dispersion. When the refractive index fluctuations are dynamic, including the first-order dispersion fluctuations results in the presence of one more fluctuating term in the nonlinear Schrödinger equation that depends on fluctuations in the group velocity and can lead to a new source of timing jitter. However, if dynamic fluctuations happen on a sufficiently long

time scale, the effect of fluctuations in the group velocity may be compensated by electronically.

Finally, we analyzed the role of distributed amplification in controlling ASE-indused timing jitter in DM systems. We have derived an analytical expression for the timing jitter at any position within the fiber link in the case of ideal distributed amplification for which losses are exactly compensated by gain at every point. We showed that in the case of a low erbium-dopant density timing jitter is well approximated by this formula. We also derived an analytical expression for the timing jitter for lumped amplifiers and compare it to the case of distributed amplification. The comparison have shown that timing jitter is reduced by about 50% in a system with ideal distributed amplification, having an inversion parameter equal to its quantum limit of 1.

As a next step, we calculated timing jitter accounting for local gain variations which occur invariably in real DM systems, and considering the actual values of the inversion parameter. The ASE-induced timing jitter in dispersion-managed systems has been compared for the cases of lumped, distributed, and hybrid Raman amplification schemes. We have shown that while the erbium-based distributed amplification gives the smallest timing jitter value, considerable reduction occurs when bidirectional, backward, or even partial Raman amplification is employed.

Bibliography

[1] G. P. Agrawal, *Fiber-Optic Communication Systems*, 3rd ed., New York: Wiley, 2002.

[2] I. Kaminov and T. Li,*Optical Fiber Telecommunications IV*, Academic Press, San Diego, 2002.

[3] G. P. Agrawal, *Applications of Nonlinear Fiber Optics*, Academic Press, New York, 2001.

[4] P. C. Becker, N. A. Olsson, and J. R. Simpson, *Erbium-Doped Fiber Amplifiers: Fundamentals and Technology*, Academic Press, San Diego, 1999.

[5] I. Tomkos, M. Vasilyev, J.-K. Rhee, M. Mehendale, B. Hallock, B. Szalabofka, M. Williams, S. Tsuda, and M. Sharma, "80 × 10.7 Gb/s ultra-long-haul (+4200 km) DWDM network with reconfigurable "broadcast and select" OADMs", *Optical Fiber Communications conf.*, paper FC1, 2002.

[6] A. H. Gnauck, G. Raybon, S. Chandrasekhar, J. Leuthold, C. Doerr, L. Stulz, A. Agarwal, S. Banerjee, D. Grosz, S. Hunsche, A. Kung, A. Marhelyuk, D. Maywar, M. Movassaghi, X. Liu, C. Xu, X. Wei, and D. M. Gill, "2.5 Tb/s (64 × 42.7 Gb/s) transmission over 40 × 100 km NZDSF using RZ-DPSK format and all-Raman-amplified spans",*Optical Fiber Communications conf.*, paper FC2, 2002.

[7] D. G. Foursa, C. R. Davidson, M. Nissov, M. A. Mills, L. Xu, J. X. Cai, A. N. Pilipetskii, Y. Cai, C. Breverman, R. R. Cordell, T. J. Carvelli, P. C. Corbett, H. D. Kidorf, and N. S. Bergano, "2.56 Tb/s (256 × 10 Gb/s) transmission over 11,000 km using hybrid Raman/EDFAs with 80 nm of continuous bandwidth",*Optical Fiber Communications conf.*, paper FC3, 2002.

[8] J.-X. Cai, M. Nissov, C. R. Davidson, Y. Cai, A. N. Pilipetskii, H. Li, M. A. Mills, R.-M. Mu, U. Feiste, L. Xu, A. J. Lucero, D. G. Foursa, and N. S. Bergano, "Transmission of thirty-eight 40 Gb/s channels (> 1.5

Tb/s) over transoceanic distance", *Optical Fiber Communications conf.*, paper FC4, 2002.

[9] H. Sugahara, K. Fukuchi, A. Tanaka, Y. Inada, and T. Ono, "6,050 km transmission of 32×42.7 Gb/s DWDM signals using Raman-amplified quadruple-hybrid span configuration", *Optical Fiber Communications conf.*, paper FC6, 2002.

[10] L. Fenghai, J. Bennike, S. Dey, C. Rasmussen, B. Mikkelsen, P. Mamyshev, D. Gapontsev, and V. Ivshin, "1.6 Tbit/s (40×42.7 Gbit/s) transmission over 3600 km UltraWave TM fiber with all-Raman amplified 100 km terrestrial spans using ETDM transmitter and receiver", *Optical Fiber Communications conf.*, paper FC7, 2002.

[11] B. Zhu, L. Leng, L. E. Nelson, L. Gruner-Nielsen, Y. Qian, J. Bromage, S. Stulz, S. Kado, Y. Emori, S. Namiki, P. Gaarde, A. Judy, B. Palsdottir, and R. L. Lingle, "3.2Tb/s (80×42.7 Gb/s) transmission over 20×100 km of non-zero dispersion fiber with simultaneous C + L-band dispersion compensation", *Optical Fiber Communications conf.*, paper FC8, 2002.

[12] D. Chen, S. Wheeler, D. Nguyen, B. Davis, M. Glavanovic, J. Khaydarov, I. Koruga, S. Hegarty, F. Cokic, and Zhu Fei, "40 channels 4000 km DWDM ULH transmission field trial without Raman amplification and regeneration", *Optical Fiber Communications conf.*, paper FC10, 2002.

[13] F. Di Pasquale, F. Meli, E. Griseri, A. Sguazzotti, C. Tosetti, and F. Forghieri, "All-Raman transmission of 192 25-GHz spaced WDM channels at 10.66 Gb/s over 30×22 dB of TW-RS fiber", *Optical Fiber Communications conf.*, paper WE2, 2003.

[14] G. Charlet, J.-C. Antona, S. Lanne, and S. Bigo, "From 2100 to 2700 km distance using phase-shaped binary transmission at 6.3 Tbit/s capacity", *Optical Fiber Communications conf.*, paper WE3, 2003.

[15] H. Bissessur, G. Charlet, E. Gohin, C. Simonneau, L. Pierre, and W. Idler, "1.6 Tbit/s (40×40 Gbit/s) DPSK transmission over 3×100 km of TeraLight fibre with direct detection", *Electron. Lett.* **39**, pp. 192-193, 2003.

[16] H. Bissessur, G. Charlet, W. Idler, C. Simonneau, S. Borne, L. Pierre, R. Dischler, C. De Barros, and P. Tran, "3.2 Tbit/s (80×40 Gbit/s) phase-shaped binary transmission over 3×100 km with 0.8 bit/s/Hz efficiency", *Electron. Lett.* **38**, pp. 377-379, 2003.

[17] Y. Frignac, G. Charlet, W. Idler, R. Dischler, P. Tran, S. Lanne, S. Borne,

C. Martinelli, G. Veith, A. Jourdan, J.-P. Hamaide, and S. Bigo, "Transmission of 256 wavelength-division and polarization-division-multiplexed channels at 42.7Gb/s (10.2Tb/s capacity) over 3×100 km of TeraLight TM fiber", *Optical Fiber Communications conf.*, paper FC5, 2002.

[18] T. Otani, M. Hayashi, M. Daikoku, K. Ogaki, Y. Nagao, K. Nishijima, and M. Suzuki, "Field trial of 63 channels 40 Gbit/s dispersion-managed soliton WDM signal transmission over 320 km NZ-DSFs", *Optical Fiber Communications conf.*, paper FC9, 2002.

[19] T. Otani, M. Hayashi, M. Daikoku, K. Ogaki, Y. Nagao, K. Nishijima, and M. Suzuki, "Investigation of system upgradability over installed fiber-optic cable using 40-Gb/s WDM signals toward multiterabit optical networks", *J. Lightwave Technol* **21**, pp. 947-952, 2003

[20] B. Mikkelsen, G. Raybon, R.-J. Essiambre, A.J. Stentz, T. N. Nielsen, D. W. Peckham, L. Hsu, L. Gruner-Nielsen, K. Dreyer, and J. E. Johnson, " 320-Gb/s single-channel pseudolinear transmission over 200 km of nonzero-dispersion fiber", *IEEE Photon. Technol. Lett.* **12**, pp. 1400-1402, 2000.

[21] J. Lou, G. Nowak, W. Kaechele, M. Dennis,, I. Duling, and T. Carruthers, "Raman-pumped, dense dispersion-managed soliton transmission of 80 Gb/s OTDM data", *Optical Fiber Communications conf.*, paper WE7, 2003.

[22] L. G. Cohen, C. Lin, W. G. French, "Tailoring zero chromatic dispersion into the 1.5-1.6 mu m low-loss spectral region of single-mode fibres", *Electron. Lett.* **15**, pp. 334-335, 1979.

[23] C. T. Chang, K. I. White, and B. P. Nelson, "Minimum dispersion at 1.55 μm for single-mode step-index fibres", *Electron. Lett.* **15**, pp. 765-767, 1979.

[24] C. T. Chang, "Minimum dispersion in a single-mode step-index optical fiber", *Appl. Opt.* **18**, pp. 2516-2522, 1979.

[25] G. P. Agrawal, *Applications of Nonlinear Fiber Optics* 3rd ed., Academic Press, New York, 2001.

[26] R. G. Waarts and R.-P Braun, "System limitations due to four-wave mixing in single-mode optical fibres", *Electron. Lett.* **22**, pp. 873-875, 1986.

[27] M. W. Maeda, W. B. Sessa, and W. I Way, , A. Yi-Yan, L. Curtis, R. Spicer, R. I. Laming, "The effect of four-wave mixing in fibers on optical frequency-division multiplexed systems", *J. Lightwave Technol.* **8**, pp. 1402-1408, 1990.

[28] K. Inoue, K. Nakanishi, K. Oda, and H. Toba, "Crosstalk and power penalty due to fiber four-wave mixing in multichannel transmissions", *J. Lightwave Technol.* **12**, pp. 1423-1439, 1994.

[29] R. W. Tkach, A. R. Chraplyvy, F. Forghieri, A. H. Gnauck, and R. M. Derosier, "Four-photon mixing and high-speed WDM systems", *J. Lightwave Technol.* **13**, pp. 841-849, 1995.

[30] F. Forghieri, R. W. Tkach, and A. R. Chraplyvy, "WDM systems with unequally spaced channels", *J. Lightwave Technol.* **13**, pp. 889-897, 1995.

[31] A. Rafel, J. Roldan, J. Prat, J. C. Sarrasi, A. Amrani, and G. Junyent, "WDM signal degradation due to FWM in dispersion shifted fibers", *Proc. SPIE - Int. Soc. Opt. Eng. (USA)* **3531**, pp. 16-26, 1998

[32] S. Song and J. Livas, "Four-wave mixing induced Q-factor variations in WDM systems", *Conference on Lasers and Electro-Optics, Technical Digest*, pp. 341-342, 2000

[33] S. Bjornstad, M. Nord, G. Hanssen, B. Slagsvold, and D. R. Hjelme, "Impact of four-wave-mixing in polarisation multiplexed 12.5 GHz channel spacing WDM systems", *LEOS 2001. 14th Annual Meeting of the IEEE Lasers and Electro-Optics Society* , pp. 285-286, 2001

[34] G. Shiming, Y. Changxi, and J. Guofan, "Comparison of interchannel pulses four-wave mixing in SMF, NZDSF and HNLF", *Opt. Commun.* **206**, pp. 439-443, 2002.

[35] A. J. Antos and D. K. Smith, "Design and characterization of dispersion compensating fiber based on the LP01 mode", *J. Lightwave Technol.* **12**, pp. 1739-1745, 1994.

[36] A. M. Vengsarkar, A. E. Miller, M. Haner, A. H. Gnauck, W. A. Reed, and K. L. Walker, "Fundamental-mode dispersion-compensating fibers: design considerations and experiments", *Optical Fiber Communication conf.*, paper ThK2, pp. 225-227, 1994.

[37] R. J. Nuyts, Y. K. Park, and P. Gallion, "Performance improvement of 10 Gb/s standard fiber transmission systems by using the SPM effect in the dispersion compensating fiber", *IEEE Photon. Technol. Lett.* **8**, pp. 1406-1408, 1996.

[38] A. H. Gnauck, J. M. Wiesenfeld, L. D. Garrett, R. M. Derosier, F. Forghieri, V. Gusmeroli, and D. Scarano, "4 $\times$ 40 Gb/s 75-km WDM transmission

over conventional fiber using a broad-band fiber grating", *IEEE Photonics Technol. Lett.* **11**, pp. 1503-1505, 1999.

[39] A. H. Gnauck, J. M. Wiesenfeld, L. D. Garrett, M. Eiselt, F. Forghieri, L. Arcangeli, B. Agogliati, V. Gusmeroli, and D. Scarano, "16 × 20 Gbit/s-400 km WDM transmission over NZDSF using a slope-compensating fiber-grating module", *IEEE Photonics Technol. Lett.* **12**, pp. 437-439, 2000.

[40] A. H. Gnauck, L. D. Garrett, Y. Danziger, U. Levy, and M. Tur, "Dispersion and dispersion-slope compensation of NZDSF over the entire C band using higher-order-mode fibre", *Electron. Lett.* **36**, pp. 1946-1947, 2000.

[41] C. D. Poole, J. M. Wiesenfeld, D. J DiGiovanni, and A. M. Vengsarkar, "Optical fiber-based dispersion compensation using higher order modes near cutoff", *J. Lightwave Technol.* **12**, pp. 1746-1758, 1994.

[42] J. H. Winters and R. D. Gitlin, "Electrical signal processing techniques in long-haul fiber-optic systems", *IEEE Transactions on Communications* **38**, pp. 1439-1453, 1990.

[43] J. H. Winters, "Equalization in coherent lightwave systems using a fractionally spaced equalizer", *J. Lightwave Technol.* **8**, pp. 1487-1491, 1990.

[44] M. I. Hayee and A. E. Willner, "Pre- and post-compensation of dispersion and nonlinearities in 10-Gb/s WDM systems", *IEEE Photon. Techol. Lett.* **9**, pp. 1271-1273, 1997.

[45] T. Yamamoto, E. Yoshida, K. R. Tamura, K. Yonenaga, and M. Nakazawa, "640-Gbit/s optical TDM transmission over 92 km through a dispersion-managed fiber consisting of single-mode fiber and reverse dispersion fiber", *IEEE Photon. Techol. Lett.* **12**, pp. 353-355, 2000.

[46] Y. W. Song, Z. Pan, S. M. R. Motaghian Nezam, C. Yu, Y. Wang, D. Starodubov, V. Grubsky, J. E. Rothenberg, J. Popelek, H. Li, Y. Li, R. Caldwell, R. Wilcox, and A.E. Willner, "Tunable dispersion slope compensation for 40-Gb/s WDM systems using broadband nonchannelized third-order chirped fiber Bragg gratings", *J. Lightwave Technol.* **20**, pp. 2239-2246, 2002.

[47] Z. Pan, Q. Yu, Y. W. Song, and A. E. Willner, "40-Gb/s RZ 120-km transmission using a nonlinearly-chirped fiber Bragg grating (NL-FBG) for tunable dispersion compensation", *Optical Fiber Communications conf.*, Post-conference Technical Digest, pp. 682-683, 2002.

[48] S. Namiki and Y. Emori, "Recent advances in ultra-wideband Raman ampli-

fiers", *Optical Fiber Communications conf.*, Postconference Technical Digest, paper FF1, **4** pp. 98-99, 2000.

[49] H. Masuda, "Review of wideband hybrid amplifiers", *Optical Fiber Communications Conf.*, Postconference Technical Digest, paper TuA1, **1** pp. 2-4, 2000.

[50] K. L. Bacher, C. Fuchs, J. S. Paslaski, R. P. Espindola, A. Benzoni, W. C. Dautremont-Smith, S. Srinivasan, G.C. Cho, and L. Monro, "High-power 14xx-nm pump laser modules for optical amplification systems", *Semiconductor Lasers for Lightwave Communication Systems conference*, Proceedings of the SPIE, **4533**, pp. 47-59, 2001.

[51] N. Tsukiji, J. Yoshida, T. Kimura, S. Koyanagi, and T. Fukushima, "Recent progress of high power 14XXnm pump lasers", *Active and Passive Optical Components for WDM Communication conference*, Proceedings of the SPIE, **4532**, pp. 349-360, 2001.

[52] R. P. Espindola, K. L. Bacher, K. Kojima, N. Chand, S. Srinivasan, G. C. Cho, F. Jin, C. Fuchs, V. Milner, and W. C.Dautremont-Smith, "High power, low RIN, spectrally-broadened 14xx DFB pump for application in co-pumped Raman amplification", *Proceedings 27th European Conference on Optical Communication* **6**, pp. 36-37, 2001.

[53] J. Yoshida, N. Tsukiji, T. Kimura, , M. Funabashi, and T. Fukushima, "Novel concepts in 14XX-nm pump lasers for Raman amplifiers", *Active and Passive Optical Components for WDM Communication II conference* Proceedings of the SPIE, **4870**, pp. 169-182, 2002.

[54] R. P. Espindola, K. L. Bacher, K. Kojima, N. Chand, S. Srinivasan, G. C. Cho, F. Jin, C. Fuchs, V. Milner, and W. Dautremont-Smith, "Penalty-free 10 Gbit/s single-channel co-pumped distributed Raman amplification using low RIN 14xx nm DFB pump", *Electron. Lett.* **38**, pp. 113-115, 2002.

[55] S. S.-H. Yam, F.-T. An, E. S.-T. Hu, M. E. Marhic, T. Sakamoto, L. G. Kazovsky, and Y. Akasaka, "Gain-clamped S-band discrete Raman amplifier", *Optical Fiber Communications conf.*, paper ThB4, 2002.

[56] S. K. Turitsyn, M. P. Fedoruk, W. Forysiak, and N. J. Doran, "Dispersion-management in fiber communication lines using Raman amplification'. *Opt. Commun.* **170**, pp. 23-27, 1999.

[57] J. B. Leroy, P. Marmier, C. Laval, and O. Gautheron, "32 $\times$ 10 Gbit/s

transmission over 8000 km using hybrid Raman-erbium doped fiber optical amplifiers", *Optical Fiber Communications conf.*, paper TuJ4, 2000.

[58] T. Matsuda, M. Murakami, and T. Imai, "Experimants on long-haul broadband WDM transmission with Raman amplification". *Electron. Lett.* **37**, pp. 237-239, 2001.

[59] R. E. Neuhauser, P. M. Krummrich, H. Bock, and C. Glingener, "Impact of nonlinear pump interaction on broadband distributed Raman amplification", *Optical Fiber Communications conf.*, paper MA4, 2001.

[60] M. N. Islam, "Raman amplifiers for telecommunications", *IEEE J. Select. Topics Quantum Electron.* **8**, pp. 548-559, 2002

[61] T. Okuno, T. Tsuzaki, and M. Nishimura, "Novel optical hybrid line configuration for quasi-lossless transmission by distributed Raman amplification", *IEEE Photon. Tochnol. Lett.* **13**, pp. 806-808, 2001

[62] A. F. Evans, J. Grochocinski, A. Rahman, C. Reynolds, and M. Vasilyev, "Distributed amplification: how Raman gain impacts other fiber nonlinearities", *Optical Fiber Communications conf.*, paper MA7, 2001.

[63] A. Evans, "Raman amplification in broadband WDM systems", *Optical Fiber Communications conf.*, paper TuF4, 2001.

[64] I. Morita, K. Tanaka, and N. Edagawa, "Benefit of Raman amplification in ultra-long distance 40 Gbit/s-based WDM transmission", *Optical Fiber Communications conf.*, paper TuF5, 2001.

[65] A. Carena, and V. Curri, "Comparison between different configurations of Hybrid/Raman/Erbium-doped fiber amplifiers", *Optical Fiber Communications conf.*, paper TuA3, 2001.

[66] N. Shimojoh, T. Naito, T. Tanaka, H. Nakamoto, T. Ueki, A. Sugiyama, K. Torii, and S. Muyama, "0.4 Tbit/s WDM transmission over 7400 km using all Raman amplifier repeaters with 74 nm continuous single band", *Proceedings 27th European Conference on Optical Communication* **6**, pp.8-9, 2001.

[67] A. Bernston, S. Popov, E. Vanin, G. Jacobsen, and J. Karlsson, "Polarization dependence and gain tilt of Raman amplifiers for WDM systems", *Optical Fiber Communications conf.*, paper MI2, 2001.

[68] P. M. Krummrich, R. E. Neuhauser, C. Glingener, and A. G. Siemens,

"Bandwidth limitations of broadband distributed Raman fiber amplifiers for WDM systems", *Optical Fiber Communications conf.*, paper MI2, 2001.

[69] H. Suzuki, N. Takachio, H. Masuda, and K. Iwatsuki,, "WDM transmission technology in the zero-dispersion region employing distributed Raman amplification", *J. Lightwave Technol.* **21**, pp. 973-981, 2003.

[70] C.R.S. Fludger, and V. Handerek, "Fundamental noise limits in broadband raman amplifiers', *Optical Fiber Communications conf.*, paper MA5, 2001

[71] M. A. Farahani, and T. Gogolla, "Spontaneous Raman scattering in optical fibers with modulated probe light for distributed temperature Raman remote sensing", *J. Lightwave Technol.* **17**, pp. 1379-1391, 1999.

[72] D. A. Long, *Raman Spectroscopy*, New York, McGraw Hill, 1977.

[73] A. Yariv, "Signal-to-noise considerations in fiber links with periodic or distributed optical amplification", *Opt. Lett.* **15**, pp. 1064-1066, 1990.

[74] R.-M. Mu, T. Yu, V. S. Grigoryan, and C. R. Menyuk, "Dynamics of the chirped return-to-zero modulation format", *J. Lightwave Technol.* **20**, pp. 47-57, 2002.

[75] R.-M. Mu, and C. R. Menyuk, "Convergence of the chirped return-to-zero and dispersion managed soliton modulation formats in WDM systems ", *J. Lightwave Technol.* **20**, pp. 608-617, 2002.

[76] K. Hirokazu and N. Masataka, "Partial soliton communication system", *Opt. Commun.* **87**, pp. 15-18, 1992.

[77] A. Berntson, N. J. Doran, W. Forysiak, and J. H. B. Nijhof, "Power dependence of dispersion-managed solitons for anomalous, zero, and normal path-average dispersion", *Opt. Lett.* **23**, pp. 900-902, 1998.

[78] J. Nathan Kutz, P. Holmes, S. G. Evangelides, and J. P. Gordon, "Hamiltonian dynamics of dispersion-managed breathers", *J. Opt. Soc. Am. B* **15**, pp. 87-96, 1998.

[79] S. K. Turitsyn, I. Gabitov, E. W. Laedke, V. K. Mezentsev, S. L. Musher, E. G. Shapiro, T. Schfer and K. H. Spatschek, "Variational approach to optical pulse propagation in dispersion compensated transmission systems", *Opt. Commun.* **151**, pp. 117-135, 1998.

[80] T. I. Lakoba and D. J. Kaup, "Hermite-Gaussian expansion for pulse propa-

gation in strongly dispersion managed fibers", *Phys. Rev. E* **151**, pp. 6728-6741, 1998.

[81] J. Martensson and A. Berntson, "Dispersion-managed solitons for 160-Gb/s data transmission", *IEEE Photon. Technol. Lett.* **13**, pp. 666-668, 2001.

[82] J.-K. Rhee, D. Chowdhury, S. C. Kwok, and U. Gliese, "DPSK 32×10 Gb/s transmission modeling on 5×90 km terrestrial system", *IEEE Photon. Technol. Lett.* **12**, pp. 1627-1629, 2000.

[83] J. Leibrich, C. Wree, and W. Rosenkranz, "CF-RZ-DPSK for suppression of XPM on dispersion-managed long-haul optical WDM transmission on standard single-mode fiber", *IEEE Photon. Technol. Lett.* **14**, pp. 155-157, 2002.

[84] Y. Miyamoto, H. Masuda, A. Hirano, S. Kuwahara, Y. Kisaka, H. Kawakami, M. Tomizawa, Y. Tada, and S. Aozasa, "S-band WDM coherent transmission of 40×43-Gbit/s CS-RZ DPSK signals over 400 km DSF using hybrid GS-TDFAs/Raman amplifiers", *Electron. Lett.* **38**, pp. 1569-1570, 2002.

[85] R. Griffin, R. Johnstone, R. Walker, J. Hall, S. Wadsworthm, K. Berry, A. Carter, M. Wale, P. Jerram, and N. Parsons, "10 Gb/s optical differential quadrature phase shift key (DQPSK)transmission using GaAs/AlGaAs integration", *Optical Fiber Communications conf.*, paper FD6, 2002.

[86] H. Bissessur, G. Charlet, E. Gohin, C. Simonneau, L. Pierre, and W. Idler, "1.6 Tbit/s (40×40 Gbit/s) DPSK transmission over 3×100 km of TeraLight fibre with direct detection", *Electron. Lett.* **39**, pp. 192-193, 2003.

[87] B. Zhu, C. R. Doerr, P. Gaarde, L. E. Nelson , S. Stulz, L. Stulz, L. Gruner-Nielsen, "Broad bandwidth seamless transmission of 3.56 Tbit/s over 40*100 km of NZDF fibre using CSRZ-DPSK format", *Electron. Lett.* **39**, pp.1528-1530, 2003.

[88] K. Hoon and A. H. Gnauck, "Experimental investigation of the performance limitation of DPSK systems due to nonlinear phase noise", *IEEE Photon. Technol. Lett.* **15**, pp. 320-322, 2003.

[89] A. H. Gnauck, G. Raybon, S. Chandrasekhar, J. Leuthold, C. Doerr, L. Stulz, and E. Burrows, "25×40-Gb/s copolarized DPSK transmission over 12×100-km NZDF with 50-GHz channel spacing", *IEEE Photon. Technol. Lett.* **15**, pp. 467-469, 2003.

[90] M. I. Hayee and A. E. Willner, "NRZ versus RZ in 10-40-Gb/s dispersion-

managed WDM transmission systems", *IEEE Photon. Technol. Lett.* **11**, pp. 991-993, 1999.

[91] L.-S. Yan, Y. Xie, Q. Yu, A.E. Willner, D. Starodubov, and J. Feinberg, "Performance optimization of chirped return-to-zero format in 10-Gb/s terrestrial transmission systems", *Optical Fiber Communications conf.*, paper MF1, 2001.

[92] R. Khosravani, S. Lee, M.I. Hayee, and A. E. Willner, "Soliton sampling of subcarrier multiplexed signals to suppress dispersion-induced RF power fading", *IEEE Photon. Technol. Lett.* **12**, pp. 1275-1277, 2000.

[93] B. Bakhshi, M. Vaa, E. A. Golovchenko, W. W. Patterson, R. L. Maybach, and N. S. Bergano, ". Comparison of CRZ, RZ and NRZ modulation formats in a 64×12.3 Gb/s WDM transmission experiment over 9000 km", *Optical Fiber Communications conf.*, paper WF4, 2001.

[94] D. Anderson, "Variational approach to nonlinear pulse propagation in optical fibers", *Phys. Rev. A.* **27**, pp. 3135-3145, 1983.

[95] L. E. Elsgoltz, *Differential equations and variational calculus*, Nauka, Moskva 1969.

[96] S. K. Turitsyn and E. G. Shapiro, "Variational approach to the design of optical communication systems with dispersion management", *Opt. Fiber Technol* **4**, pp. 151-188, 1998.

[97] A. Berntson, N. J. Doran, W. Forysiak, and J. H. B. Nijhof, "Power dependence ofdispersion-managed solitons for anomalous, zero, and normal path-average dispersion", *Opt. Lett.* **23**, pp. 900-902, 1998.

[98] J. N.Kutz, P. H., S. G. Evangelides, and J. P. Gordon, "Hamiltonian dynamics of dispersion-managed breathers", *J. Opt. Soc. Am. B* **15**, pp. 87-96, 1998.

[99] S. K. Turitsyn, I. Gabitov, E. W. Laedke, V. K. Mezentsev, S. L. Musher, E. G. Shapiro, T. Schfer and K. H. Spatschek, "Variational approach to optical pulse propagation in dispersion compensated transmission systems", *Opt. Commun.* **151**, pp. 117-135, 1998.

[100] H. Onaka, K. Otsuka, H. Miyata, and T. Chikama, "Measuring the longitudinal distribution of four-wave mixing efficiency in dispersion-shifted fibers", *IEEE Photon. Technol. Lett.* **6**, pp. 1454-1457, 1994.

[101] K. Ishiba, K. Tadayoshi, and T. Mikio, "Soliton System Evaluations using fibers with Dispersion and Loss Fluctuations", *Electronics and Communications in Japan, Part 2* **79**, pp. 780-786, 1996.

[102] L. F. Mollenauer, P. V. Mamyshev, and M. J. Neubelt, "Method for facile and accurate measurement of optical fiber dispersion maps", *Opt. Lett.***21**, pp. 1724-1726, 1996.

[103] K. Nakajima, M. Ohashi, and M. Tateda, "Chromatic dispersion distribution measurement along single mode optical fiber", *J. Lightwave Technol.* **15**, pp. 1095-1101, 1997.

[104] J. Gripp and L. F. Mollenauer, "Enhanced range for OTDR-like dispersion map measurements", *Opt. Lett.* **23**, pp. 1603-1605, 1998.

[105] J. P. Gordon and H. A. Haus, "Random walk of coherently amplified solitons in optical fiber transmission", *Opt. Lett.* **11**, pp. 665-667, 1986.

[106] H. A. Haus, "Quantum noise in a solitonlike repeater system", *J. Opt. Soc. Am. B* **8**, pp. 1122-1126, 1991.

[107] D. Marcuse, "An Alternative derivation of the Gordon-Haus Effect", *J. Lightwave Technol* **10**, pp. 273-278, 1992.

[108] V. S. Grigoryan, C. R. Menyuk, and R.-M Mu, "Calculation of timing and amplitude jitter in dispersion-managed optical fiber communications using linearization", *J. Lightwave Technol* **17**, pp. 1347-1356, 1999.

[109] S. Kumar and F. Lederer, "Gordon-Haus effect in dispersion-managed soliton systems", *Opt. Lett.* **22**, pp. 1870-1873, 1997.

[110] R.-M Mu, V. S Grigoryan, C. R Menyuk, E. A Golovchenko, and A. N Pilipetskii, "Timing-jitter reduction in a dispersion-managed soliton system", *Opt. Lett.* **23**, pp. 930-932, 1998.

[111] B. A Malomed, F. Matera, and M. Settembre, "Performance of optically amplified dispersion-compensated links: reduction of the time jitter for return to zero signals", *Opt. Commun.* **143**, pp. 193-198, 1997.

[112] K. Rottwitt, J. H. Povlsen, and A. Bjarklev, "Long distance transmission through distributed erbium-doped fibers", *J. Lightwave Technol.* **11**, pp. 2105-2112, 1993.

[113] K. Rottwitt, A. Bjarklev, J. H. Povlsen, O. Lumholt, and T. P. Ras-

museen, "Fundamental Design of a Distributed Erbium-doped fiber amplifier for Long-Distance Transmission", *J. Lightwave Technol.* **10**, pp. 1544-1552, 1992.

[114] F. Kh. Abdulaev and B. B. Baizakov, "Disintegration of a soliton in a dispersion-managed optical communication line with random parameters", *Opt. Lett.* **25**, pp. 93-95, 2000.

[115] Q. Lin and G. P. Agrawal, "Pulse broadening induced by dispersion fluctuations in optical fibers", *Opt. Commun.* **206**, pp. 313-317, 2002.

[116] F. Kh. Abdulaev, J. C. Bronski, and G. Papanicolaou, "Soliton perturbations and the random Kepler problem", *Physica D* **135**, pp. 369-386, 2000.

[117] T. I. Lakoba and D. J. Kaup, "Shape of Stationary Pulse in Strong Dispersion Management Regime", *Electron. Lett.* **34**, pp. 1124-1125, 1998.

[118] V. S. Grigoryan, T. Yu, E. A. Golovchenko, C. R. Menyuk, and A. N. Pilipetski, "Dispersion-managed soliton dynamics", *Opt. Lett.* **22**, pp.1609-1611, 1997.

[119] Y. Takushima, T. Douke, W. Xiaomin and K. Kikuchi, "Dispersion tolerance and transmission distance of a 40-Gb/s dispersion management soliton transmission system", *J. Lightwave Technol.* **20**, pp. 360-367, 2002.

[120] R. W. Boyd, *Nonlinear Optics*, 2nd ed., Academic Press, San Diego, 2003.

[121] Y. R. Shen, *Principles of Nonlinear Optics*, Wiley, New York, 1984.

[122] S. N. Vlasov, V. A. Petrishchev, and V. I. Talanov, "Averaged description of wave beams in linear and nonlinear media", *Radiophys. Quantum Electron.* **14**, p. 1353, 1971.

[123] S. K. Turitsyn, M. F. Fedoruk, E. G. Shapiro, V. K. Mezentsev, and E. G. Turitsyna, "Novel Approaches to Numerical Modeling of Periodic Dispersion-Managed Fiber Communicaion Systems", *IEEE J. Select. Topics Quantum Electron.* **6**, pp. 263-275, 2000.

[124] T. I. Lakoba and D. J. Kaup, "Shape of Stationary Pulse in Strong Dispersion Management Regime", *Electron. Lett.* **34**, pp. 1124-1125, 1998.

[125] T. Yu, E. A. Golovchenko, A. N. Pilipetskii, and C. R. Menyuk, "Dispersion-managed soliton interactions in optical fibers", *Opt. Lett.* **22**, pp. 793-795, 1997.

[126] A. H. Liang, H. Toda, and A. Hasegawa, "High speed soliton transmission in dense periodic fibers", *Opt. Lett.* **24**, pp. 799-801, 1999.

[127] S. K. Turitsyn, M. P. Fedoruk, and A. Gornakova, "Reduced-power optical solitons in fiber lines with short-scale dispersion management", *Opt. Lett.* **24**, pp. 869-871, 1999.

[128] L. J. Richardson, W. Forysiak, and N. J. Doran, "Dispersion-managed soliton propagation in short-period dispersion maps", *Opt. Lett.* **25**, pp. 1010-1012, 2000.

[129] A. Maruta, Y. Yamamoto, S. Okamoto, A. Suzuki, T. Morita, A. Agata, and A. Hasegawa, "Effectiveness of densely dispersion managed solitons in ultra-high speed transmission", *Electron. Lett.* **36**, pp. 1947-1949, 2000.

[130] N. J.Smith, N. J. Doran, F. M. Knox, and W. Forysiak, "Energy-scaling characteristics of solitons in strongly dispersion-managed fibers", *Opt. Lett.* **21**, pp. 1981-1983, 1996.

[131] S. K. Turitsyn, J. H. B. Nijhof, V. K. Mezentsev, and N. J. Doran, "Symmetries, chirp-free points, and bistability in dispersion-managed fiber lines", *Opt. Letts.* **24**, pp. 1871-1873, 1999.

[132] L. J. Richardson, W. Forysiak, and N. J. Doran, "Trans-oceanic 160-Gb/s single-channel transmission using short-period dispersion management", *Photonics Technol. Lett.* **13**, pp. 209-211, 2001.

[133] I. Gabitov, E. G. Shapiro, and S. K. Turitsyn, "Asymptotic breathing pulse in optical transmission systems with dispersion compensation", *Phoys.Rev.E.* **55**, pp. 3624-3633, 1997.

[134] M. J. Ablowitz and G. Biondini, "Multiscale pulse dynamicsin communication systems with strong dispersion management", *Opt. Lett.* **23**, pp. 1668-1670, 1998.

[135] C. Paré and P.-A. Bélanger, "Spectral domain analysis of dispersion management without averaging", *Opt. Lett.* **25**, pp. 881-883, 2000.

[136] R. H. Stolen, E. P. Ippen, and A. R. Tynes, "Raman Oscillation in Glass Optical Waveguide", *Appl. Phys. Lett.* **20**, pp. 62-64, 1972.

[137] R. H. Stolen, E. P. Ippen, "Raman gain in glass optical waveguides", *Appl. Phys. Lett.* **22**, pp. 276-278, 1973.

[138] L. J. Richardson, V. K. Mezentsev, and S. K. Turitsyn, "Limitations of 40 Gbit/s based dispersion managed WDM transmission: solitons versus quasi-linear propagation regime", *Optical Fiber Communications conf.*, paper MF5, Mar. 2001.

[139] W. L. Barnes, R. I. Laming, E. J. Tarbox, and P. R. Morkel, "Absorption and Emission Cross Section of Er3+ Doped Silica Fibers", *IEEE J. of Quantum Electron.* **27**, pp.1004-1010, 1991.

[140] K. Rottwitt, J. H. Povlsen, and A. Bjarklev, "Long Distance Transmission through Distributed Erbium-Doped Fibers", *J. Lightwave Technol.* **11**, pp.2105-2112, 1993.

[141] K. Rottwitt, J. H. Povlsen, A. Bjarklev, O. Lumholt, B. Pedersen, and T. Rasmuseen, "Noise in Distributed Erbium-doped Fibers", *IEEE Photon. Technol. Lett.* **11**, pp.218-219, 1993.

Appendix A

Reduced Lagrangian

In this appendix, we derive the reduced lagrangian (2.30) used in variational analysis of chapter 2.4. Representing Gaussian function (2.26) as

$$\begin{aligned} V(z,t) &= p(z)\exp\left[-(1+iC)\frac{(t-t_p)^2}{2T^2} - i\Omega(t-t_p) + i\phi\right] \\ &\equiv \nu\exp(i\Phi), \end{aligned} \tag{A.1}$$

where $p(z) \equiv \sqrt{E_0/\sqrt{\pi}T(z)}$ is a peak amplitude, and ν and Φ are the modulus and the phase of the complex quantity $V(z,t)$:

$$\nu \equiv p(z)\exp\left(-\frac{[t-t_p(z)]^2}{2T^2}\right), \tag{A.2}$$

$$\Phi \equiv -\frac{C(t-t_p)^2}{2T^2} - \Omega(z)[t-t_p(z)] + \varphi(z), \tag{A.3}$$

we can write the first term in Lagrangian density (2.25) as

$$\frac{i}{2}\left[V\frac{\partial V^*}{\partial z} - V^*\frac{\partial V}{\partial z}\right] = \frac{i}{2}\left[\nu e^{i\Phi}(\nu_z - i\nu\Phi_z)e^{-i\Phi} - \nu e^{-i\Phi}(\nu_z + i\nu\Phi_z)e^{i\Phi}\right]$$

$$
\begin{aligned}
&= -\frac{i}{2}\left[\nu\nu_z + i\nu^2\Phi_z - \nu\nu_z + i\nu^2\Phi_z\right] \\
&= \nu^2\Phi_z \qquad \text{(A.4)}
\end{aligned}
$$

Using Eq. (A.4), this first term can be integrated as

$$
\begin{aligned}
&\int_{-\infty}^{\infty} \frac{i}{2}\left[V\frac{\partial V^*}{\partial z} - V^*\frac{\partial V}{\partial z}\right]dt = \\
&\quad \int_{-\infty}^{\infty} p^2 e^{-\frac{(t-t_p)^2}{T^2}}\left[\varphi_z - (t-t_p)^2\left(\frac{C}{2T^2}\right)_z + \frac{C}{T^2}\frac{dt_p}{dz}(t-t_p) - (t-t_p)\,\Omega_z + \Omega\frac{dt_p}{dz}\right]dt \\
&\quad = p^2\left[\varphi_z + \Omega\frac{dt_p}{dz}\right]T\int_{-\infty}^{\infty} e^{-x^2}dx \\
&\quad + p^2\left[\frac{C}{T^2}\frac{dt_p}{dz} - \Omega_z\right]T^2\int_{-\infty}^{\infty} xe^{-x^2}dx \\
&\quad - p^2\left(\frac{C}{2T^2}\right)_z T^3\int_{-\infty}^{\infty} x^2e^{-x^2}dx \\
&\quad = \sqrt{\pi}p^2T\left[\varphi_z + \Omega\frac{dt_p}{dz} - \frac{T^2}{2}\left(\frac{C}{2T^2}\right)_z\right]. \qquad \text{(A.5)}
\end{aligned}
$$

We follow the same procedure for integrating the rest of the terms in Eq. (2.25).

For example,

$$
\begin{aligned}
&-\frac{\beta_2}{2}\left|\frac{\partial V}{\partial t}\right|^2 = \\
&\quad -\frac{\beta_2}{2}\left|pe^{-i\varphi - i\Omega(t-t_p)}\left(-\frac{(1+iC)(t-t_p)}{T^2} - i\Omega\right)\exp\left[-\frac{(1+iC)(t-t_p)^2}{2T^2}\right]\right|^2 \\
&\quad = -\frac{\beta_2}{2}p^2\left[\frac{(1+C^2)(t-t_p)^2}{T^4} + \frac{2\Omega C(t-t_p)}{T^2} + \Omega^2\right]\exp\left[-\frac{(t-t_p)^2}{T^2}\right]. \qquad \text{(A.6)}
\end{aligned}
$$

We can now perform integration to obtain

$$
\int_{-\infty}^{\infty} -\frac{\beta_2}{2}\left|\frac{\partial V}{\partial t}\right|^2 dt =
$$

$$
\begin{aligned}
&-\frac{\beta_2}{2}p^2\left[\left(1+C^2\right)\int\limits_{-\infty}^{\infty}e^{-\frac{(t-t_p)^2}{T^2}}\frac{(t-t_p)^2}{T^4}dt\right.\\
&\left.+2\Omega C\int\limits_{-\infty}^{\infty}\frac{(t-t_p)}{T^2}e^{-\frac{(t-t_p)^2}{T^2}}dt+\Omega^2\int\limits_{-\infty}^{\infty}e^{-\frac{(t-t_p)^2}{T^2}}dt\right]\\
&=-\frac{\beta_2}{2}p^2\left[\frac{(1+C^2)}{T}\int\limits_{-\infty}^{\infty}x^2e^{-x^2}dx+2\Omega C\int\limits_{-\infty}^{\infty}xe^{-x^2}dx+\Omega^2\int\limits_{-\infty}^{\infty}e^{-x^2}dx\right]
\end{aligned}
$$

$$
=-\frac{\sqrt{\pi}}{2}\frac{\beta_2}{2}p^2\left[\frac{(1+C^2)}{T}+2\Omega^2T\right], \tag{A.7}
$$

Similarly, using

$$
-\frac{\gamma(z)}{2}|V|^4=-\frac{1}{2}\gamma p^4e^{-2\frac{(t-t_p)^2}{T^2}}, \tag{A.8}
$$

$$
\begin{aligned}
\int\limits_{-\infty}^{\infty}-\frac{\gamma(z)}{2}|V|^4dt&\equiv-\frac{1}{2}\gamma p^4\frac{T}{\sqrt{2}}\int\limits_{-\infty}^{\infty}e^{-x^2}dx\\
&=-\sqrt{\frac{\pi}{2}}\frac{1}{2}\gamma p^4T.
\end{aligned} \tag{A.9}
$$

Using the Eqs. (A.5), (A.7), and (A.9) in Eq. (2.29), we arrive at the following expression for the reduced Lagrangian $\mathcal{R}$:

$$
\mathcal{R}=\frac{\sqrt{\pi}}{2}p^2\left\{2\Omega\frac{dt_p}{dz}+2T\varphi_z-\frac{C_zT}{2}+CT_z-\frac{\gamma}{\sqrt{2}}p^2T-\frac{\beta_2}{2}\frac{1+C^2}{T}-\beta_2\Omega^2T\right\}. \tag{A.10}
$$

Appendix B

Variational equations

We present here in detail the derivation of variational equations (2.33)-(2.36). Let $\eta = \varphi$ in Eq. (2.32). Using Eq. (2.29) in Eq. (2.32) for $\mathcal{R}$, we receive in this case

$$0 = \mathcal{R}_{\varphi} - \frac{d}{dz}\mathcal{R}_{\varphi_z} = \frac{d}{dz}\left(Tp^2\right), \tag{B.1}$$

which leads to the energy conservation law

$$E_0 \equiv \sqrt{\pi}Tp^2 = \text{const.} \tag{B.2}$$

Similarly, for $\eta = p$ in Eq. (2.32), noticing that $2p \neq 0$, and $T \neq 0$, we obtain:

$$0 = CT_z - \frac{C_z T}{2} + 2T\varphi_z - \sqrt{2}\gamma T p^2 - \beta_2 \frac{1+C^2}{2T} - \beta_2 \Omega^2 T + 2\Omega T \frac{dt_p}{dz}, \tag{B.3}$$

or

$$2\varphi_z = \frac{C_z}{2} - \frac{CT_z}{T} + \sqrt{2}\gamma p^2 + \beta_2 \frac{1+C^2}{2T^2} + \beta_2 \Omega^2 - 2\Omega \frac{dt_p}{dz}. \tag{B.4}$$

Let now $\eta = T$ in Eq. (2.32). We have

$$0 = 2\Omega p^2 \frac{dt_p}{dz} + 2p^2\varphi_z - \frac{p^2 C_z}{2} - \frac{\gamma p^4}{\sqrt{2}} + \beta_2 \frac{1+C^2}{2T^2} p^2 - \beta_2 \Omega^2 p^2 - \frac{d}{dz}\left(p^2 C\right). \quad \text{(B.5)}$$

Using Eq. (B.2), we can write

$$\frac{d}{dz}\left(p^2 C\right) = \frac{d}{dz}\left(p^2 T \frac{C}{T}\right) = p^2 C_z - \frac{C p^2 T_z}{T}. \quad \text{(B.6)}$$

Using Eq. (B.6) in Eq. (B.5) and noticing that $p^2 \neq 0$, we receive

$$2\varphi_z = \frac{C_z}{2} - \frac{C T_z}{T} + \frac{1}{\sqrt{2}}\gamma p^2 - \beta_2 \frac{(1+C^2)}{2T^2} + \beta_2 \Omega^2 - 2\Omega \frac{dt_p}{dz} + C_z. \quad \text{(B.7)}$$

Comparing (B.4) and (B.7), we find

$$\frac{dC}{dz} = \frac{\gamma p^2}{\sqrt{2}} + \beta_2 \frac{1+C^2}{T^2}, \quad \text{(B.8)}$$

and, noticing that $p^2 = E_0/\sqrt{\pi}T$ and $\gamma \equiv \gamma_0 G$, we arrive at the following expression describing evolution of the pulse chirp $C(z)$ in each fiber section of a DM system:

$$\frac{dC}{dz} = \frac{\gamma_0 E_0 G}{\sqrt{2\pi}T} + \frac{\beta_2 \left(1+C^2\right)}{T^2}. \quad \text{(B.9)}$$

Using now $\eta = C$ in Eq. (2.32), we have

$$0 = T_z p^2 - \frac{\beta_2 p^2}{T} C - \frac{1}{2}\frac{d}{dz}\left(p^2 T\right). \quad \text{(B.10)}$$

Using Eq. (B.2) in (B.10) and noticing that $p^2 \neq 0$, we obtain the following equation for pulse width evolution in each fiber section

$$\frac{dT}{dz} = \frac{\beta_2 C}{T}. \quad \text{(B.11)}$$

Similarly, considering $\eta = \Omega$ and $\eta = t_p$, we receive:

$$0 = \frac{\sqrt{\pi}}{2} p^2 T \left[2\frac{dt_p}{dz} - 2\beta_2 \Omega \right], \tag{B.12}$$

and

$$0 = \frac{\sqrt{\pi}}{2} p^2 T \left[-\frac{2d\Omega}{dz} \right]. \tag{B.13}$$

Noticing that $\frac{\sqrt{\pi}}{2} p^2 T \neq 0$, we obtain the following equations for the pulse position t_p and for the central frequency shift Ω:

$$\frac{dt_p}{dz} = \beta_2 \Omega, \tag{B.14}$$

$$\frac{d\Omega}{dz} = 0. \tag{B.15}$$

Finally, using Eqs. (B.11) and (B.9) in Eq. (B.4), we have

$$2\varphi_z = \frac{\gamma p^2}{2\sqrt{2}} + \beta_2 \frac{(1+C^2)}{2T^2} - \frac{C}{T}\left(\frac{\beta_2 C}{T}\right) + \frac{2\gamma p^2}{\sqrt{2}} + \beta_2 \frac{(1+C^2)}{2T^2} + \beta_2 \Omega^2 - 2\beta_2 \Omega^2, \tag{B.16}$$

and we obtain the following expression for pulse phase evolution in each fiber section

$$\frac{d\varphi}{dz} = \frac{5\gamma p^2}{4\sqrt{2}} + \frac{\beta_2}{2T^2} - \frac{1}{2}\beta_2 \Omega^2, \tag{B.17}$$

which can be rewritten in terms of the input energy $E_0 \equiv \sqrt{\pi} p^2 T$ and of the nonlinear parameter $\gamma_0 \equiv \gamma / G$ as

$$\frac{d\varphi}{dz} = \frac{5\gamma_0 E_0 G}{4\sqrt{2\pi} T} + \frac{\beta_2}{2T^2} - \frac{\beta_2}{2}\Omega^2. \tag{B.18}$$

Eqs. (B.2), (B.9), (B.11), (B.14), (B.15), and (B.18) are the final variational equation describing the evolution of pulse parameters within each fiber section.

Appendix C

Details of timing jitter calculation

We derive here the correlation terms $\langle F^2 \rangle$, $\langle FS \rangle$, and $\langle S^2 \rangle$ used in Eq. (4.15) for timing jitter. According to Eq. (4.12), since we assume here the dispersion β_2 to have a deterministic value, correlation $\langle F^2 \rangle$ can be expressed as

$$\left\langle F^2 \right\rangle = \int_0^z \int_0^z \beta_2 (z_1) \beta_2 (z_2) \left\langle \delta\Omega (z_1) \, \delta\Omega^* (z_2) \right\rangle dz_1 dz_2. \tag{C.1}$$

We first find the correlation $\langle \delta\Omega(z_1)\delta\Omega^*(z_2) \rangle$. Noticing that all the quantities in Eq.(4.14) are deterministic except for f_n, we can represent this correlation as

$$\left\langle \delta\Omega (z_1) \, \delta\Omega^* (z_2) \right\rangle = \frac{1}{E_0^2}(a + a^*), \tag{C.2}$$

where

$$a \equiv \int_0^{z_1} \int_0^{z_2} \frac{dz_1' dz_2'}{\sqrt{G (z_1') \, G (z_2')}} \int_{-\infty}^{\infty} \int_{-\infty}^{\infty} q_t^* (z_1', t') \, q_t (z_2', t'') \left\langle f_n (z_1', t') \, f_n^* (z_2', t'') \right\rangle e^{-i\Omega(t''-t')} dt' dt''$$

(C.3)

Using Eq. (4.2) and noticing that integration limits over time are infinite for both t' and t'' in Eq. (C.3), we have for the a term:

$$\begin{aligned} a &\equiv \int_0^{z_1}\int_0^{z_2} \frac{dz_1' dz_2'}{G(z_1')\,G(z_2')} \int_{-\infty}^{\infty}\int_{-\infty}^{\infty} \{q_t^*(z_1', t')\, q_t(z_2', t'')\, g(z_1')\, n_{sp}(z_1')\, h\upsilon_0 \\ &\quad \times \delta(z_1' - z_2')\,\delta(t' - t'')\, e^{-i\Omega(t''-t')}\Big\}\, dt' dt'' \\ &= \int_0^{z_1}\int_0^{z_2} \frac{dz_1' dz_2'}{G(z_1')\,G(z_2')} \int_{-\infty}^{\infty} q_t^*(z_1', t)\, q_t(z_2', t)\, g(z_1')\, n_{sp}(z_1')\, h\nu_0 \delta(z_1' - z_2')\, dt. \end{aligned} \tag{C.4}$$

Care should be taken in integrating over the δ-function $\delta(z_1' - z_2')$ since the result depends on the relative values of z_1 and z_2, both of which vary between 0 and z. Let us define

$$\theta(z_1', z_2', t) \equiv \frac{q_t^*(z_1', t)\, q_t(z_2', t)\, g(z_1')\, n_{sp}(z_1')\, h\nu_0}{G(z_1')\,G(z_2')}, \tag{C.5}$$

so that Eq. (C.4) can be written as

$$a = \int_{-\infty}^{\infty} \left\{ \int_0^{z_1}\int_0^{z_2} \theta(z_1', z_2', t)\, \delta(z_1' - z_2') dz_1' dz_2' \right\} dt. \tag{C.6}$$

One can show that

$$\int_0^{z_1}\int_0^{z_2} \theta(z_1', z_2', t)\, \delta(z_1' - z_2') dz_1' dz_2' = \int_0^{\min(z_1, z_2)} \theta(z'', t) dz'', \tag{C.7}$$

where $\min(x, y)$ denotes the minimal of the values x and y. The proof of Eq. (C.7) is straightforward. We can represent the integral in Eq. (C.7) as

$$\int_0^{z_1}\int_0^{z_2} \theta(z_1', z_2', t)\, \delta(z_1' - z_2') dz_1' dz_2' = \int_0^{z_2} \bar{\theta}(z_2', z_1, t)\, dz_2', \tag{C.8}$$

where

$$\bar{\theta}\left(z_2', z_1, t\right) \equiv \int_0^{z_1} \theta\left(z_1', z_2', t\right) \delta\left(z_1' - z_2'\right) dz_1'. \tag{C.9}$$

The integral in Eq. (C.9) can be easily shown to be

$$\bar{\theta}\left(z_2', z_1, t\right) = \begin{cases} \theta\left(z_2', t\right), & \text{if } z_2' \in [0, z_1] \\ 0, & \text{if } z_2' \notin [0, z_1]. \end{cases} \tag{C.10}$$

For simplicity of discussion, we do not consider the boundary point $z_1 = z_2'$; taking it into account does not change the final result. Using the result of Eq. (C.10) and noticing that z_2' always varies from 0 to z_2, the integral in Eq. (C.8) is found to be

$$\begin{aligned} \int_0^{z_2} \bar{\theta}\left(z_2', z_1, t\right) dz_2' &= \begin{cases} \int_0^{z_1} \theta\left(z_2', t\right) dz_2', & \text{if } z_2 > z_1 \\ \int_0^{z_2} \theta\left(z_2', t\right) dz_2', & \text{if } z_2 < z_1 \end{cases} \\ &= \int_0^{\min(z_1, z_2)} \theta\left(z_2', t\right) dz_2', \end{aligned} \tag{C.11}$$

which proves Eq. (C.7). Using Eqs. (C.6), (C.7), and (C.5), the a term is found to be

$$a = h\nu_0 \int_0^{\min(z_1, z_2)} \int_\infty^\infty \left|q_t\left(z'', t\right)\right|^2 g\left(z''\right) n_{sp}\left(z''\right) G^{-1}\left(z''\right) dt dz''. \tag{C.12}$$

Using the result (C.12) in Eq. (C.2), the whole correlation in Eq. (C.2) is then equal to

$$\begin{aligned} \left\langle \delta\Omega\left(z_1\right) \delta\Omega^*\left(z_1\right) \right\rangle &= \frac{2h\nu_0}{E_0^2} \int_0^{\min(z_1, z_2)} \int_\infty^\infty \left|q_t\left(z'', t\right)\right|^2 g\left(z''\right) n_{sp}\left(z''\right) G^{-1}\left(z''\right) dt dz'' \\ &\equiv f\left(z_1, z_2\right). \end{aligned} \tag{C.13}$$

Using this result in Eq. (C.1), we have

$$\left\langle F^2 \right\rangle = \int_0^z \int_0^z \beta_2 (z_1) \beta_2 (z_2) f (z_1, z_2) \, dz_1 dz_2, \tag{C.14}$$

where $f(z_1, z_2)$ is defined in Eq. (C.13). Since both z_1 and z_2 take arbitrary (positive) values on the plane (z_1, z_2), while $f(z_1, z_2)$ depends on the relative values of z_1 and z_2, we need to consider separately the regions $z_1 < z_2$ and $z_1 > z_2$. We can represent the $\langle F^2 \rangle$ term as a sum of two integrals, $\langle F^2 \rangle = I_1 + I_2$, where the integration in I_1 and I_2 is considered on the half-planes $z_1 < z_2$ and $z_1 > z_2$, respectively. Consider the half-plane $z_1 < z_2$. In this region, z_2 varies from 0 to z, while z_1 changes from 0 to z_2, and $\min(z_1, z_2) = z_1$, so that $f(z_1, z_2)$, according to the definition (C.13), is equal to

$$f (z_1, z_2) = \frac{2h\nu_0}{E_0^2} \int_0^{z_1} \int_\infty^\infty |q_t (z'', t)|^2 \, g (z'') \, n_{sp} (z'') \, G^{-1} (z'') \, dt dz''. \tag{C.15}$$

The integral I_1 is then found to be

$$I_1 = \frac{2h\nu_0}{E_0^2} \int_0^z \beta_2 (z_2) \, dz_2 \int_0^{z_2} \beta_2 (z_1) \, dz_1 \int_0^{z_1} \int_\infty^\infty |q_t (z', t)|^2 \, g (z') \, n_{sp} (z') \, G^{-1} (z') \, dt dz'. \tag{C.16}$$

Similarly, for I_2 we have

$$I_2 = \frac{2h\nu_0}{E_0^2} \int_0^z \beta_2 (z_1) \, dz_1 \int_0^{z_1} \beta_2 (z_2) \, dz_2 \int_0^{z_2} \int_\infty^\infty |q_t (z', t)|^2 \, g (z') \, n_{sp} (z') \, G^{-1} (z') \, dt dz'. \tag{C.17}$$

We see that integration in the regions $z_1 < z_2$ and $z_1 > z_2$ produces the same result, i.e. $I_1 = I_2$, and we have the following final expression for $\langle F^2 \rangle$:

$$\left\langle F^2 \right\rangle \;\; = \;\; I_1 + I_2$$

$$= \frac{4h\nu_0}{E_0^2}\int_0^z \beta_2(z_1)\,dz_1 \int_0^{z_1} \beta_2(z_2)\,dz_2 \int_0^{z_2} \frac{g(z')\,n_{sp}(z')}{G(z')} \int_\infty^\infty |q_t(z',t)|^2\,dt dz'. \tag{C.18}$$

Consider now the cross-correlation term $\langle FS\rangle$. Using Eqs. (4.12, (4.13), and (4.14), and using again the fact that all the quantities are deterministic in those equations except for f_n, we can write:

$$\begin{aligned}
\langle FS\rangle = & \\
& \frac{i}{E_0^2}\left\langle \int_0^z \beta_2(z_1)dz_1 \int_0^{z_1} \frac{dz'}{G(z')} \int_{-\infty}^\infty \left(q_t^*(z',t')\,f_n(z',t')\,e^{i\Omega(t'-t_p)}\right.\right. \\
& \left. + q_t(z',t')\,f_n^*(z',t')\,e^{-i\Omega(t'-t_p)}\right)dt' \\
& \times \int_0^z \frac{dz_2}{G(z'')} \int_{-\infty}^\infty (t''-t_p)\left(q(z_2,t'')\,f_n^*(z_2,t'')\,e^{-i\Omega(t''-t_p)}\right. \\
& \left.\left. - q^*(z_2,t'')\,f_n(z_2,t'')\,e^{i\Omega(t''-t_p)}\right)dt''\right\rangle \\
= & \frac{i}{E_0^2}\int_0^z \beta_2(z_1)dz_1 \int_0^z \left\{\frac{dz_2}{G(z_2)}\int_0^{z_1}\frac{dz'}{G(z')}\int_{-\infty}^\infty\int_{-\infty}^\infty (t''-t_p)\left[q_t^*(z',t')\,q(z_2,t'')\,e^{-i\Omega(t''-t')}\right.\right. \\
& \left.\left. - q_t(z',t')\,q^*(z_2,t'')\,e^{i\Omega(t''-t')}\right]\langle f_n(z',t')\,f_n^*(z_2,t'')\rangle\,dt'dt''\right\} \\
= & \frac{ih\nu_0}{E_0^2}\int_0^z \beta_2(z_1)dz_1 \int_0^z \frac{dz_2}{G(z_2)}\int_0^{z_1}\frac{dz'}{G(z')}\int_{-\infty}^\infty\int_{-\infty}^\infty \left\{(t''-t_p)\left[q_t^*(z',t')\,q(z_2,t'')\,e^{-i\Omega(t''-t')}\right.\right. \\
& \left.\left. - q_t(z',t')\,q^*(z_2,t'')\,e^{i\Omega(t''-t')}\right]g(z')\,n_{sp}(z')\,\delta(z'-z_2)\,\delta(t'-t'')\right\}dt'dt''
\end{aligned} \tag{C.19}$$

where we used the fact that $\langle f_n(z',t')\,f_n^*(z_2,t'')\rangle = \langle f_n^*(z',t')\,f_n(z_2,t'')\rangle$. Noticing that the integration over both t' and t'' is in the same infinite limits, we can accomplish the integration over time to obtain:

$$\begin{aligned}
\langle FS\rangle = & \frac{i}{E_0^2}\int_0^z \beta_2(z_1)dz_1 \int_0^z \frac{dz_2}{G(z_2)}\int_0^{z_1}\frac{dz'}{G(z')}\int_{-\infty}^\infty \{(t-t_p) \\
& \times \left(q_t^*(z',t)\,q(z_2,t) - q_t(z',t)\,q^*(z_2,t)\right)\delta(z'-z_2)\}\,dt.
\end{aligned} \tag{C.20}$$

We proceed further by considering, first, the integration over z'. Let us define

$$f\left(z',z_2\right)\equiv\frac{1}{G\left(z'\right)}\int\limits_{-\infty}^{\infty}\left(t-t_p\right)\left(q_t^*\left(z',t\right)q\left(z_2,t\right)-q_t\left(z',t\right)q^*\left(z_2,t\right)\right)dt, \tag{C.21}$$

and

$$\bar{f}\left(z_2,z_1\right)\equiv\int\limits_0^{z_1}dz'f\left(z',z_2\right)\delta\left(z'-z_2\right). \tag{C.22}$$

Integrating Eq. (C.22) over z', we obtain

$$\bar{f}\left(z_2,z_1\right)=\begin{cases} f\left(z_2\right), & \text{if } \mathrm{z_2}\in[0,\mathrm{z_1}] \\ 0, & \text{if } \mathrm{z_2}\notin[0,\mathrm{z_1}] \end{cases} \tag{C.23}$$

Since we always have $z_1\leq z$, we can represent the integral over z_2 in Eq. (C.20) as a sum of two integrals: from 0 to z_1 and from z_1 to z. Using the result of Eq. (C.23), we have

$$\int\limits_0^z dz_2\bar{f}\left(z_2,z_1\right)=\int\limits_0^{z_1}\bar{f}\left(z_2,z_1\right)dz_2+\int\limits_{z_1}^{z}\bar{f}\left(z_2,z_1\right)dz_2=\int\limits_0^{z_1}f\left(z_2\right)dz_2. \tag{C.24}$$

Note that the same result one could obtain considering, first, integration over z_2. With the result of Eq. (C.24), the final expression for the cross-correlation $\langle FS\rangle$ is found to be

$$\langle FS\rangle=\frac{ih\nu_0}{E_0^2}\int\limits_0^z\beta_2(z_1)dz_1\int\limits_0^{z_1}g(z')n_{sp}(z')G^{-1}\left(z'\right)\int\limits_{-\infty}^{\infty}\left(t-t_p\right)\left[q_tq^*-q_t^*q\right]dtdz'. \tag{C.25}$$

Similarly, we calculate the expression for the $\langle S^2\rangle$ term:

$$\begin{aligned}\left\langle S^2\right\rangle &= \frac{1}{E_0^2}\int\limits_0^z\int\limits_0^z\frac{dz_1dz_2}{\sqrt{G\left(z_1\right)}G\left(z_2\right)}\int\limits_{-\infty}^{\infty}\int\limits_{-\infty}^{\infty}\Big\{\left(t_1-t_p\right)\left(t_2-t_p\right)\Big[q\left(z_1,t_1\right)q^*\left(z_2,t_2\right)e^{-i\Omega(t_1-t_2)} \\ &\quad +q^*\left(z_1,t_1\right)q\left(z_2,t_2\right)e^{i\Omega(t_1-t_2)}\Big]\left\langle f_n\left(z_1,t_1\right)f_n^*\left(z_2,t_2\right)\right\rangle\Big\}dt_1dt_2 \\ &= \frac{2h\nu_0}{E_0^2}\int\limits_0^z g\left(z'\right)n_{sp}\left(z'\right)G^{-1}\left(z'\right)\int\limits_{-\infty}^{\infty}\left(t-t_p\right)^2\left|q\left(z',t\right)\right|^2dtdz'.\end{aligned} \tag{C.26}$$

Equations (C.18), (C.25), and (C.26) provide the final expressions for the three terms composing the timing jitter in Eq. (4.15).

Appendix D

List of abbreviations

ASE	Amplified spontaneous emission
BER	Bit error rate
CRZ	Chirped return to zero
DCF	Dispersion compensating fiber
DM	Dispersion managed
DPSK	Differential phase shift keying
DRA	Distributed Raman amplification
EDFAs	Erbium-doped fiber amplifiers
FBGs	Fiber Bragg gratings
FWHM	Full width at half maximum
FWM	Four wave mixing
GVD	Group velocity dispersion

NLS	Nonlinear Schrödinger equation
NRZ	Non-return to zero
RZ	Return-to zero
SMF	Single mode fiber
SNR	Signal-to-noise ratio
SPM	Self-phase modulation
WDM	Wavelength division multiplexing
XPM	Cross-phase modulation